5-2015

Facile Synthesis and Electrochemical Analysis of Cobalt Sulfide Nanostructures for Supercapacitor Applications

Esam Alqurashi
Pittsburg State University

FACILE SYNTHESIS AND ELECTROCHEMICAL ANALYSIS OF COBALT SULFIDE NANOSTRUCTURES FOR SUPERCAPACITOR APPLICATIONS

A Thesis Submitted to the Graduate School
In Partial Fulfillment of the Requirements
For The Degree of Master of Science

Esam Alqurashi

Pittsburg State University

Pittsburg, Kansas

May, 2015

FACILE SYNTHESIS AND ELECTROCHEMICAL ANALYSIS OF COBALT SULFIDE NANOSTRUCTURES FOR SUPERCAPACITOR APPLICATIONS

Esam Alqurashi

APPROVED:

Thesis Advisor _____
Dr. Ram Gupta, Chemistry Department

Committee Member _____
Dr. Khamis Siam, Chemistry Department

Committee Member _____
Dr. Irene Zegar, Chemistry Department

Committee Member _____
Dr. John Franklin, Department of English and Modern Languages

ACKNOWLEDGEMENTS

First of all, I would like to thank my lovely parents and wife for their support and great patience at all times. Also, I would like to thank my brothers, sisters and my future babies.

I would like to thank my advisor Dr. Ram Gupta for his guidance and motivation to achieve this work. I would like to thank him for his teaching and for his patience to improve my skills. This process would not have been nearly as successful or enjoyable without his knowledge, friendship and dedication.

In addition, I would like to express my sincere thanks to all my committee members Dr. Khamis Siam, Dr. Irene Zegar and Dr. John Franklin and other faculty members. Also, this thesis would not have been completed without the help of Dr. Lifeng Dong from Missouri State University (for recording SEM and EDX images) and Dr. Dhananjay Kumar from North Carolina A&T State University (for magnetic measurements).

I would like to thank my sponsor Al-Baha University that give me the opportunity to continue my studies and my knowledge.

Last but not least, I would like to thank Esam Allehyani, Ali Hroobi, John Candler, all my nice friends and my classmates. Words cannot describe my feeling toward them: thank you for everything.

FACILE SYNTHESIS AND ELECTROCHEMICAL ANALYSIS OF COBALT SULFIDE NANOSTRUCTURES FOR SUPERCAPACITOR APPLICATIONS

An Abstract of the Thesis By
Esam Alqurashi

The main objective of the thesis is to understand the effect of morphologies and electrolytes on the electrochemical properties of cobalt sulfides. The nanostructured cobalt sulfides were synthesized by a facile hydrothermal method. For this, cobalt nitrate $Co(NO_3)_2.H_2O$, cetyl trimethylammonium bromide (CTAB), thioacetamide (TTA), poly (vinyl pyrrolidone) (PVP) and ethylene glycol were used. The effect of growth parameters such as solvent and presence of surfactants on the size and morphology of the cobalt sulfides were investigated. It was observed that these variations could provide cobalt sulfides with a range of sizes, shapes and morphologies. The nanostructured cobalt sulfides were structurally and electrochemically characterized using various techniques. The structural characterizations were performed using X-ray diffraction (XRD) technique. The XRD analysis showed mixed phases of cobalt sulfides such as CoS and CoS_2. The morphology and size of the cobalt sulfides were studied using scanning electron microscopy (SEM). It was observed that the morphology and the size of the cobalt sulfides depend on the growth conditions. The crystallite size of the cobalt sulfide was estimated using XRD data. Energy-dispersive X-ray spectrometer (EDS) was used to further confirm the cobalt sulfide formation.

Electrochemical measurements were performed in a standard three electrode cell containing a platinum wire as a counter electrode, a saturated calomel electrode as a

reference electrode and cobalt sulfide on nickel foam as a working electrode. The potential application of cobalt sulfides for supercapacitors was tested using cyclic voltammeter and galvanostatic charge-discharge methods. It was seen that the specific capacitance of cobalt sulfides depends on its morphology and electrolyte. The specific capacitance was observed to be decreasing with increasing scan rate. In galvanostatic charge-discharge measurements, it was observed that the specific capacitance of cobalt sulfides decreases with increasing current. The charge storage capacity depends on electrolyte and a maximum specific capacitance of 335 F/g was observed in 3 M NaOH solution. The electrochemical stability of these electrodes was also investigated using cyclic voltammetry and galvanostatic charge-discharge techniques. A quasi-solid state supercapacitor device was fabricated by sandwiching two electrodes separated by an ion transporting layer. The effect of temperature on the charge storage properties of the device was investigated for high temperature applications. The specific capacitance of the device improved when the operational temperature of the device was elevated from 10 to 70 ^{o}C. The results suggest that cobalt sulfides could be used as an electrode material for fabrication of supercapacitor devices.

TABLE OF CONTENTS

LIST OF TABLES

LIST OF FIGURES

CHAPTER I

INTRODUCTION

Due to increasing demand for energy, there is an urgent need to develop efficient and low cost energy conversion and storage devices. There are many other ways to get energy apart from conventional sources such as coal and petroleum. Some of the typical non-conventional (green) energy sources are solar light, hydro power, and wind energy. Devices based on conversion of solar light into electricity are the most common for practical applications. These devices are also known as photovoltaic devices or solar cells. The research on solar cells is divided into three generations. The First generation is the classic one where silicon was used for making solar cells. The silicon wafer was used for such devices. The second generation is based on development of the solar cells based on thin-film apart from silicon such as cadmium telluride. The third generation is based on using different materials such as solar dyes, conductive plastics, solar inks etc.

Hydro-energy is the other type of non-conventional energy source where power can be generated by forces of water. The Hydro-energy has many different types such as small hydro, micro hydro, conventional hydroelectric, run of the river hydroelectricity,

and pumped storage hydroelectricity. Furthermore, wind power can be also used to generate energy. These devices can generate energy which could be used for various applications. For any practical applications, we need to store the generated energy so that it could be used when needed. Batteries, fuel cells and capacitors are some of the commonly used energy storage devices. The comparison of the power density and energy density of these devices are shown in Figure 1.1.

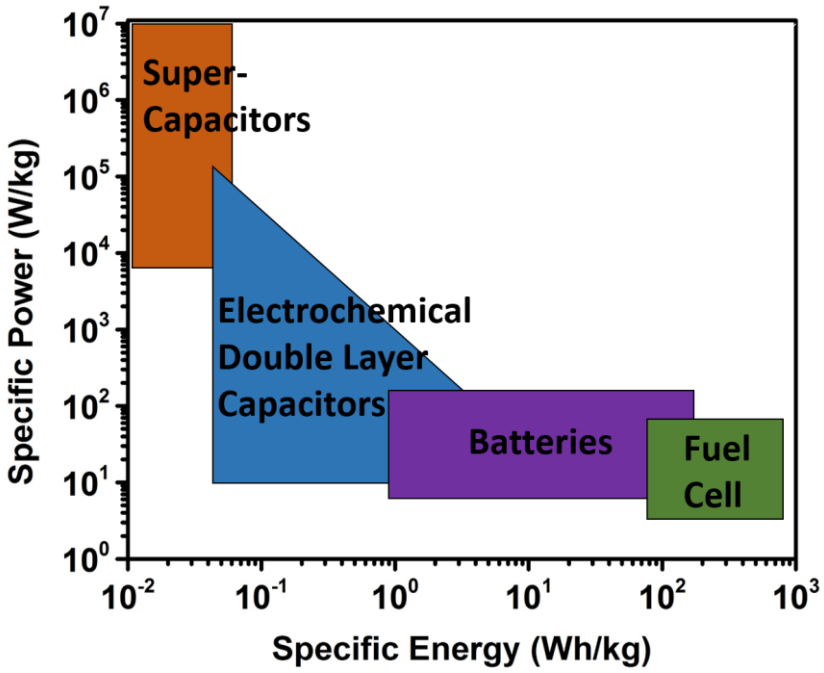

Figure 1.1: Ragone plot for various kinds of energy storage devices.

A battery is a device which converts chemical energy into electrical energy. A battery could be primary or rechargeable. The main issues facing various current batteries are the slow electrode-process kinetics and low rate of ionic diffusion/migration, resulting in limited practical energy output and battery performance. In contrast, a capacitor works

in a different and simpler way from a battery. A capacitor stores energy electrostatically in an electric field. The most common capacitors consist of conducting electrodes separated by non-conducting layer as shown in Figure 1.2. The potential difference (V) across the plates generates an electrical field in the dielectric material causing generation of positive charge (+Q) at one plate and negative charge (-Q) at the other plate. The capacitance (C) of the device is equal to Q/V. The SI unit of capacitance is farad (F), which is equal to one coulomb per volt. Capacitors are called supercapacitors when their charge storage capacity is higher than conventional capacitors. Supercapacitors (SCs), often referred to as ultracapacitors or electrochemical capacitors, demonstrate high power performance, excellent cyclic stability and very long cycle life. Supercapacitors are emerging energy storage devices that are complementary to the conventional batteries.

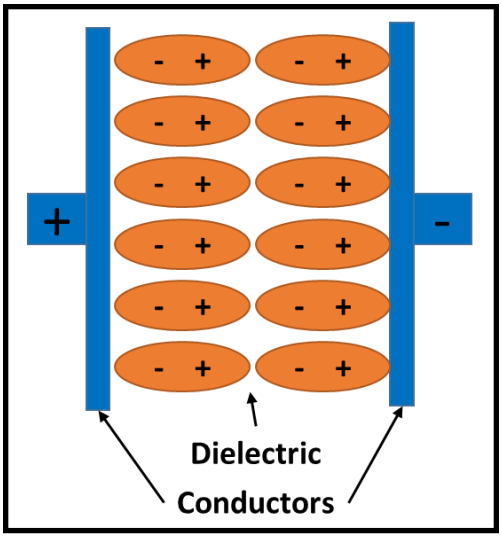

Figure 1.2: Charge separation and storage in a parallel-plate capacitor.

The charge storage mechanism of the supercapacitors can be divided into two categories: (i) electrical double-layer capacitors (EDLC) in which the capacitance arises from the charge separation at the electrode/electrolyte interface; and, (ii) redox electrochemical capacitors (pseudocapacitors) in which the capacitance arises from faradic reactions occurring at the electrode interface (Figure 1.3). The earliest model of electrical double-layer is usually attributed to Helmholtz and thus the electrical double-layer is also referred to as Helmholtz double-layers. Later, the Gouy-Chapman model and the Gouy-Chapman-Stern model were developed to more accurately describe the detailed structure of electrical double-layer. Electrical double-layer capacitors commonly use carbon-based materials, whereas metal oxides and conducting polymers are used for pseudocapacitors.

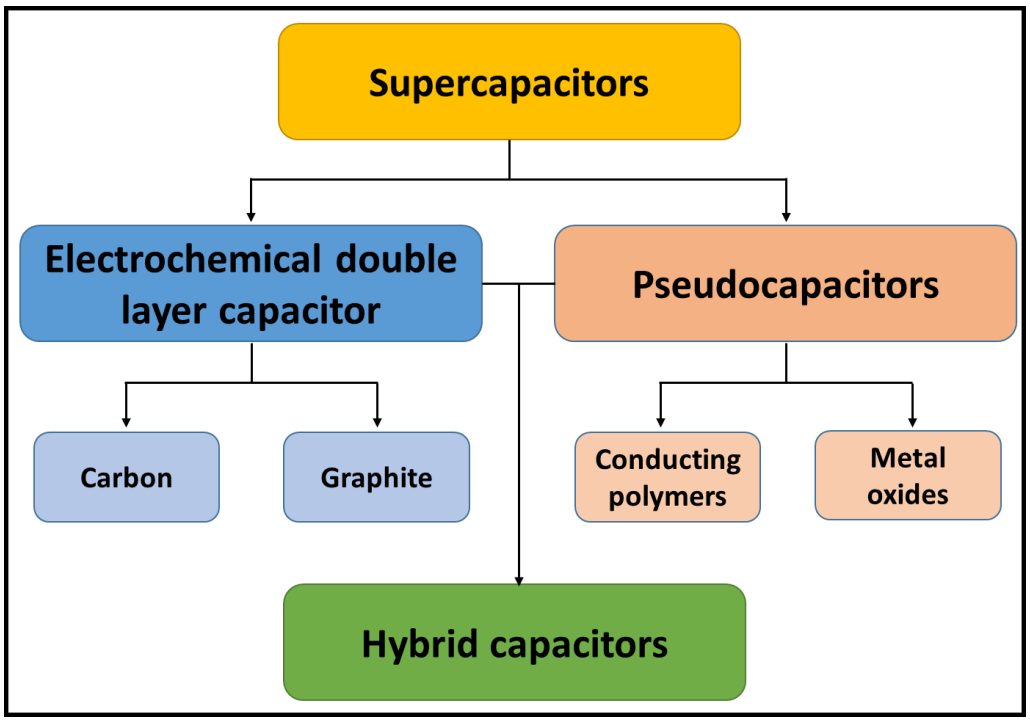

Figure 1.3: Types of supercapacitors.

1.1. Electrical Double-Layer Capacitors (EDLC)

In electrochemical double layer capacitors, the capacitance arises from the charge separation at the electrode/electrolyte interface. As capacitance is proportional to the area of the electrode, the electrode with higher surface area provides capacitor which could store a larger amount of charge. The commonly used materials for electrochemical double layer capacitors are carbon, graphite and some metal oxides. Different types of carbon such as carbon gel, carbon black, active carbon, carbon fibers, microbeads and mesocarbon are particularly useful for making such capacitors. Different types of electrolytes such as aqueous, non-aqueous, organic and inorganic can be used in fabrication of these capacitors. Aqueous electrolytes such as sulfuric acid (H_2SO_4) and potassium hydroxide (KOH) are some of the examples. The disadvantage of aqueous electrolytes is their potential limit. The potential limit for aqueous electrolytes is 1.23 V. The higher potential limit of about 2.5 V can be achieved by using organic electrolytes containing quaternary salts. The energy density for organic electrolytes is about four times higher than that of an aqueous one. The performance of a capacitor could be improved by improving properties of carbon used. For example, Zhao et al have recently reported that the N-doped carbons generated from the biomass derivatives (chitosan and glucosamine) possess an increased electronic conductivity and an unproved oxidation stability, as compared to ordinary char based carbons [1]. Recently, Wang et al have fabricated three-dimensional flower-like and hierarchical porous carbon material by carbonization method followed by chemical activation using flower-like ZnO as template and pitch as carbon precursor [2]. The electrode made using three-dimensional flower-

like and hierarchical porous carbon shows a high specific capacitance of 294 F/g with excellent cyclic stability. The symmetric supercapacitor made using modified carbon provides a high energy density of 15.9 Wh/kg at a power density of 317.5 W/kg. It is observed that the three-dimensionally hierarchical porous carbon can produce high performance capacitor [3]. These three-dimensionally hierarchical porous carbons exhibit large specific capacitance of about 300 F/g at 1 A/g in 6 M KOH aqueous electrolyte along with high capacitance retention.

1.2. Pseudocapacitors

Pseudocapacitance arises at the electrode surfaces where the charges are faradically stored. The faradaic charge transfer process across the electric double layer leads to a special potential-dependent charge accumulation. The most common active materials for pseudocapacitors are metal oxides, metal sulfides and conducting polymers. Among the metal oxides, various transition-metal oxides, such as RuO_2, Co_3O_4, NiO, Fe_2O_3, Fe_3O_4, MnO_2, etc., are being studied for supercapacitor applications [4-21]. Wang et al have used a composite of Fe_3O_4 nanoparticles grown on reduced graphene oxide for supercapacitor applications [16]. The specific capacitance of 220.1, 110.5 and 65.4 F/g was observed for Fe_3O_4/reduced graphene oxide, Fe_3O_4/carbon nano tubes and Fe_3O_4, respectively. The reduction in the particle size of Fe_3O_4 from microcrystals to nanocrystals by making composites with graphene oxide and carbon nanotubes was one of the main reasons to increase the specific capacitance. Thus, the specific capacitance of a redox active metal oxide can be improved by reducing the particle size. Recently, Mitchell et al

have used a multilayer of polyaniline and graphene to achieve better performance and higher charge storage capacity [22]. The electrochemical testing showed that the multilayer film has improved specific capacitance compared to that of pure polyaniline film. The specific capacitance of 201 F/g and 429 F/g was achieved for polyaniline and polyaniline-graphene multilayer electrodes. The high performance of the multilayers was due to presence of more active sites for the deposition of polyaniline provided by large surface areas of graphene oxide sheets.

1.3. Hybrid Capacitors

Hybrid capacitors are capacitors which hold properties of both electrochemical double layers and pseudocapacitors (Figure 1.4). In terms of charge storage capacity, hybrid capacitors are better than electrical double-layer capacitors and pseudocapacitors due to combined properties of double layer and Faradic reactions at the electrodes. There are three types of hybrid capacitors: asymmetric, composite and battery types. Sun et al have deposited hybrid films of polyaniline and manganese oxide for hybrid capacitors [23]. The hybrid film showed excellent cyclic stability. They retained more than 90% of its capacitance after 1000 charging-discharging cycles, with a coulombic efficiency of 98%. Guan et al have used iron oxide and carbon nanotubes for energy storage applications [24]. They reported that the presence of carbon nanotubes could significantly improve the charge storage capacity of the carbon nanotubes/iron oxide composite. The specific capacitance of 117.2 F/g was observed for the composite electrode which was 3 times higher than that of pure iron oxide. The improved electrochemical performance was due

to the good conductivity of carbon nanotubes as well as the anchored iron oxide particles on the carbon nanotubes.

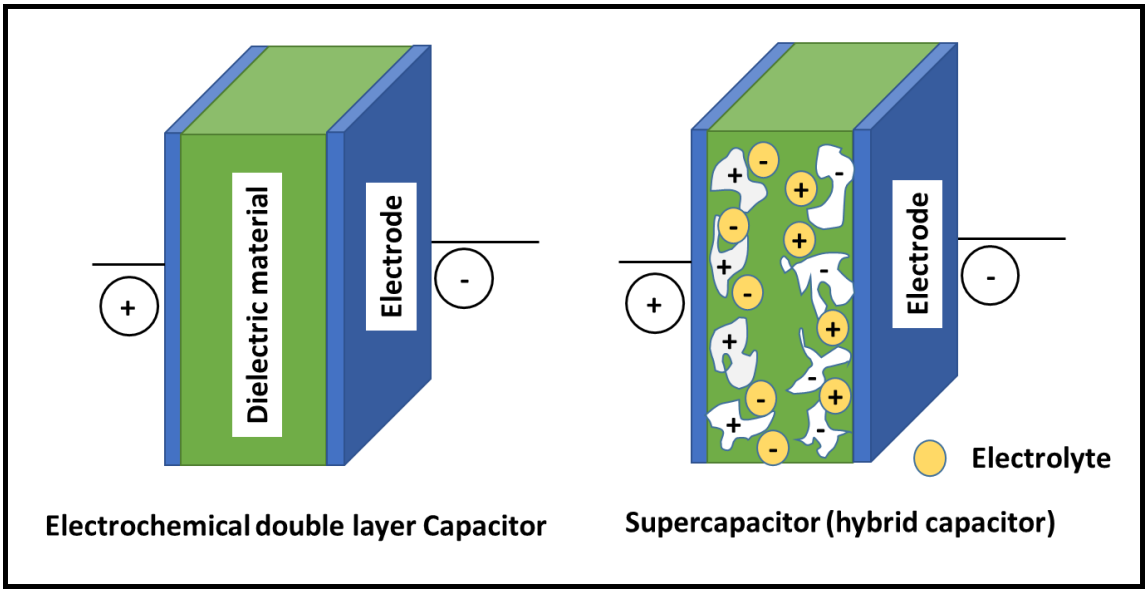

Figure 1.4: Schematic diagram of electrochemical double layer and hybrid capacitor.

1.4. Advantages and Disadvantages of Supercapacitors

The supercapacitors have certain advantages and disadvantages, which are given below:

Table 1.1: Advantages and disadvantages of supercapacitors.

Advantages	Disadvantages
✓ No chemical reaction ✓ Simple charging requires ✓ Faster than batteries ✓ Long cycle life (more than 10 years) ✓ Control the charge (no overcharge) ✓ Provides high power density	▪ Energy density is low ▪ Need cell balancing ▪ Very fast power delivery ▪ Self-discharge is high

1.5. Project Rationale

The electrochemical properties and thus the charge storage capacity of any electrode depends on its size, morphology, porosity and pore size distribution. The main objective of this thesis is to understand the effect of morphologies and electrolytes on the charge storage properties of cobalt sulfides. Cobalt sulfides could be present in different phases such as CoS, CoS_2, Co_3S_4 and Co_9S_8.

Recently, cobalt sulfides have attracted much attention because of their potential applications in catalysts, Li-ion batteries, solar cells and charge storage devices due to

their excellent physical, chemical, electronic and optical properties [25-27]. Among the cobalt sulfides, CoS_2 is emerging as one of the high performance material for energy storage applications due to its high redox activity as well as multiple convertible valence states. The charge storage capacity of the CoS_2 can be tuned by modifying its morphology. Hollow spheres, single phase ellipsoids, nono- octahedrons, nanotubes, nanorods, nanowires, mono disperse particles and polygons have been synthesized and used as an electrode material for supercapacitor applications. Xing at al have synthesized octahedron-shaped CoS_2 crystals using a hydrothermal method without any surfactant or template [28]. These CoS_2 octahedral structures showed a very uniform structure with a mean edge length of ~360 nm and exhibited a high geometric symmetry. The electrochemical performance of these octahedrals was investigated using cyclic voltammetry and galvanostatic charge discharge method. The electrochemical testing of octahedron-shaped CoS_2 showed a specific capacitance of 236.5 F/g at a current density of 1 A/g. These octahedron-shaped CoS_2 also showed an excellent cyclic stability with almost 93% capacitance retention after 2000 cycles.

A facile and efficient solvothermal method was used for the synthesis of cobalt sulfide (CoS) nanoflakes and cobalt disulfide (CoS_2) nanoparticles [29]. It was reported that the surface morphology of the cobalt sulfide depends on its phase. The CoS showed a regular hexagonal shapes whereas CoS_2 nanoparticles were of cubic structure. It was observed that the quantity of thiourea influenced the corresponding morphologies of the CoS nanostructures, but has no effect on their phase structures. Qiu et al have synthesized nanocomposites of CoS_2/reduced graphene oxides (RGO) nanocomposites for charge

storage applications [30]. It was observed through scanning electron microscopy that the size of CoS_2 particles was about 150 nm. The nanocomposites showed an outstanding capacity retention and rate performance. The enhanced electrochemical properties were attributed to the nanosize of CoS_2 and non- agglomeration of CoS_2 in graphene during the charge-discharge processes. Wang et al have fabricated hollow CoS_2 spheres and showed that the hollow spheres of CoS_2 could be used for high energy storage materials [31]. These spheres exhibited a high specific capacity of 850 mAh/g as Li-ion battery anode materials.

Magnetic properties of the CoS_2 octahedrons were studied in zero field cooled and field cooled conditions [32]. Zero field cooled and field cooled magnetic measurements showed the superparamagnetic behavior of the CoS_2 with blocking temperature of about 104 K. The magnetization versus magnetic field measurements further confirmed the superparamagnetic behavior of the CoS_2 above the blocking temperature and ferromagnetic nature below the blocking temperature. These results suggested that the CoS_2 octahedrons were ferromagnetic at low temperature. As it is apparent from the literature survey that the charge storage capacities of cobalt sulfide depends on size, morphology and phase, we present a detailed study of effect of morphology, size and electrolyte on the charge storage capacity of cobalt sulfides.

1.6. Dissertation Organization

This master thesis has been organized under four chapters.

Chapter 1 is dedicated to the introduction of the subject matter and the specific objectives for the research work. It also provides a brief introduction to various kinds of energy storage materials and their advantages.

Chapter 2 provides the experimental details about the synthesis of cobalt sulfides. It presents a comprehensive theoretical background of different techniques used for characterizations of cobalt sulfides.

Subsequently, Chapter 3 is dedicated to the results and discussion of the various experimental techniques used in this research.

Finally, the conclusion of this research work is discussed in Chapter 4.

CHAPTER II

EXPERIMENTAL DETAILS

2.1. Materials and Synthesis

All the reagents used in experiments were of analytical reagent grade and used without further purification. For the synthesis of cobalt sulfides with varying morphologies, cobalt nitrate $Co(NO_3)_2.6H_2O$, thioacetamide (TAA), cetyl trimethylammonium bromide (CTAB), poly (vinyl pyrrolidone) (PVP) and ethylene glycol were used. In typical synthesis, cobalt nitrate dissolved in solvents were added to the thioacetamide solution with or without surfactant. The experimental details are given in Table 2.1. After mixing the compounds with the help of bath sonication for 10 min, the mixed solutions were transferred to a 45 mL Teflon line stainless steel autoclave and heated at 180 ^oC for 12 h. After 12 h of reaction at 180 ^oC, the reactor was cooled to room temperature naturally. The obtained black precipitate at the bottom of the Teflon container was filtered out and washed several time with deionized water followed by isopropanol. The obtained powder was dried at 60 ^oC for 10 h.

2.2. Characterizations

The synthesized materials were characterized using various available techniques such as X-ray diffraction, scanning electron microscopy, electrochemically, vibrating sample magnetometer and X-ray energy dispersive spectrometer. The details for the characterization methods are given below:

Table 2.1: Experimental details for the synthesis of cobalt sulfides.

Sample Name	$Co(NO_3)_2.6H_2O$	TAA	PVP	CTAB	DI water	EG
CS-1	873 mg	450 mg	-	-	36 ml	-
CS-2	873 mg	450 mg	-	-	-	36 ml
CS-3	873 mg	450 mg	-	300 mg	36 ml	-
CS-4	873 mg	450 mg	300 mg	-	36 ml	-
CS-5	873 mg	450 mg	-	300 mg	-	36 ml
CS-6	873 mg	450 mg	300 mg	-	-	36 ml

2.2.1. X-Ray Diffraction

The structure of the synthesized materials was investigated using a Shimadzu X-ray diffractometer using the 2θ-θ scan with $CuK_{\alpha 1}$ (λ=1.5406 Å) radiation. 0.2 mm slits were used for the source and detector sides. A voltage of 40 kV and a current of 30 mA

were used to generate the X-ray. Diffraction patterns in the form of X-ray counts were collected by the detector while the sample was rotated through 2θ = 25° - 70°. An X-ray detector was placed at an angle to satisfy the geometry so that the angle between the atomic planes and the detector is 2θ, as shown in Figure 2.1.

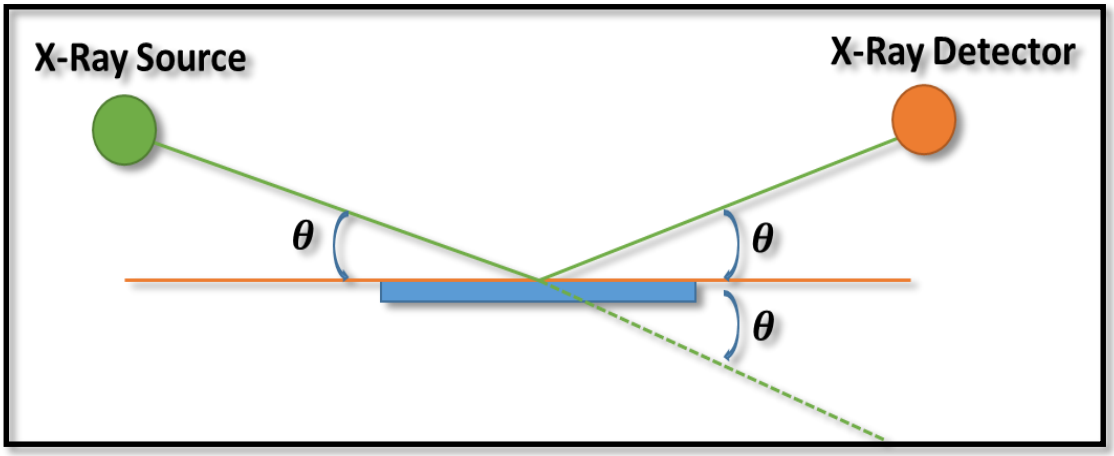

Figure 2.1: Schematic diagram of an X-ray diffractometer.

2.2.2. Scanning Electron Microscopy

The morphologies of the synthesized cobalt sulfide was examined using scanning electron microscopy (SEM). The SEM has been a valuable instrument in the development of scientific theories and has contributed greatly towards the advancement of materials science and other areas. The wide spread use of electron microscopes is based on the fact that they permit the observation and characterization of the materials on a nanometer (nm) to micrometer (μm) scale range. The particle size and morphology of the powder samples were studied using a JEOL JSM-840A scanning electron microscope and an FEI Quanta 200 field emission scanning electron microscopy (FESEM) equipped with an

Oxford INCA 250 silicon drift X-ray energy dispersive spectrometer (EDS). A schematic of a typical scanning electron microscope is shown in Figure 2.2.

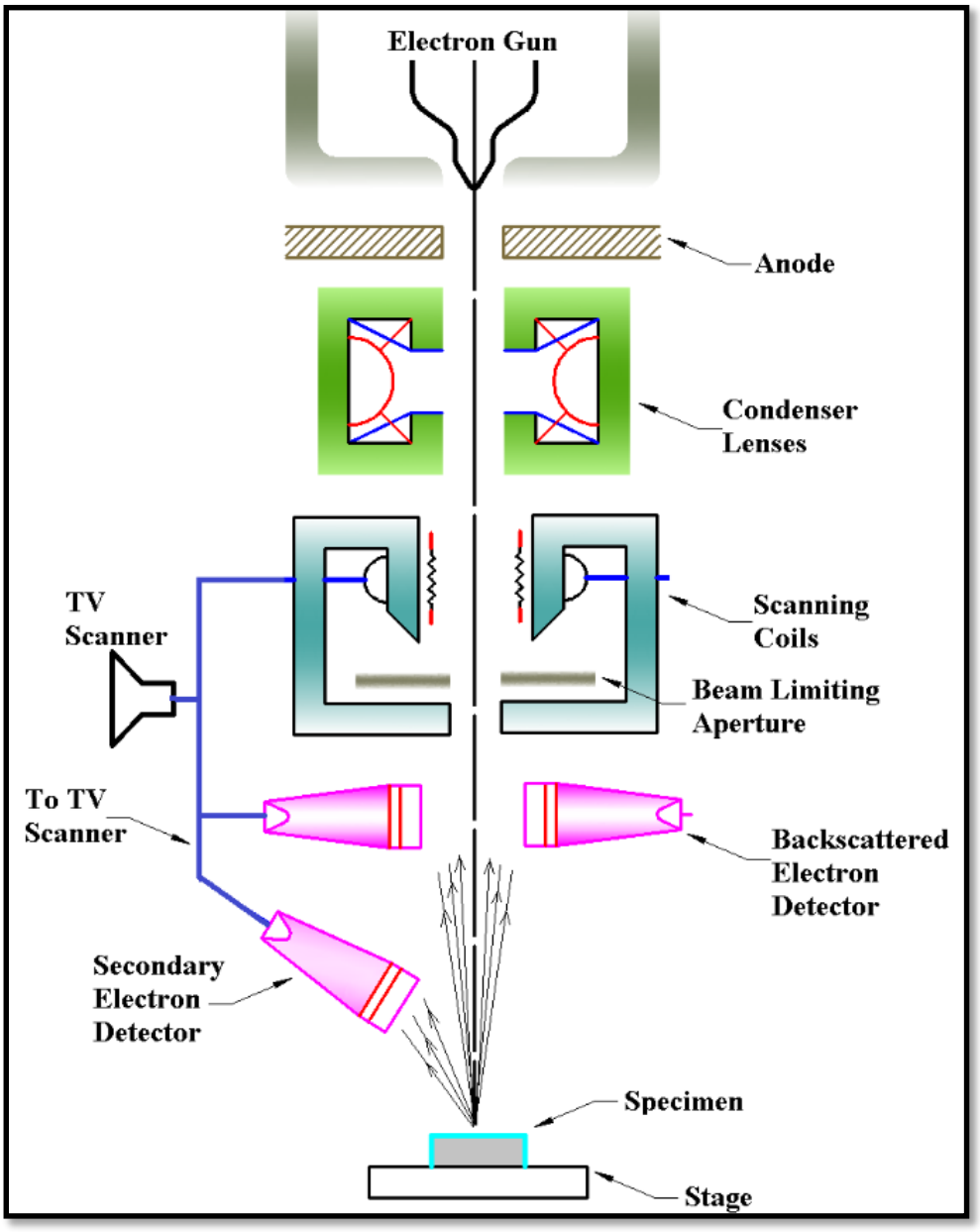

Figure 2.2: Schematics of scanning electron microscope.

2.2.3. Electrochemical Measurements

The electrochemical measurements were performed in a standard three electrode cell containing a platinum wire as a counter electrode, saturated calomel electrode as a reference electrode and as-synthesized CoS_2 on nickel foam as a working electrode. The schematic diagram of the three electrode system is shown in Figure 2.3. Before preparation of the working electrode, the nickel foam was cleaned using HCl, water and acetone successively using ultrasonication. The working electrode was prepared by mixing 80 wt.% of the cobalt sulfide, 10 wt.% of acetylene black and 10 wt.% of polyvinylidenedifluoride (PVdF) in the presence of N-methyl pyrrolidinone (NMP). After mixing the components, the slurry was pasted onto nickel foam. The prepared electrode was dried at 60 °C under vacuum for overnight. An aqueous solution containing 3 M KOH, NaOH and LiOH was used as electrolyte.

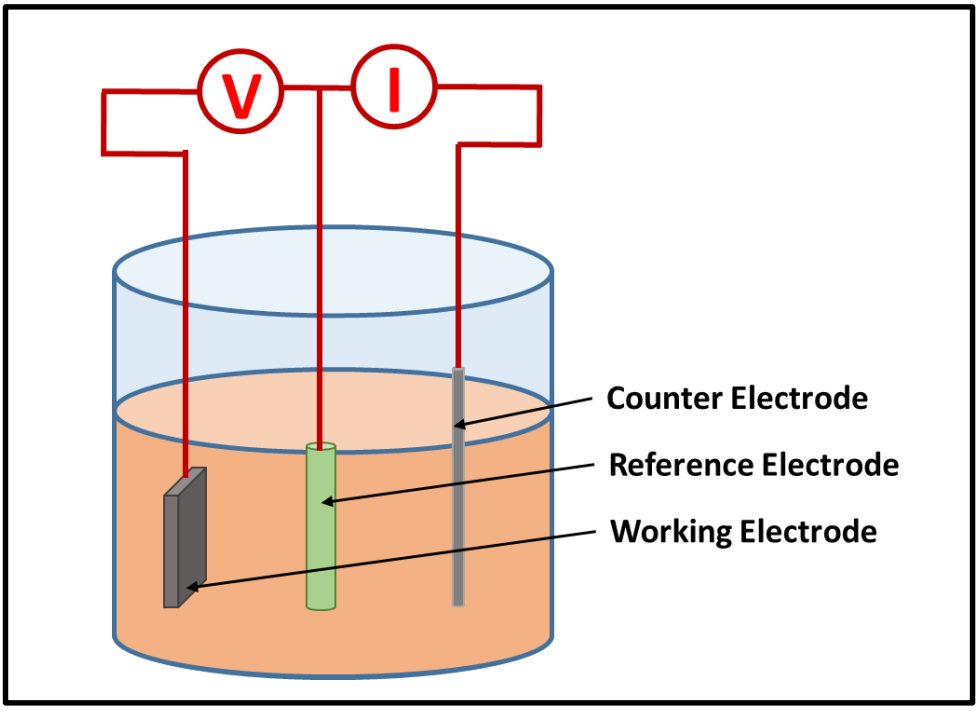

Figure 2.3: Schematic of three cell electrochemical measurement system.

The supercapacitive performance of cobalt sulfides was evaluated by cyclic voltammetry (CV) and galvanostatic charge-discharge measurements. All the electrochemical measurements were performed on a Versastat 4-500 electrochemical workstation (Princeton Applied Research, USA). The electrochemical data was analyzed using VersaStudio software provided by Princeton Applied Research.

A quasi-solid state supercapacitor was fabricated using these electrodes. The device was assembled by sandwiching ion transporting layer (Celgard, 25μm thick, 39% porosity) between two cobalt sulfide electrodes. 3M NaOH was used as an electrolyte for this assembly. The schematic diagram of the quasi-solid state supercapacitor is given in Figure 2.4. The charge storage capacity of the device was evaluated using cyclic voltammetry (CV) and galvanostatic charge-discharge measurements. We have studied the effect of temperature on the electrochemical properties of the device for its application in harsh conditions. The electrochemical impedance spectroscopy was used to further evaluate electrochemical properties of the device. All the electrochemical impedance measurements were performed in frequency range of 0.05Hz to 10,000 Hz.

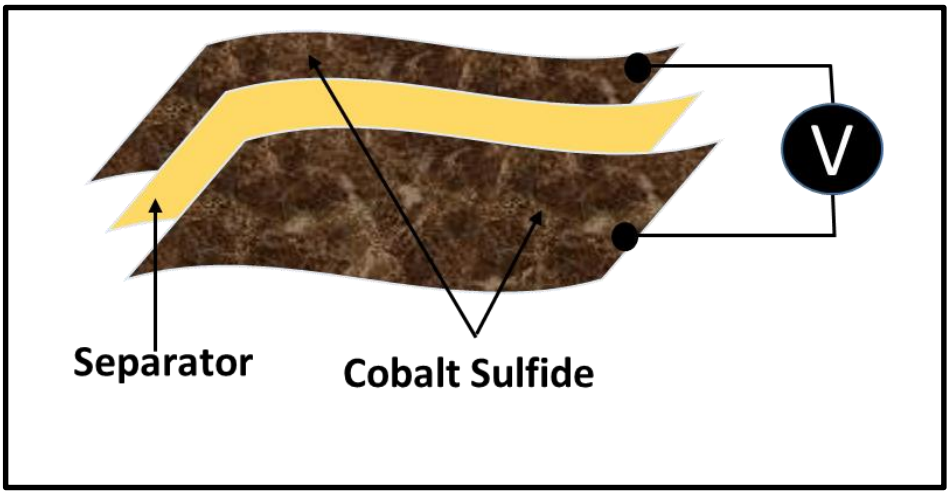

Figure 2.4: Schematic diagram of a quasi-solid state supercapacitor device.

2.2.4. Magnetic Measurements

Magnetic measurements were performed using a Quantum Design vibrating sample magnetometer (VSM). A VSM is a very sensitive magnetic characterization technique for characterizing magnetic materials when a high detection sensitivity is needed over a broad temperature range. The magnetic properties of the cobalt sulfide were investigated as a function of temperature and applied magnetic field. The temperature dependence magnetization (M *vs.* T) was studied under field cool. The field cool measurements were performed while cooling the cobalt sulfide from room temperature to 10 K under an applied external magnetic field. The magnetic nature of the cobalt sulfide was also studied using magnetic field dependence magnetization (M *vs.* H). The M *vs.* H nature of the cobalt sulfide was studied at various temperatures to better understand its magnetic properties at various temperatures.

CHAPTER III

RESULTS AND DISCUSSION

3.1. X-Ray Diffraction Analysis

The X-ray diffraction (XRD) patterns of all the samples were recorded in the two-theta range of 25-70 degree. The XRD patterns of the samples grown under different conditions are shown in Figures 3.1-3.6. As seen in the XRD patterns, all the samples show several diffraction peaks suggesting high crystalline nature of the synthesized cobalt sulfide. The diffraction peaks of all the cobalt sulfides samples can be indexed to the standard diffraction data of CoS (JCPDS no. 65-3418) and CoS_2 (JCPDS no. 65-3322).

The XRD patterns of the cobalt sulfides were used to estimate the crystallite size of the synthesized cobalt sulfide. The average crystalline size (t) of all the samples was calculated using the Debye Scherrer equation [33]:

$$t = \frac{0.9\,\lambda}{\beta\,cos\theta}$$

where λ is the X-ray wavelength, β is the full width at half maximum of the diffraction line, and θ is the diffraction angle of the XRD spectra. The average crystalline size of all the samples are given in Table 3.1.

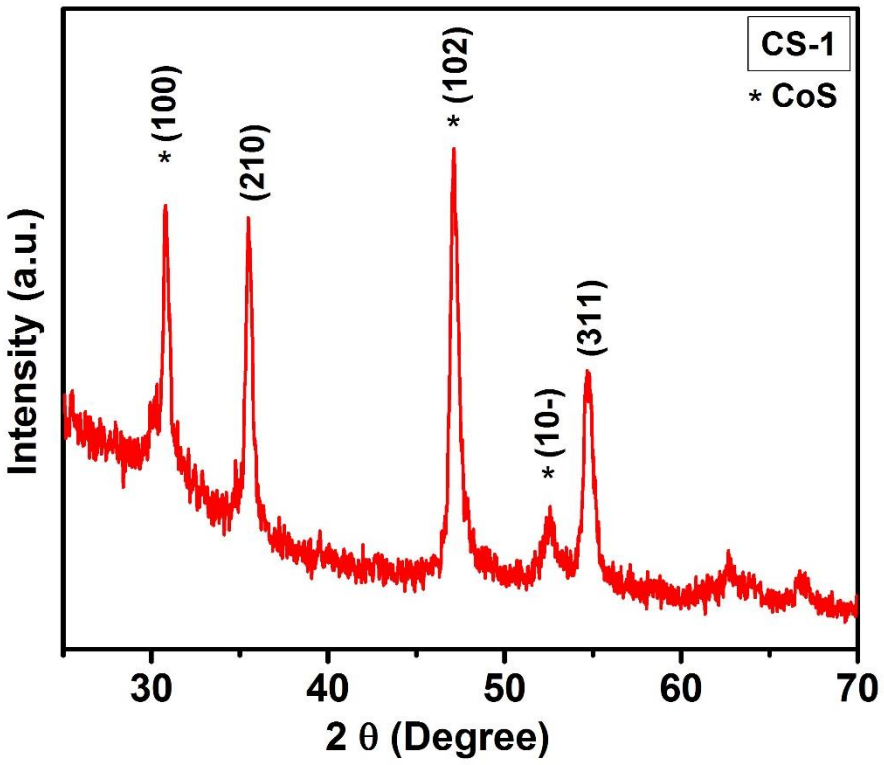

Figure 3.1: XRD patterns of CS-1.

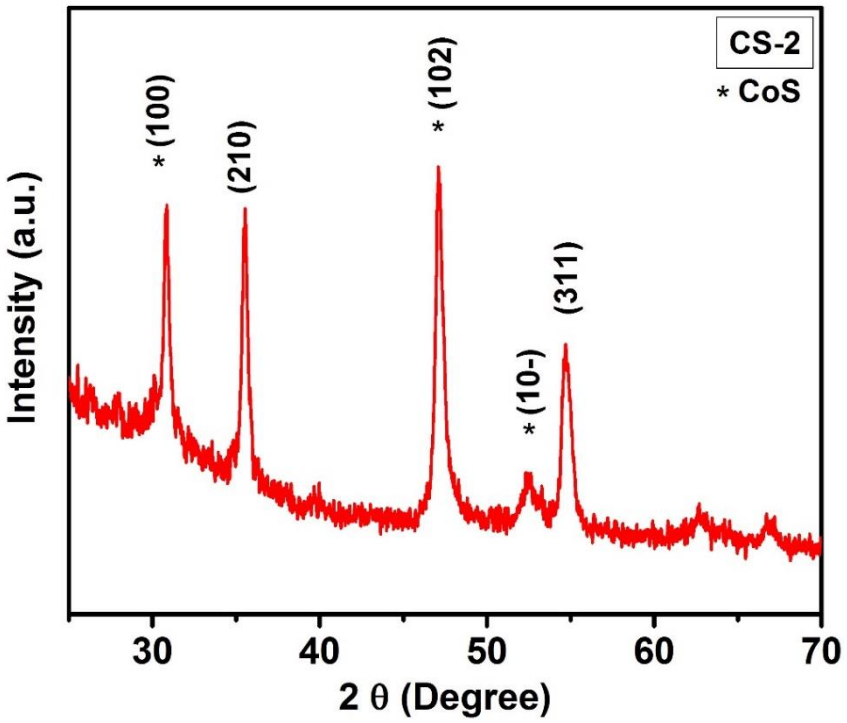

Figure 3.2: XRD patterns of CS-2.

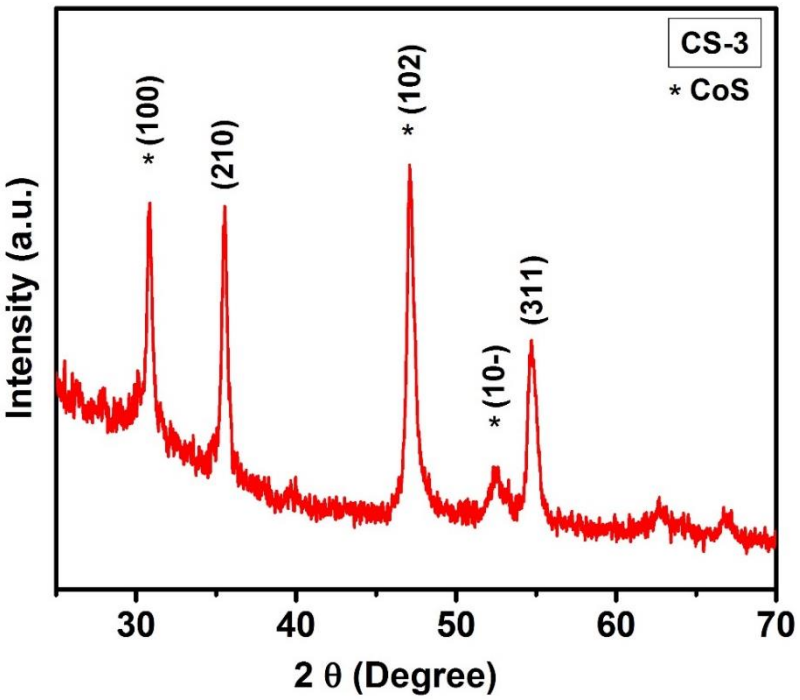

Figure 3.3: XRD patterns of CS-3.

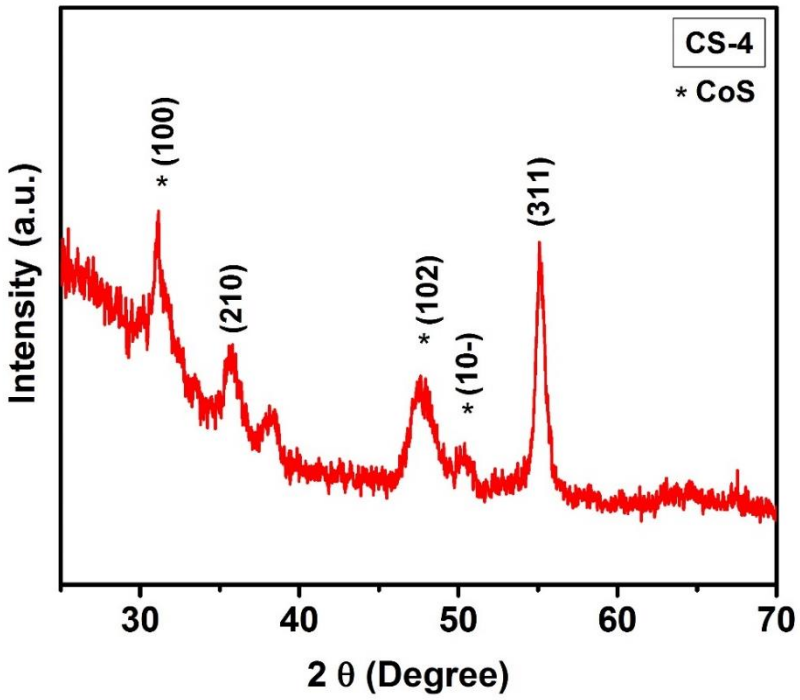

Figure 3.4: XRD patterns of CS-4.

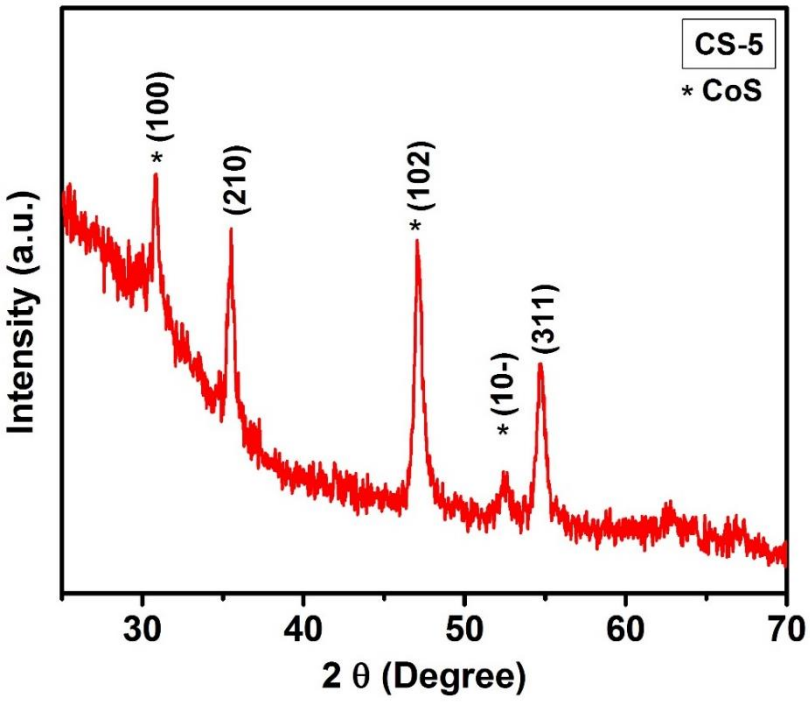

Figure 3.5: XRD patterns of CS-5.

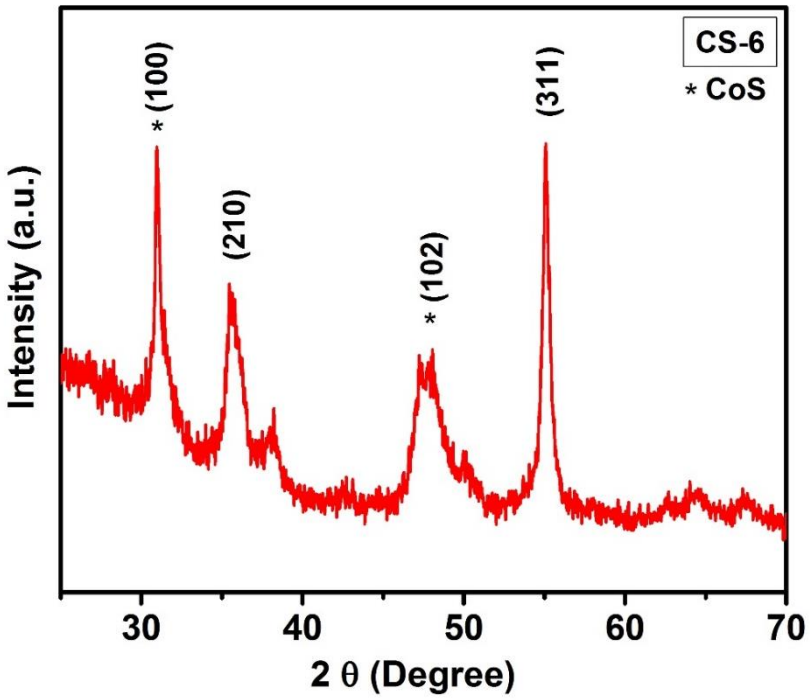

Figure 3.6: XRD patterns of CS-6.

Table 3.1: Crystalline size of the synthesized cobalt sulfides.

Sample	FWHM (Degree)	FWHM (Radian)	Crystallite Size (nm)
CS-1	0.58	0.010	18.2
CS-2	0.66	0.012	16.9
CS-3	0.63	0.011	17.3
CS-4	0.63	0.011	17.3
CS-5	0.56	0.010	18.6
CS-6	0.49	0.009	20.4

Xing et al [28] have synthesized octahedron-shaped CoS_2 crystals using a hydrothermal route without any surfactant or template. These octahedral structures were highly uniform with a mean edge length of about 360 nm and with a high geometric symmetry. The XRD patterns of the synthesized material shows CoS_2 phase. On the other hand, Kim et al have used spray deposition technique to fabricate cobalt sulfide [34]. The structural analysis using XRD revealed that the cobalt sulfide contained mixed phases. It was observed that CoS was the major phase while Co_9S_8, Co_3S_4, and CoS_2 were minor phases. A facile solvothermal route used for the synthesis of cobalt sulfide yielded multiple phases of cobalt sulfide such as CoS_2, CoS and Co_9S_8 [25]. Since all phases of cobalt sulfide participate in redox reaction and thus in charge storage, it is not very crucial to have phase pure cobalt sulfide for supercapacitor applications.

3.2. Scanning Electron Microscopic Analysis

The morphology and structure of the cobalt sulfides were investigated using field emission scanning electron microscopy (FE-SEM). The FE-SEM images of all the samples at various magnifications are shown in Figures 3.7-3.12. As seen in these SEM images, the morphology and the size of the cobalt sulfides are highly dependent on the growth conditions.

Elemental analysis of all the samples were performed using energy-dispersive X-ray spectrometer (EDS). The EDS pattern of some of the samples are shown in Figure 3.13. The EDS pattern shows the presence of Co and S. The relative concentration ratio of Co and S confirms the CoS and CoS_2 phases.

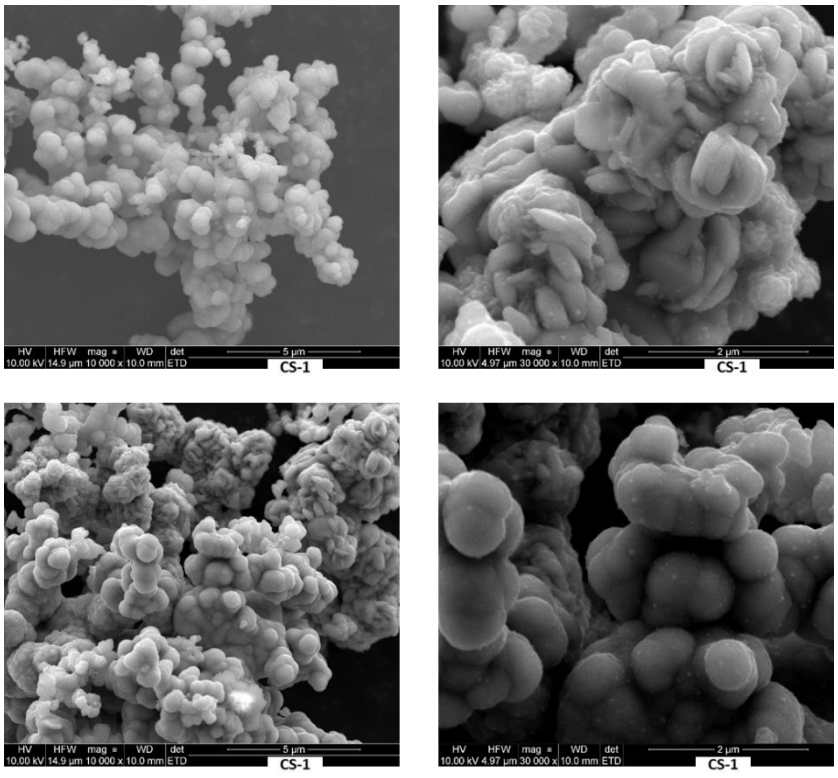

Figure 3.7: SEM images of CS-1 at various magnifications.

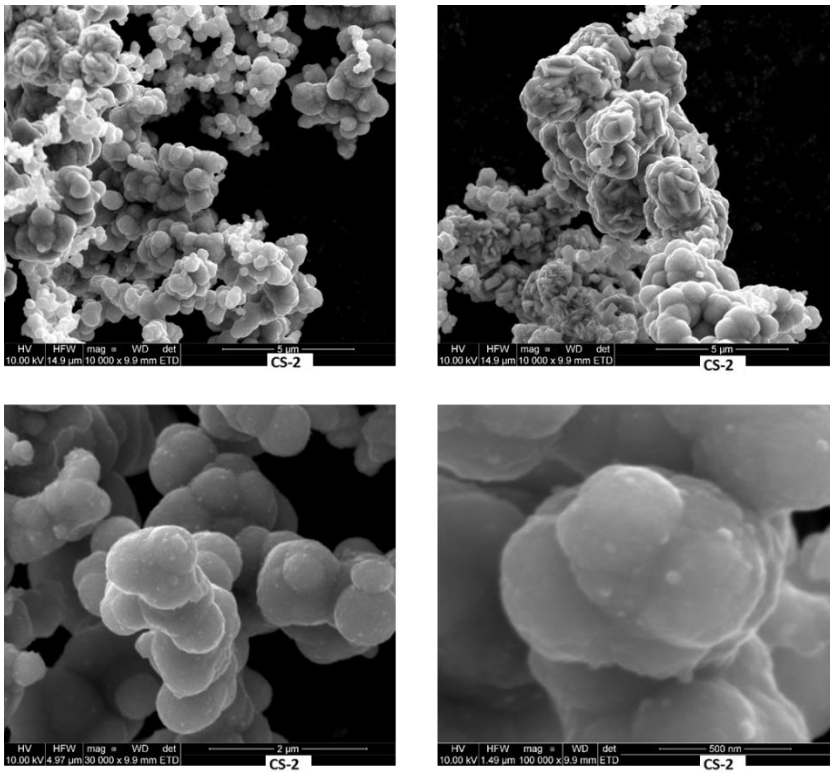

Figure 3.8: SEM images of CS-2 at various magnifications.

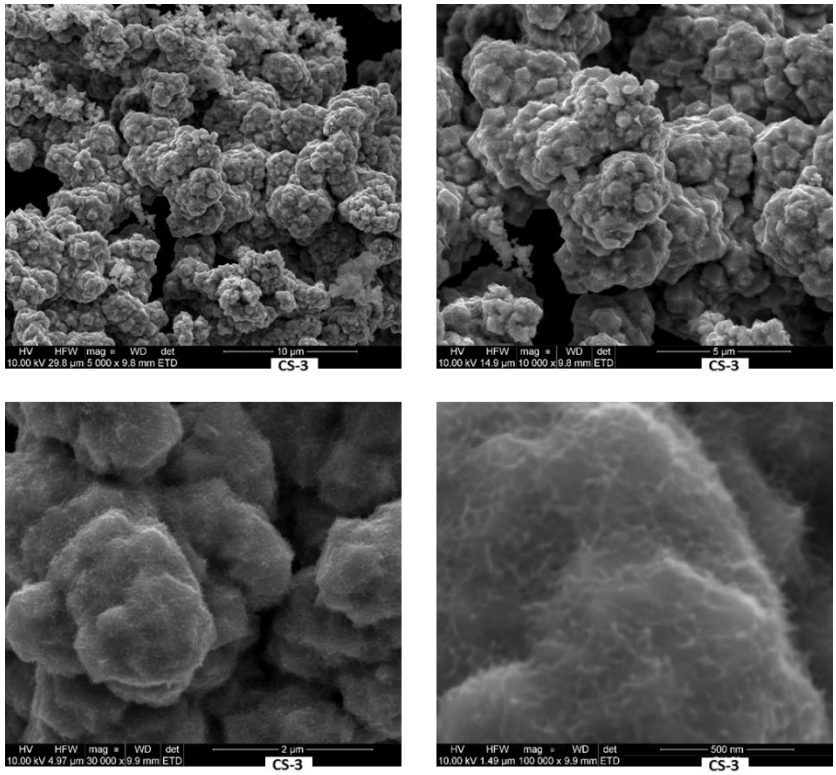

Figure 3.9: SEM images of CS-3 at various magnifications.

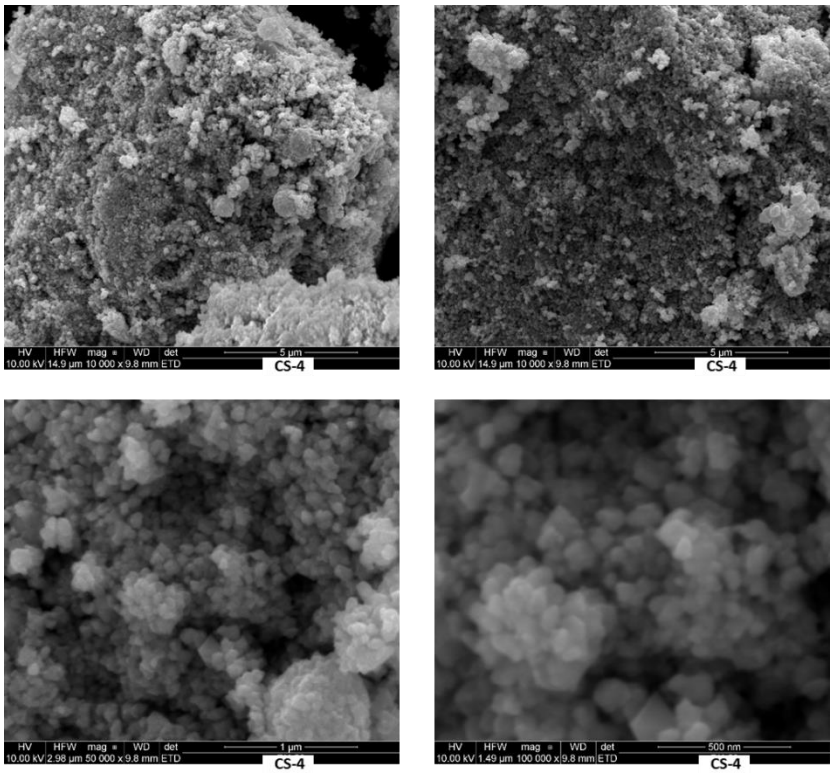

Figure 3.10: SEM images of CS-4 at various magnifications.

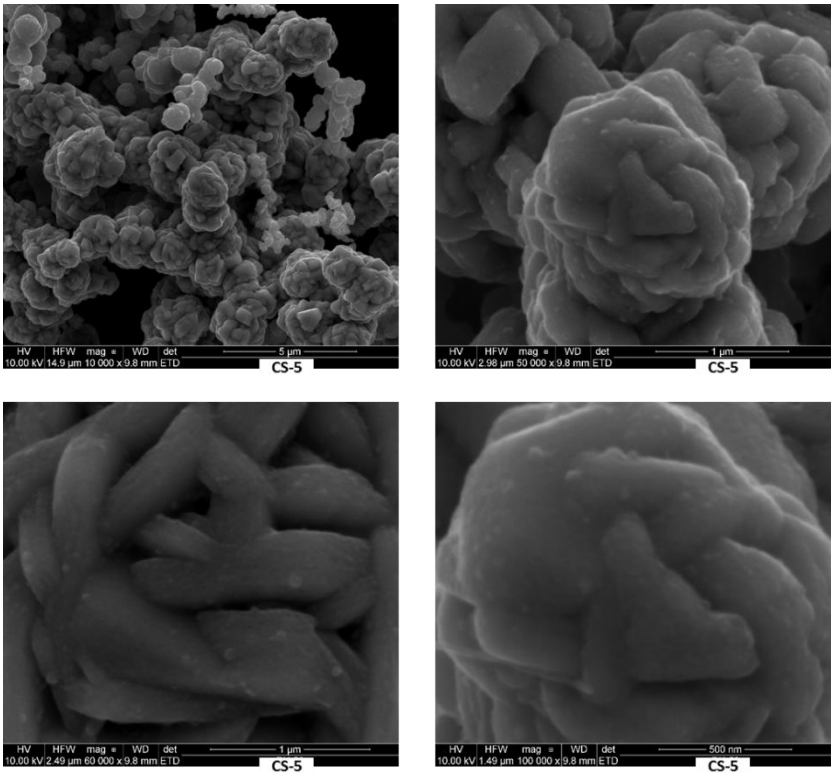

Figure 3.11: SEM images of CS-5 at various magnifications.

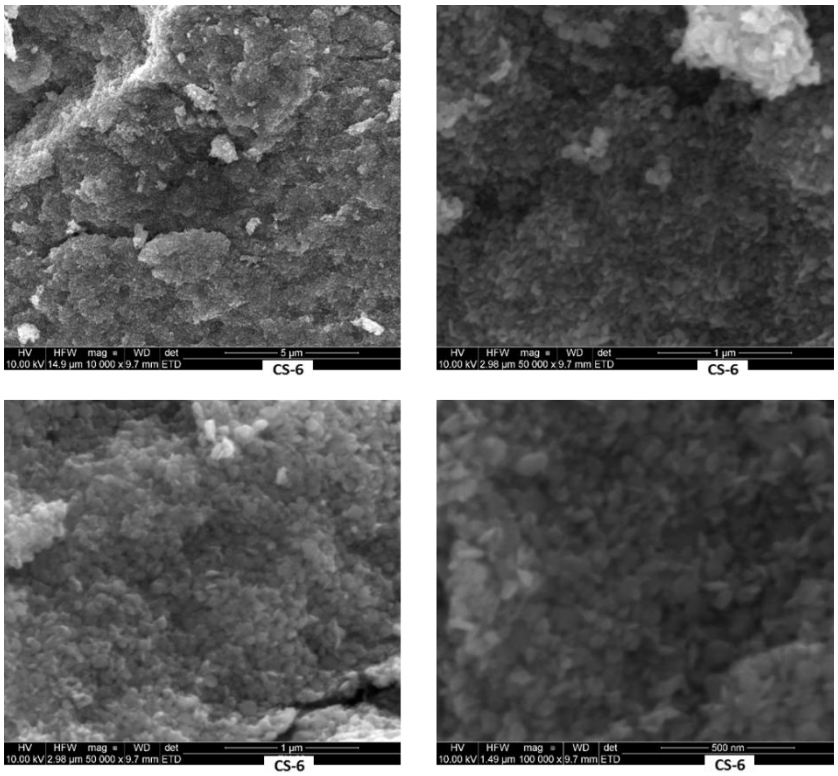

Figure 3.12: SEM images of CS-6 at various magnifications.

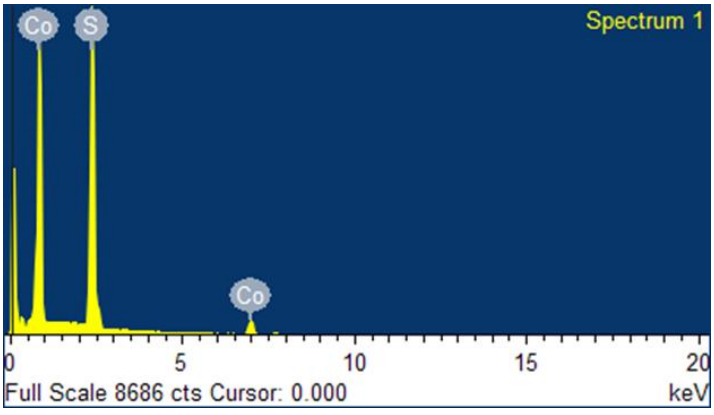

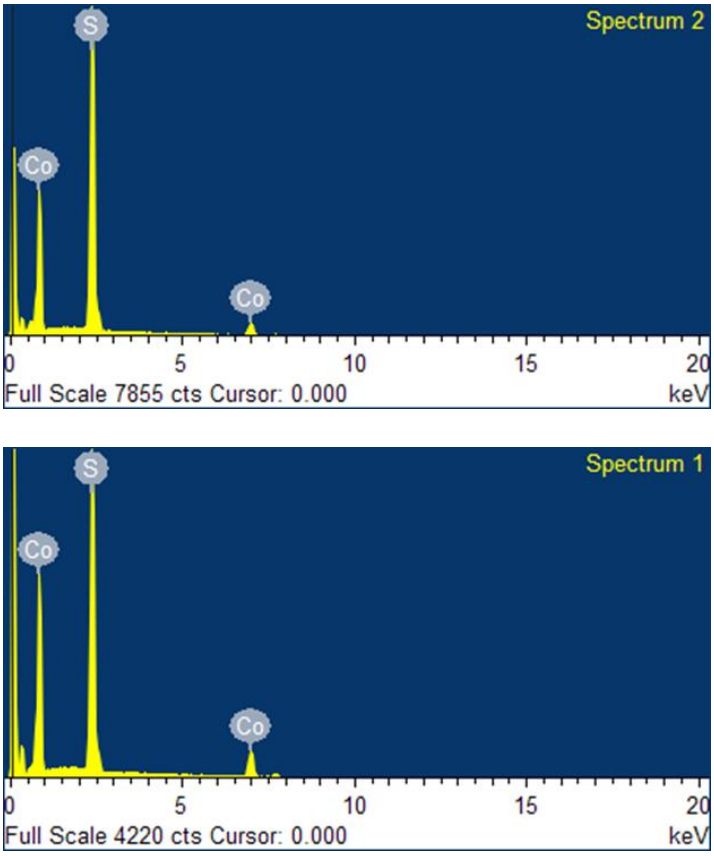

Figure 3.13: EDX images of CS-1 (Top image), CS-3 (Middle image) and CS-6 (Bottom image) (Y-axis is count).

3.3. Electrochemical Characterizations

The electrochemical properties of the synthesized cobalt sulfides were studied using cyclic voltammetry and galvanostatic charge-discharge measurements. The effect of morphologies and electrolytes on the electrochemical properties were investigated in detail. Three different electrolytes such as 3M LiOH, NaOH and KOH were used for the electrochemical measurements. Figures 3.14-3.16 shows the cyclic voltammograms of CS-1 sample in different electrolytes at various scan rates. As evident from the cyclic voltammograms, the cyclic voltammograms of the cobalt sulfide are different from that

of electrical double layer capacitor. The cyclic voltammograms of the electrical double layer capacitors are usually rectangular in shape. The shape and nature of the cyclic voltammograms of the cobalt sulfide electrode suggest that the capacitance is mainly due to pseudocapacitance. The cyclic voltammograms of the cobalt sulfide shows a pair of redox peak in oxidation and reduction process. The mechanism for such redox process in cobalt sulfide based electrode in alkaline aqueous electrolytes could be explained by the following reaction:

$$CoS_2 + OH^- \leftrightarrow CoS_2 - OH + e^-$$

The specific capacitance of the cobalt sulfide electrode was calculated using data from the cyclic voltammetric measurements. The specific capacitance (C_{sp}) of the cobalt sulfide electrode was calculated using the following expression [35]

$$C_{sp} = \frac{Q}{\Delta V \times (\frac{\partial v}{\partial t}) \times m}$$

where Q is the area under the CV curve, $\partial v/\partial t$ is the scan rate, ΔV is the potential window and m is the mass of the cobalt sulfide. The variation of specific capacitance as a function of scan rate in different electrolytes is shown in Figure 3.17. The specific capacitance was observed to be decreasing with increasing scan rate in all the studied electrolytes. The decrease in the specific capacitance with increasing scan rate could be due to insufficient time for the redox reaction at electrode. At a higher scan rate, the concentration of the ions at the electrode/electrolyte interface increases rapidly and the diffusion rate of electrolyte from electrode/electrolyte interface to electrode will be not

enough to satisfy the electrochemical reactions [36]. Specific capacitance not only depends on scan rate but also on the type of electrolyte used. The highest specific capacitance was observed in KOH electrolyte. The maximum specific capacitance of 694 F/g was calculated for CS-1 sample in 3M NaOH electrolyte at scan rate of 5 mV/s.

Figure 3.17 through Figure 3.37 shows the cyclic voltammograms and variation of specific capacitance as a function of scan rate for the rest of the cobalt sulfide samples (CS-2 to CS-6). The cyclic voltammograms of all the samples show the pseudocapacitive behavior of cobalt sulfide samples with presence of a pair of redox peaks during reduction and oxidation process. Among all the samples, CS-6 sample shows the highest specific capacitance of 702 F/g in 3M NaOH electrolyte.

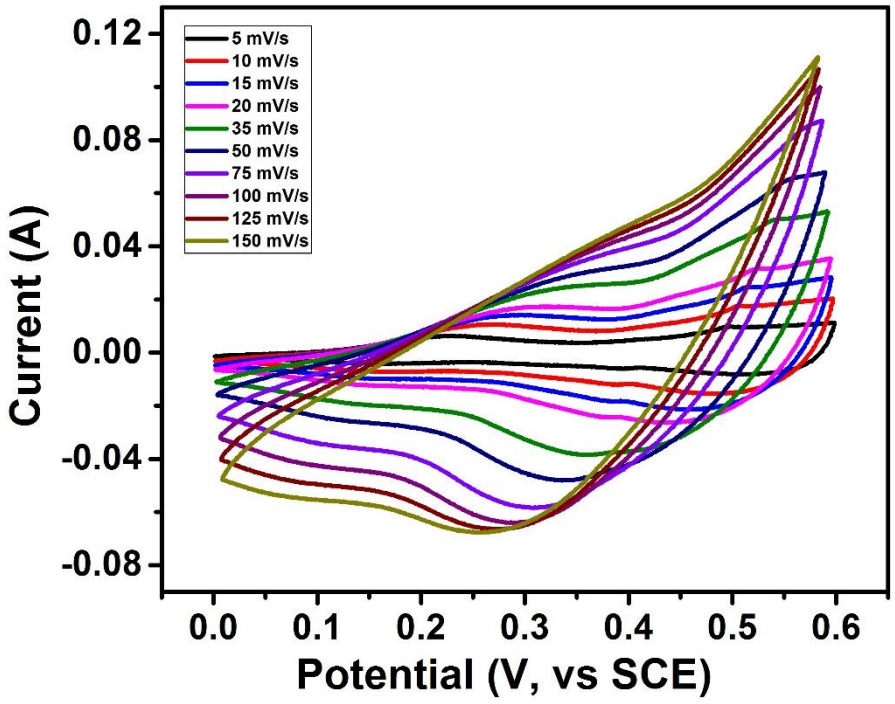

Figure 3.14: Cyclic voltammograms of CS-1 sample at various scan rates in 3 M LiOH electrolyte.

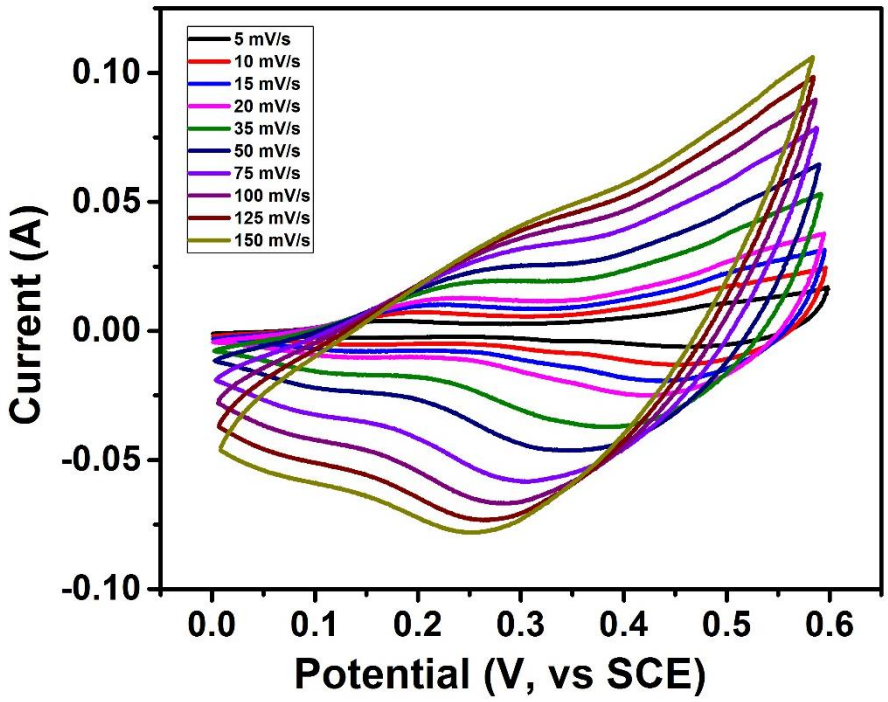

Figure 3.15: Cyclic voltammograms of CS-1 sample at various scan rates in 3 M NaOH electrolyte.

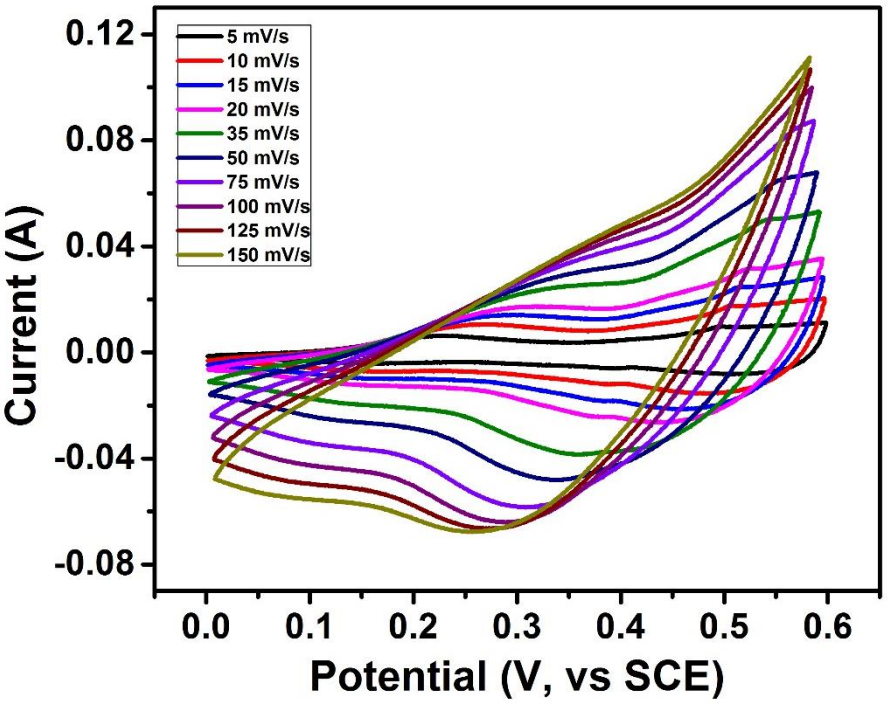

Figure 3.16: Cyclic voltammograms of CS-1 sample at various scan rates in 3 M KOH electrolyte.

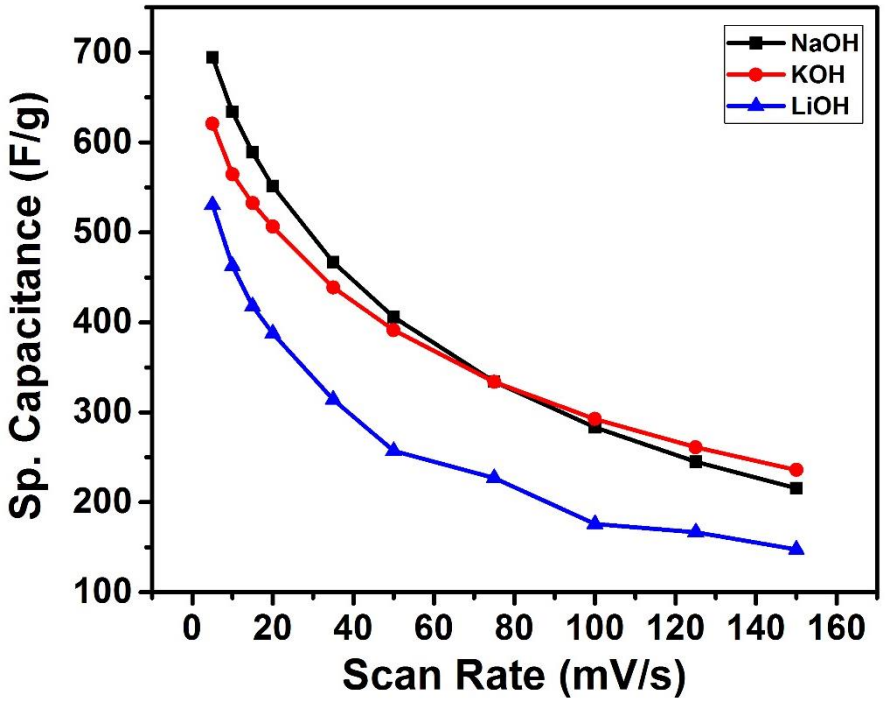

Figure 3.17: Variation of specific capacitance as a function of scan rate for CS-1 sample in different electrolytes.

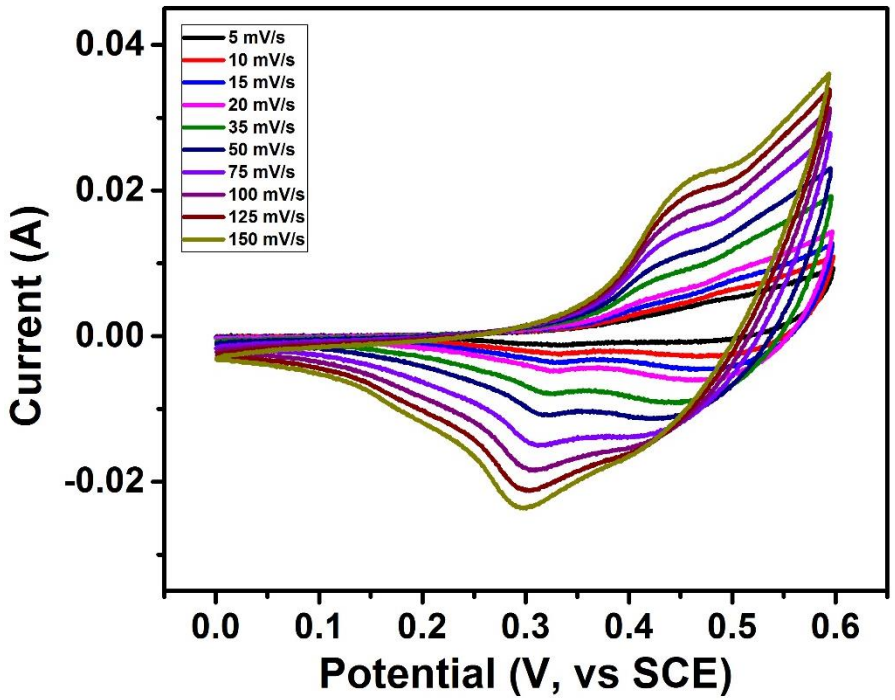

Figure 3.18: Cyclic voltammograms of CS-2 sample at various scan rates in 3 M LiOH electrolyte.

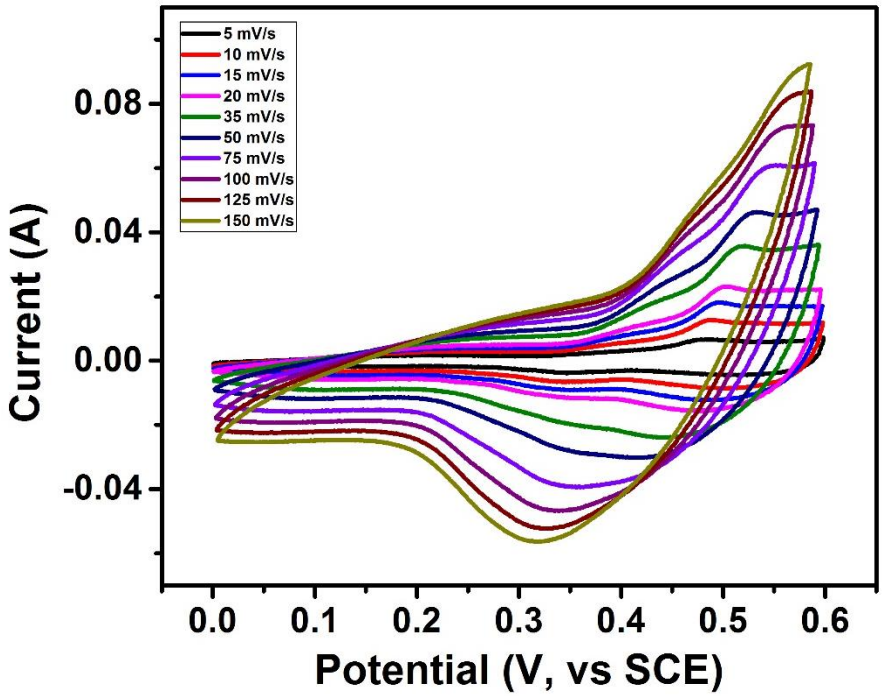

Figure 3.19: Cyclic voltammograms of CS-2 sample at various scan rates in 3 M NaOH electrolyte.

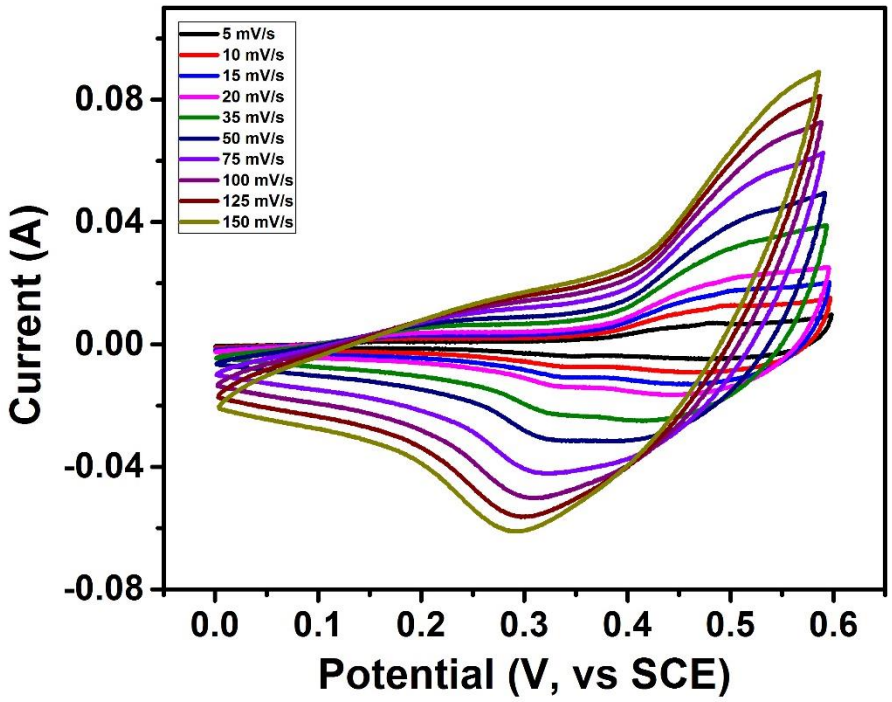

Figure 3.20: Cyclic voltammograms of CS-2 sample at various scan rates in 3 M KOH electrolyte.

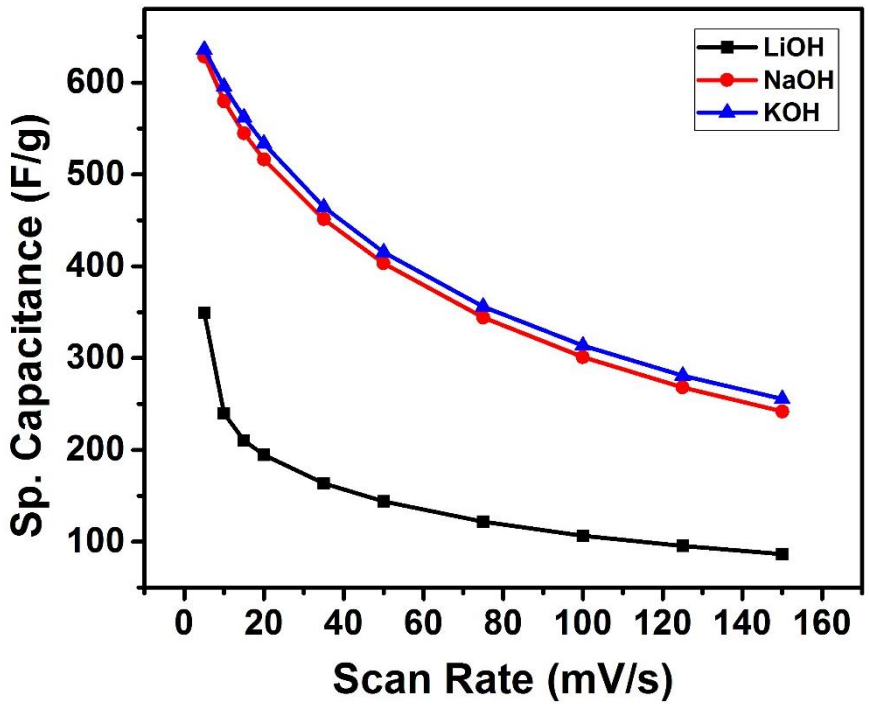

Figure 3.21: Variation of specific capacitance as a function of scan rate for CS-2 sample in different electrolytes.

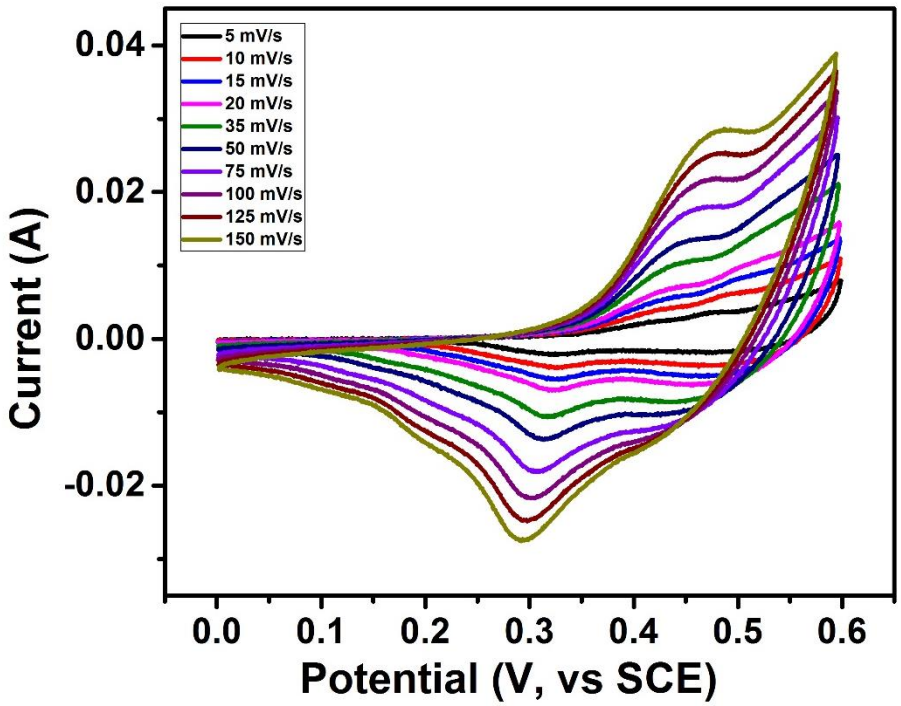

Figure 3.22: Cyclic voltammograms of CS-3 sample at various scan rates in 3 M LiOH electrolyte.

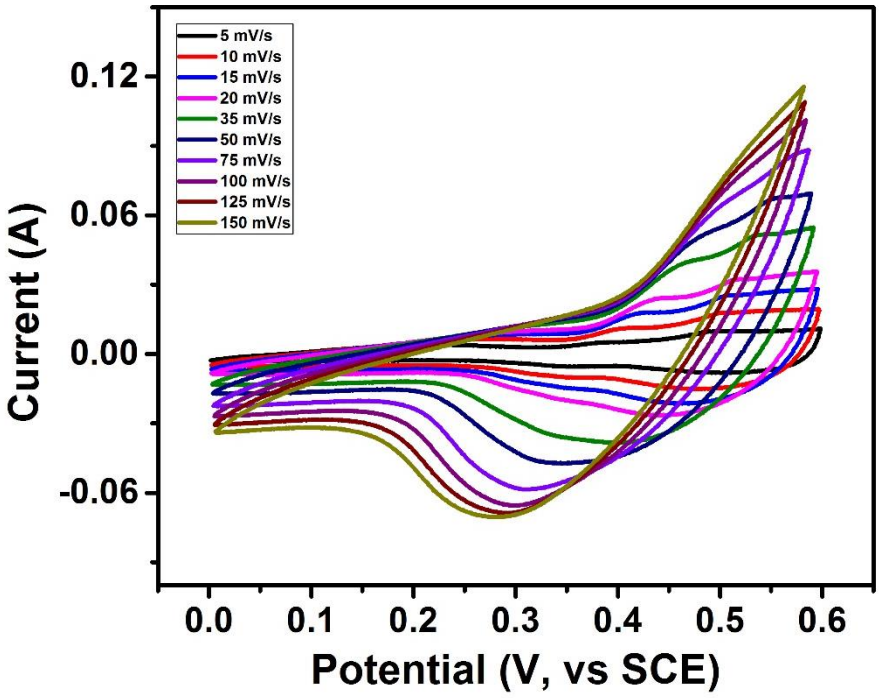

Figure 3.23: Cyclic voltammograms of CS-3 sample at various scan rates in 3 M NaOH electrolyte.

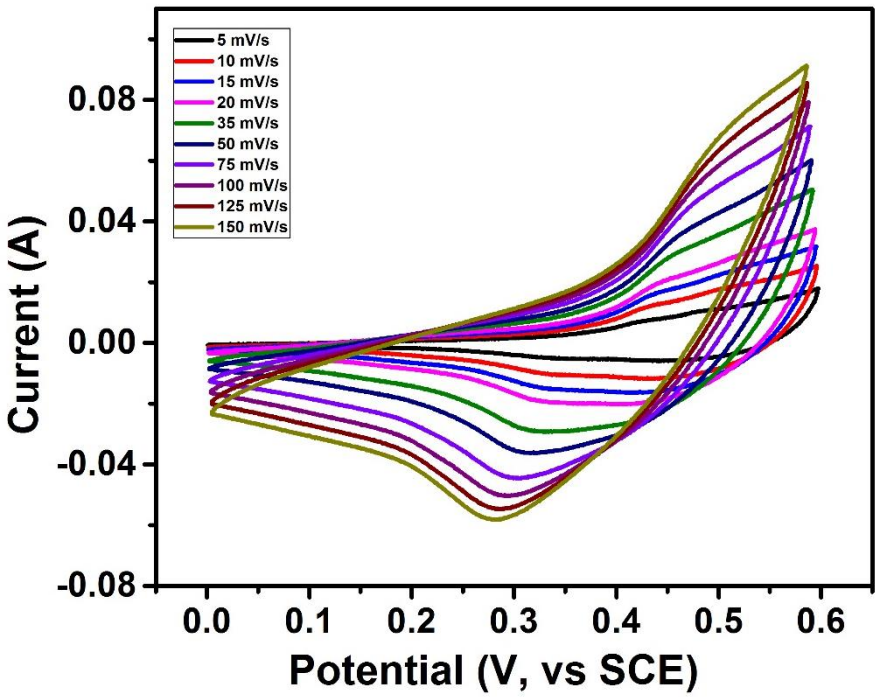

Figure 3.24: Cyclic voltammograms of CS-3 sample at various scan rates in 3 M KOH electrolyte.

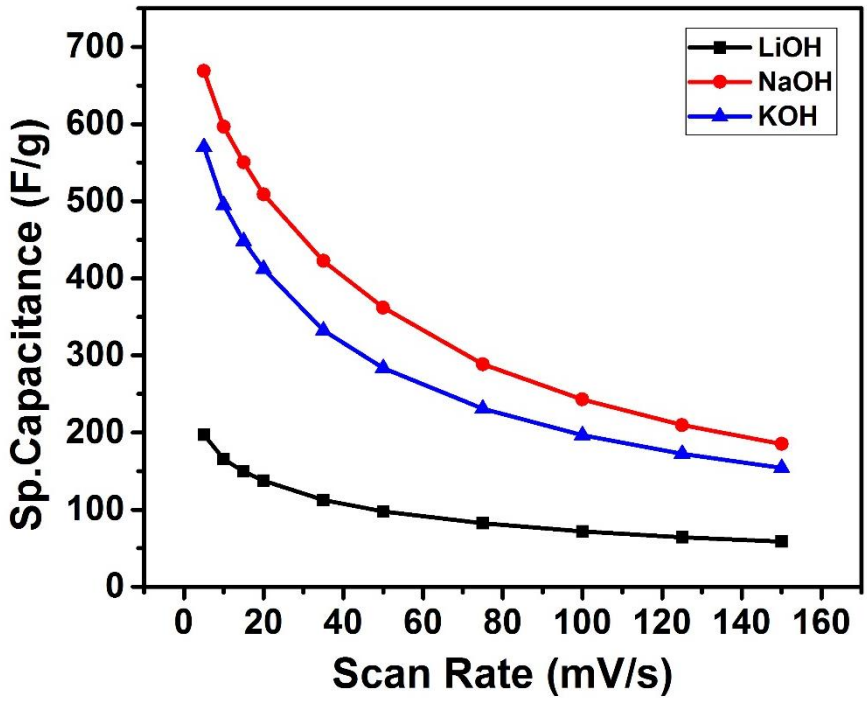

Figure 3.25: Variation of specific capacitance as a function of scan rate for CS-3 sample in different electrolytes.

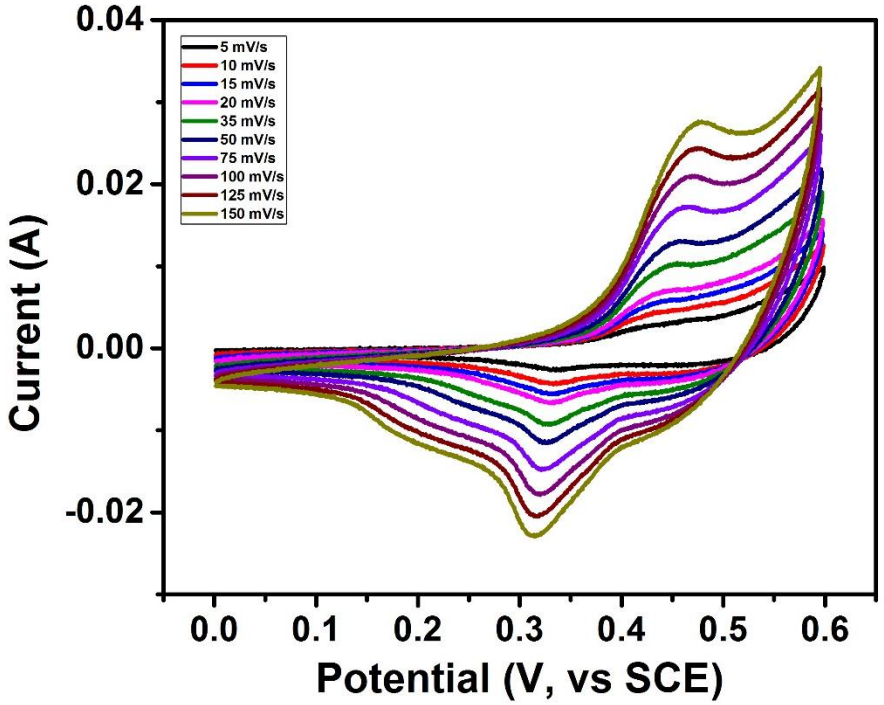

Figure 3.26: Cyclic voltammograms of CS-4 sample at various scan rates in 3 M LiOH electrolyte.

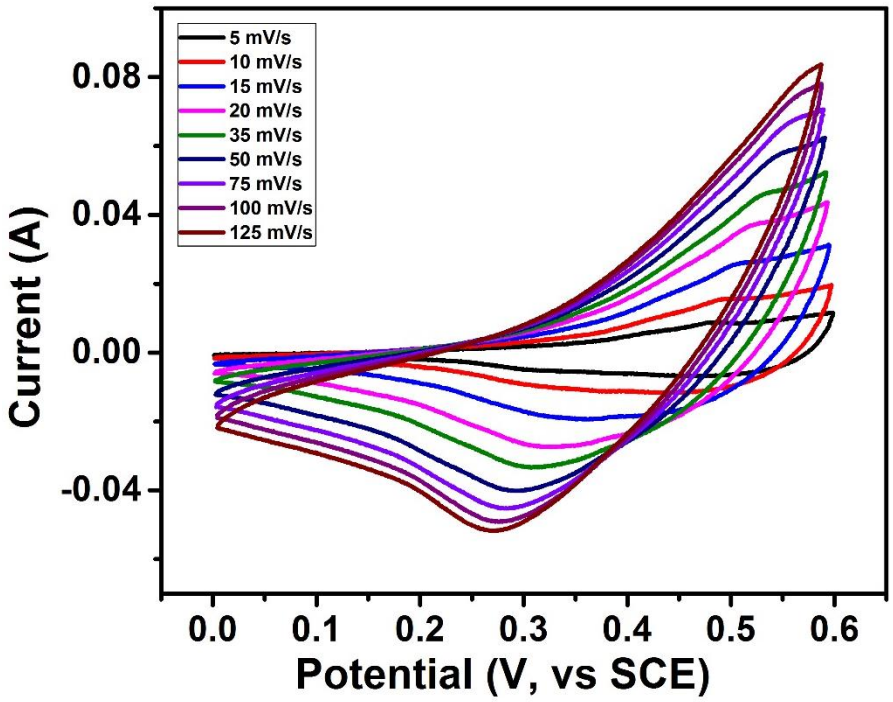

Figure 3.27: Cyclic voltammograms of CS-4 sample at various scan rates in 3 M NaOH electrolyte.

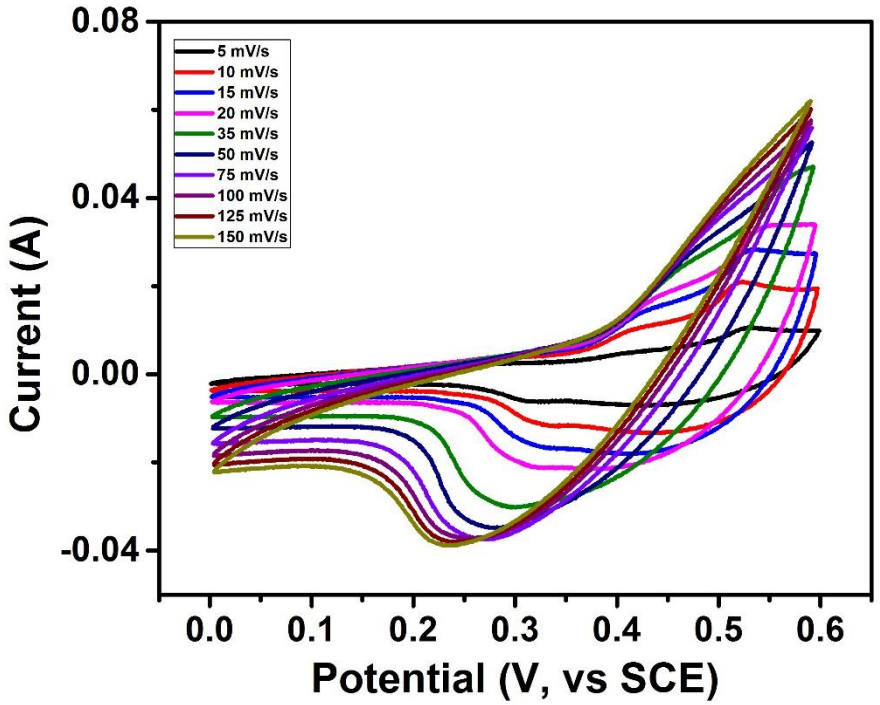

Figure 3.28: Cyclic voltammograms of CS-4 sample at various scan rates in 3 M KOH electrolyte.

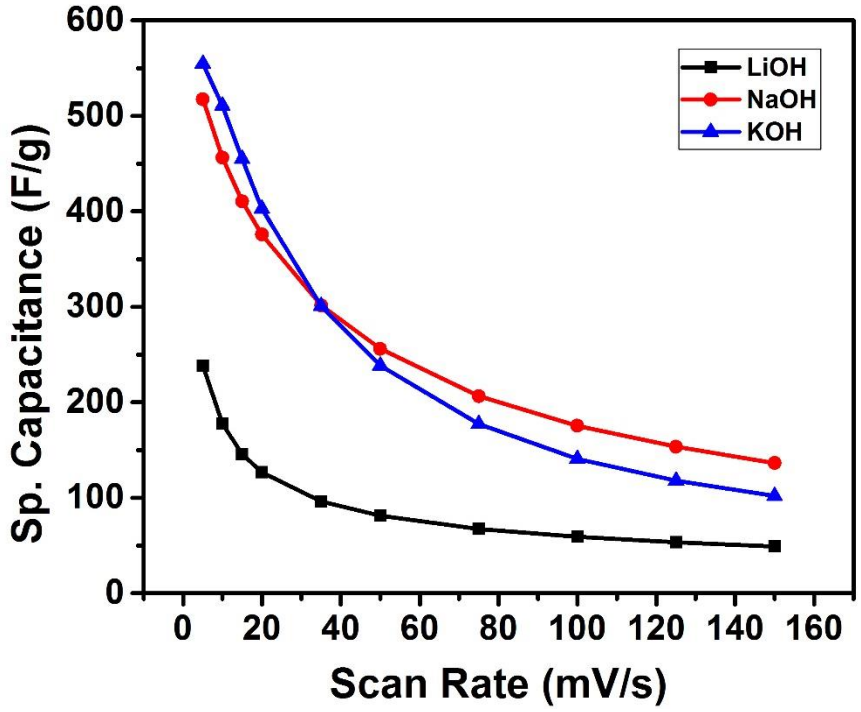

Figure 3.29: Variation of specific capacitance as a function of scan rate for CS-4 sample in different electrolytes.

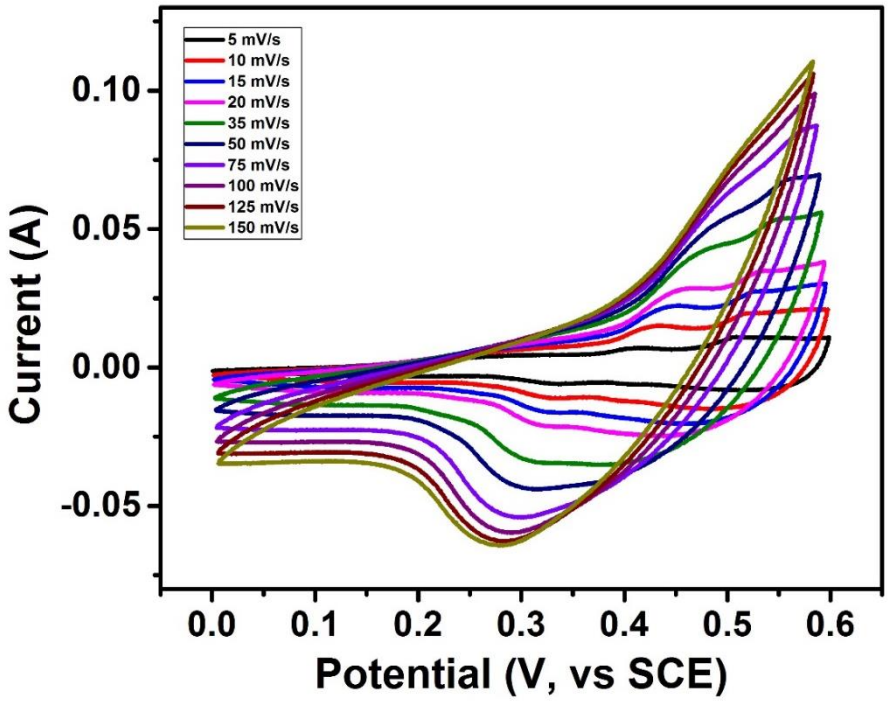

Figure 3.30: Cyclic voltammograms of CS-5 sample at various scan rates in 3 M LiOH electrolyte.

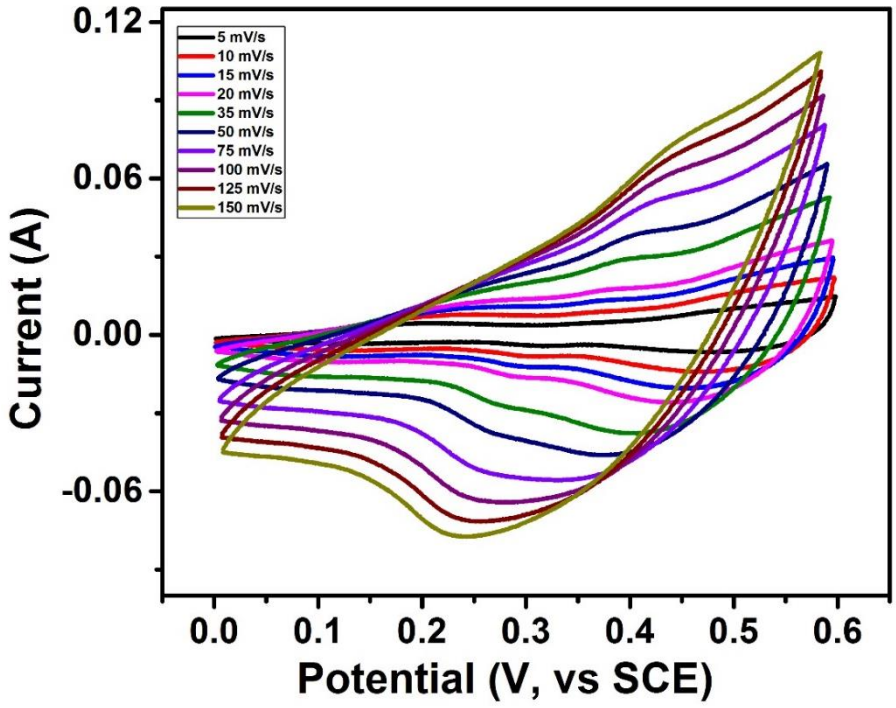

Figure 3.31: Cyclic voltammograms of CS-5 sample at various scan rates in 3 M NaOH electrolyte.

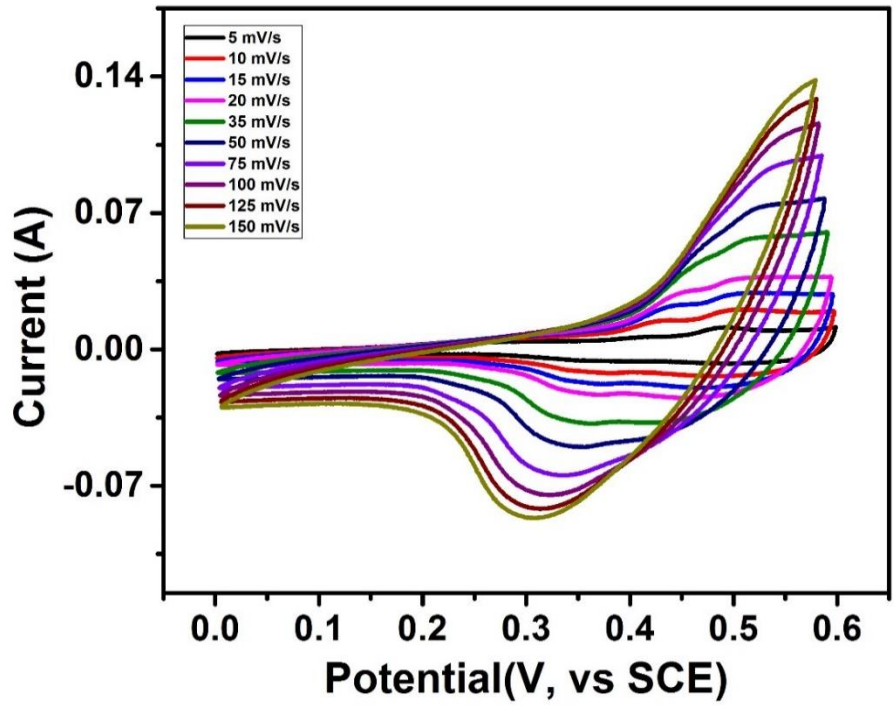

Figure 3.32: Cyclic voltammograms of CS-5 sample at various scan rates in 3 M KOH electrolyte.

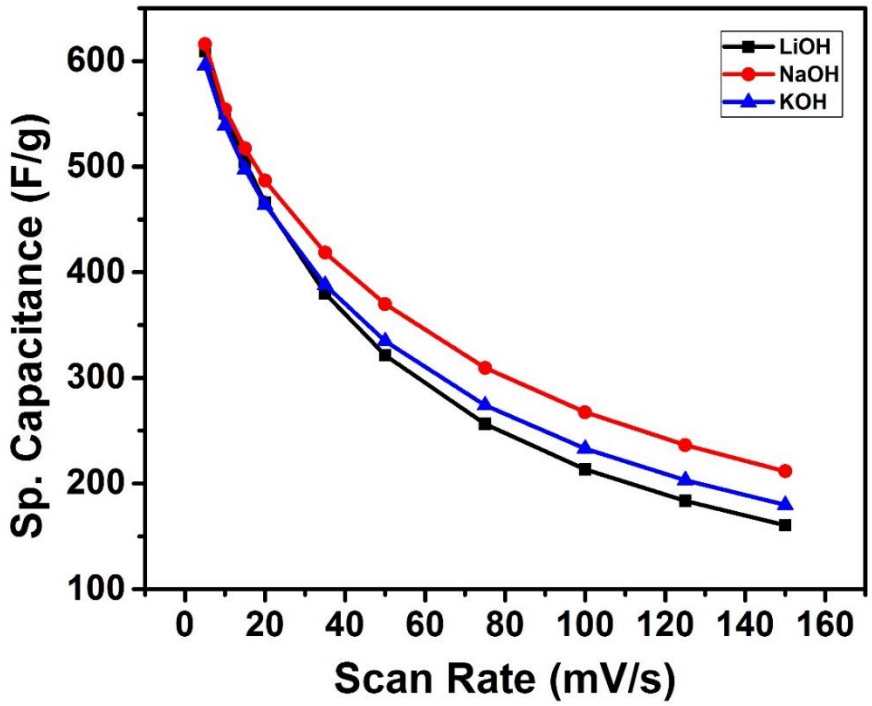

Figure 3.33: Variation of specific capacitance as a function of scan rate for CS-5 sample in different electrolytes.

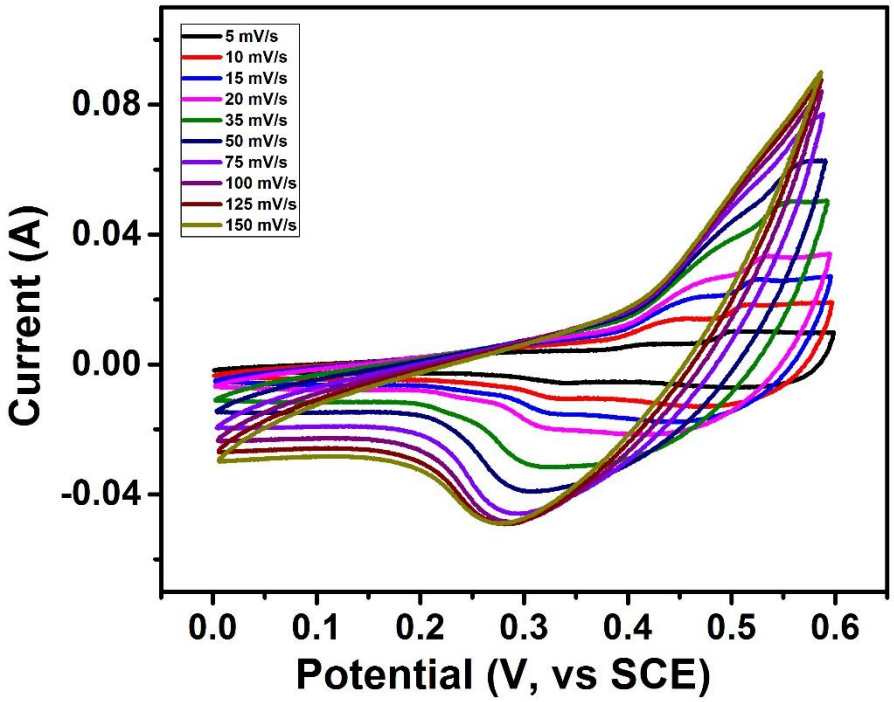

Figure 3.34: Cyclic voltammograms of CS-6 sample at various scan rates in 3 M LiOH electrolyte.

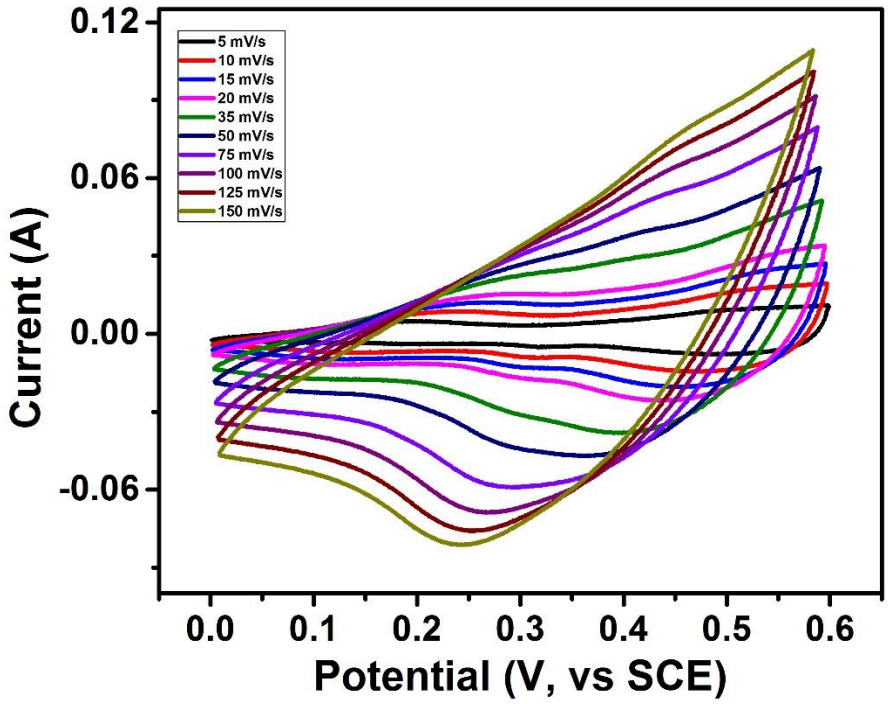

Figure 3.35: Cyclic voltammograms of CS-6 sample at various scan rates in 3 M NaOH electrolyte.

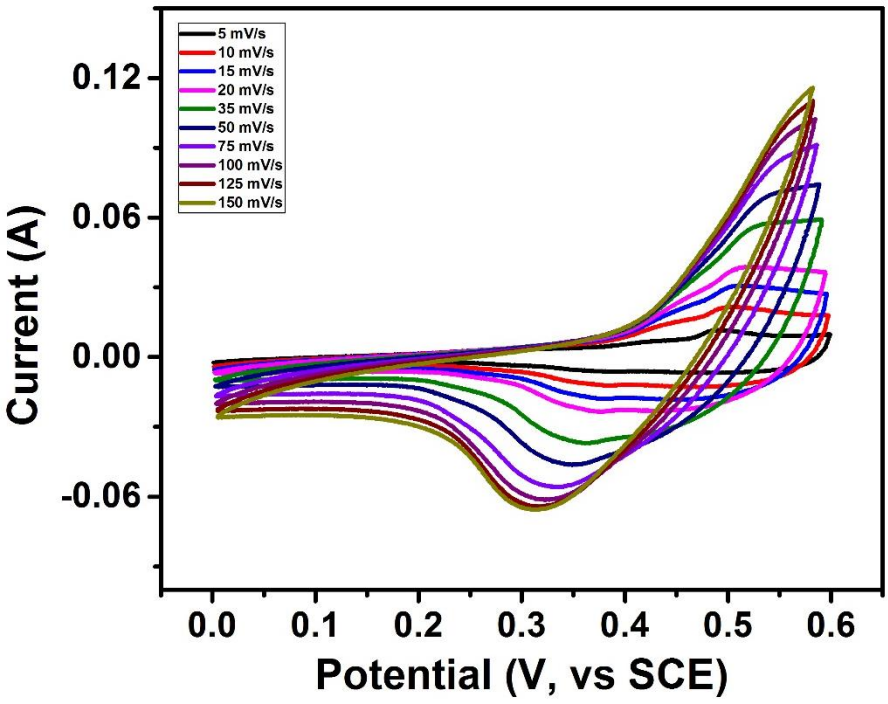

Figure 3.36: Cyclic voltammograms of CS-6 sample at various scan rates in 3 M KOH electrolyte.

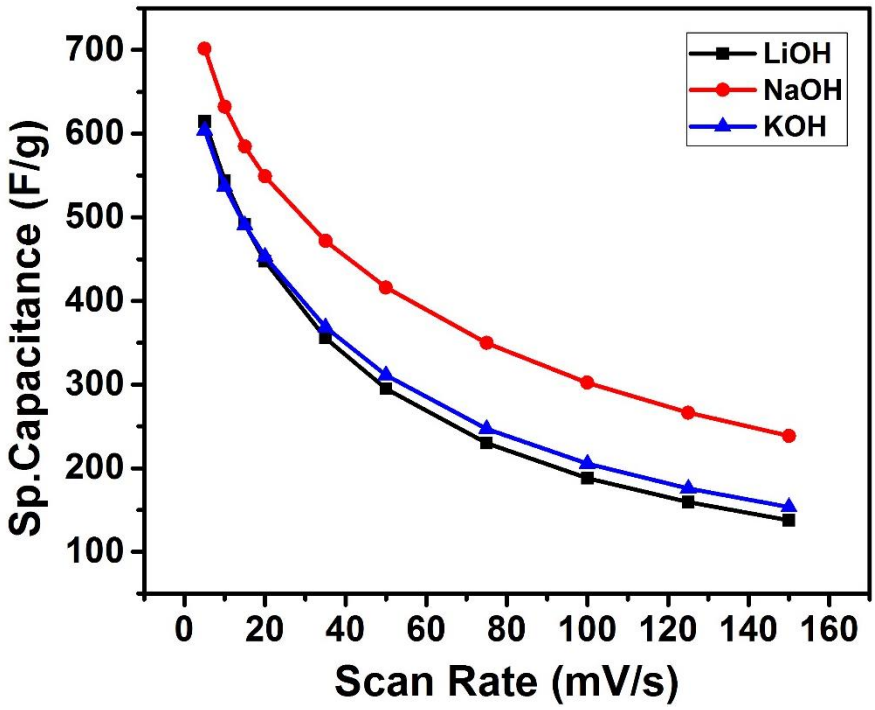

Figure 3.37: Variation of specific capacitance as a function of scan rate for CS-6 sample in different electrolytes.

The cyclic stability of the synthesized cobalt sulfide samples were further tested using cyclic voltammetry. All the cobalt sulfide electrodes were tested for 500 cycles in potential range of 0-0.6 volt in three different electrolytes (3M LiOH, NaOH, KOH). All the cyclic stability measurements were performed at the scan rate of 50 mV/s. Figures 3.38-3.55 show the cyclic voltammograms of all the cobalt sulfide electrodes at various numbers of cycles. As seen in these cyclic voltammograms, the shape and area of the voltammograms are very similar, suggesting high cyclic stability of the electrodes based on cobalt sulfides.

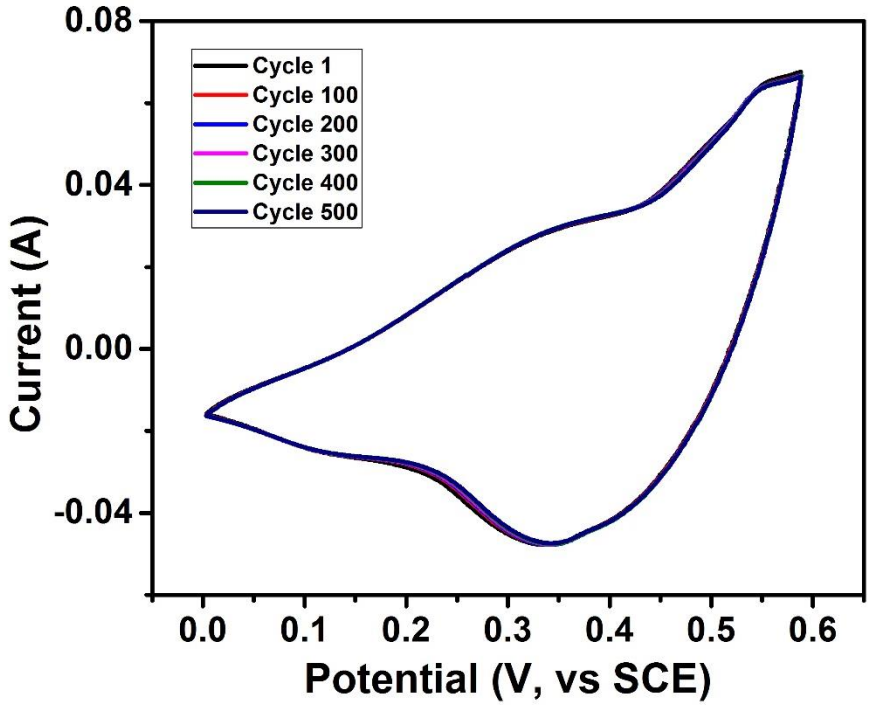

Figure 3.38: Cyclic voltammograms of CS-1 electrode at various cycles in 3M LiOH electrolyte.

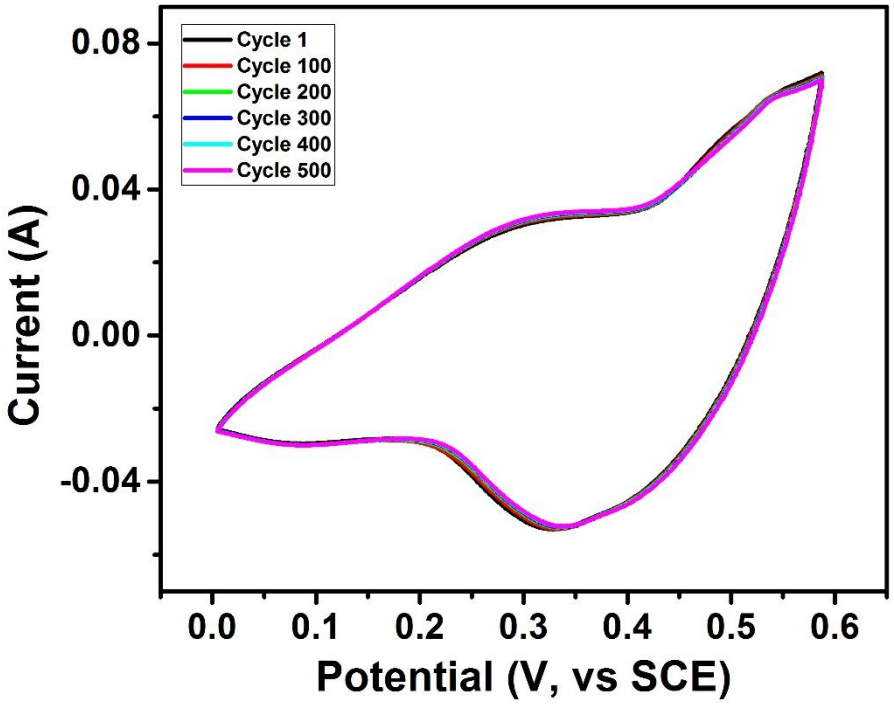

Figure 3.39: Cyclic voltammograms of CS-1 electrode at various cycles in 3M NaOH electrolyte.

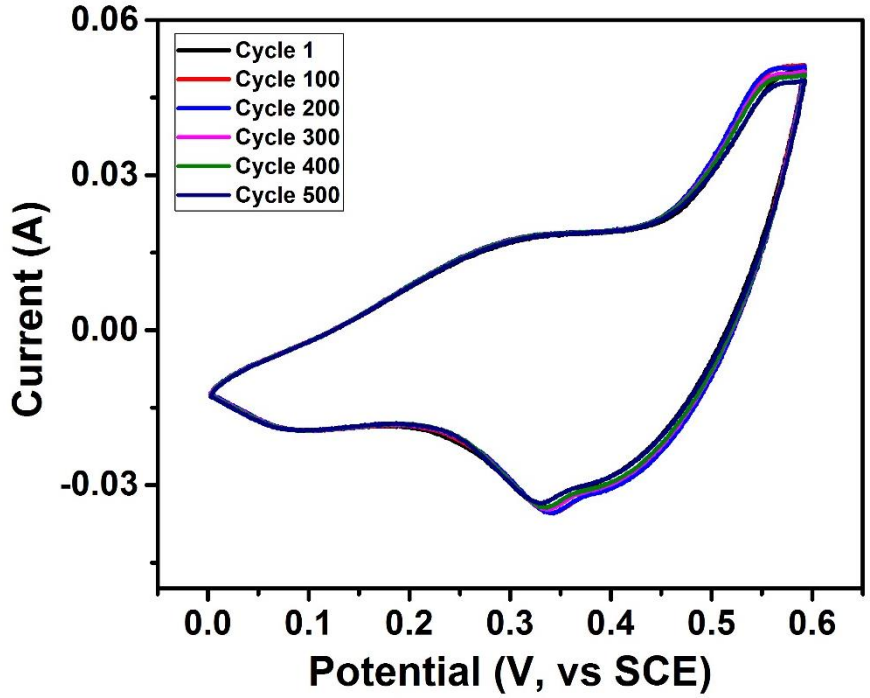

Figure 3.40: Cyclic voltammograms of CS-1 electrode at various cycles in 3M KOH electrolyte.

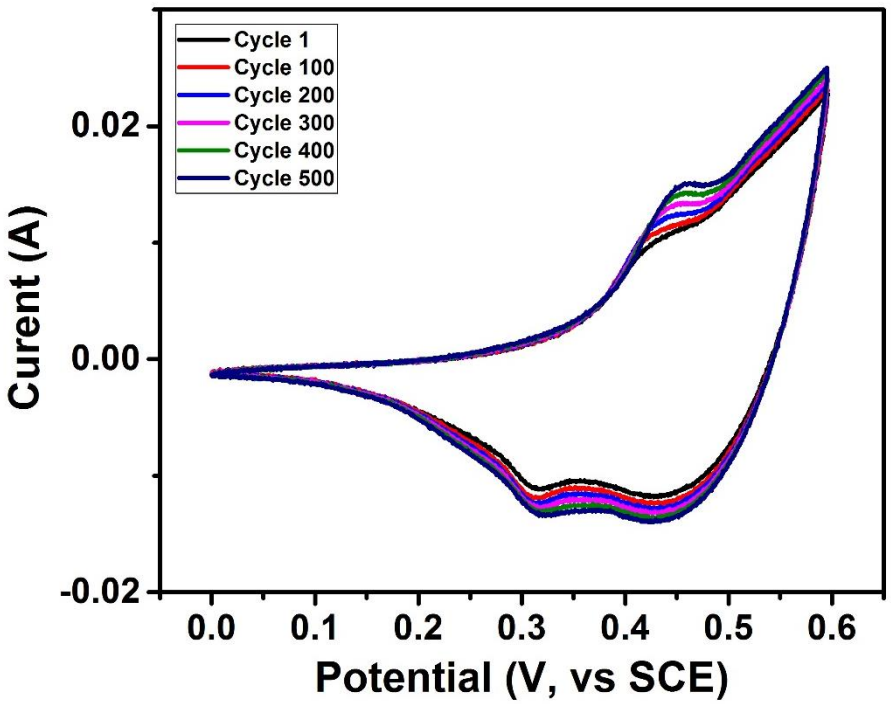

Figure 3.41: Cyclic voltammograms of CS-2 electrode at various cycles in 3M LiOH electrolyte.

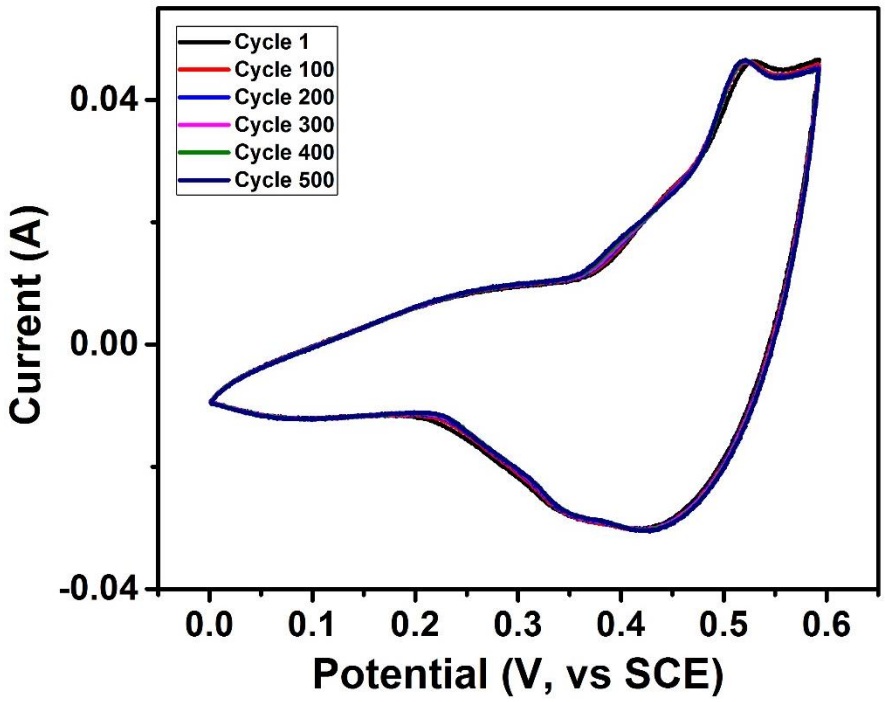

Figure 3.42: Cyclic voltammograms of CS-2 electrode at various cycles in 3M NaOH electrolyte.

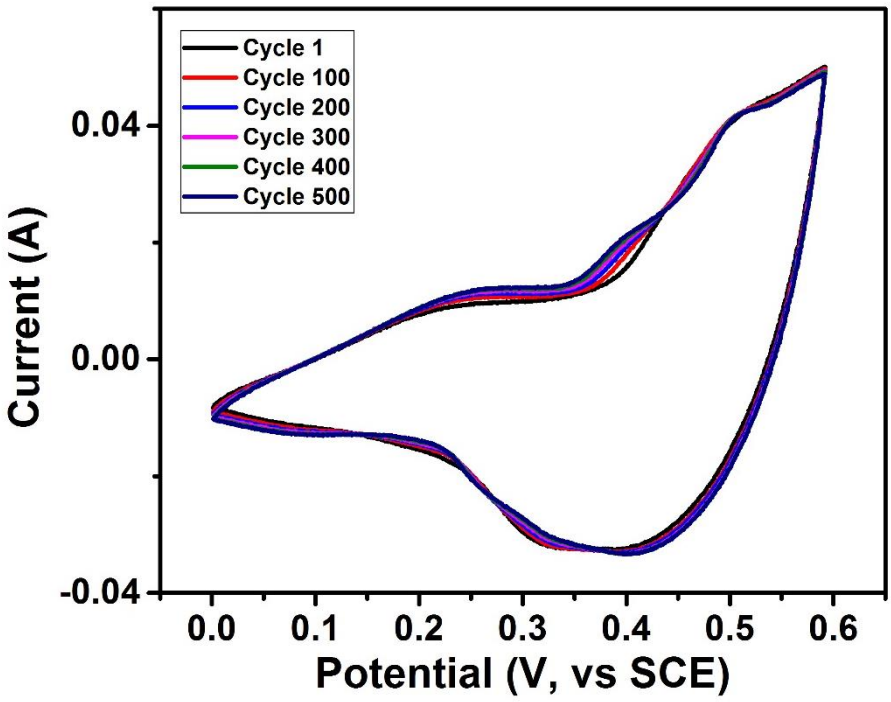

Figure 3.43: Cyclic voltammograms of CS-2 electrode at various cycles in 3M KOH electrolyte.

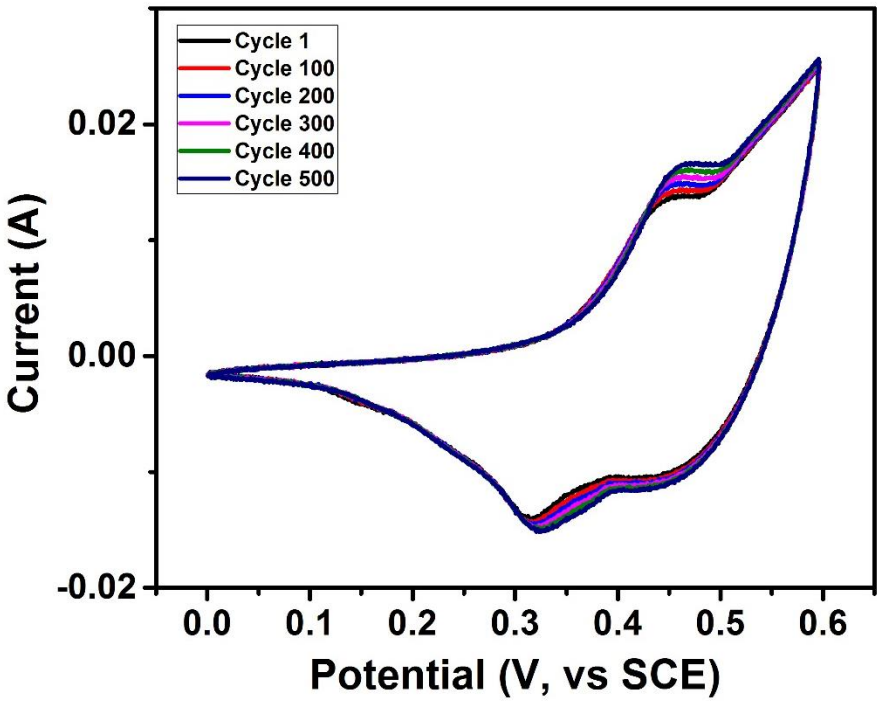

Figure 3.44: Cyclic voltammograms of CS-3 electrode at various cycles in 3M LiOH electrolyte.

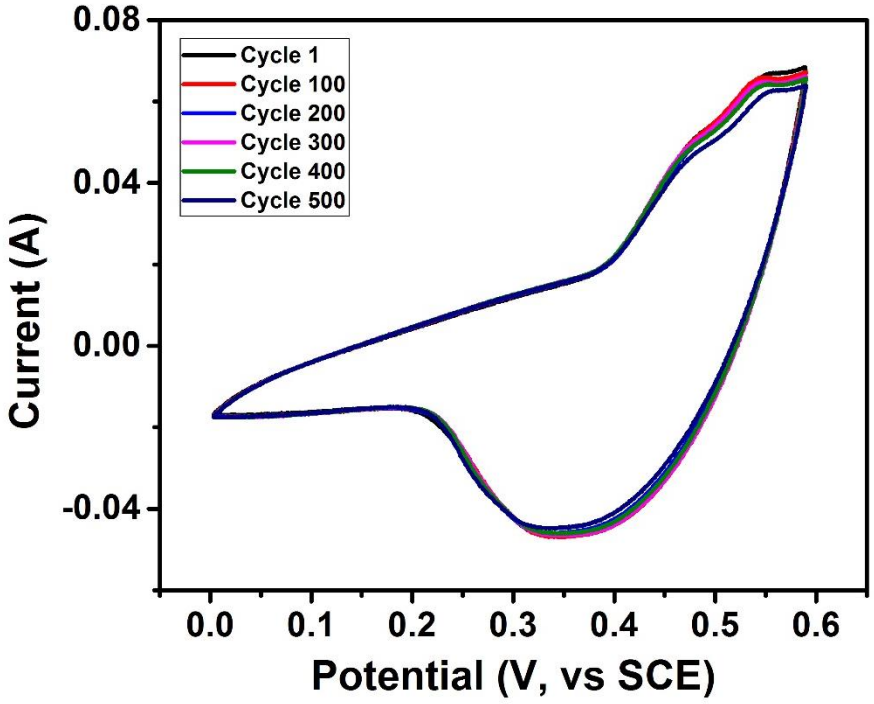

Figure 3.45: Cyclic voltammograms of CS-3 electrode at various cycles in 3M NaOH electrolyte.

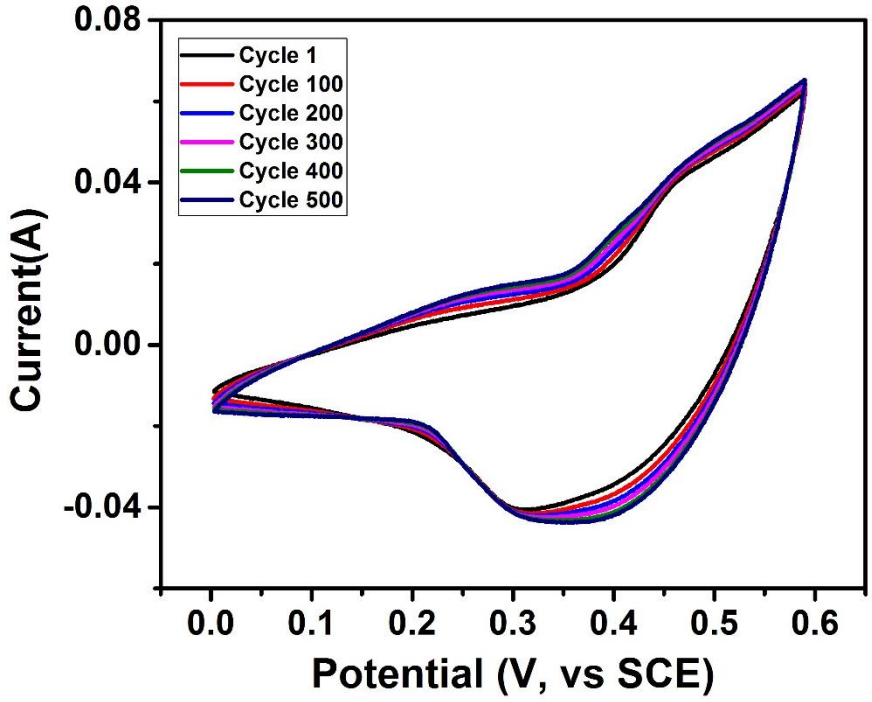

Figure 3.46: Cyclic voltammograms of CS-3 electrode at various cycles in 3M KOH electrolyte.

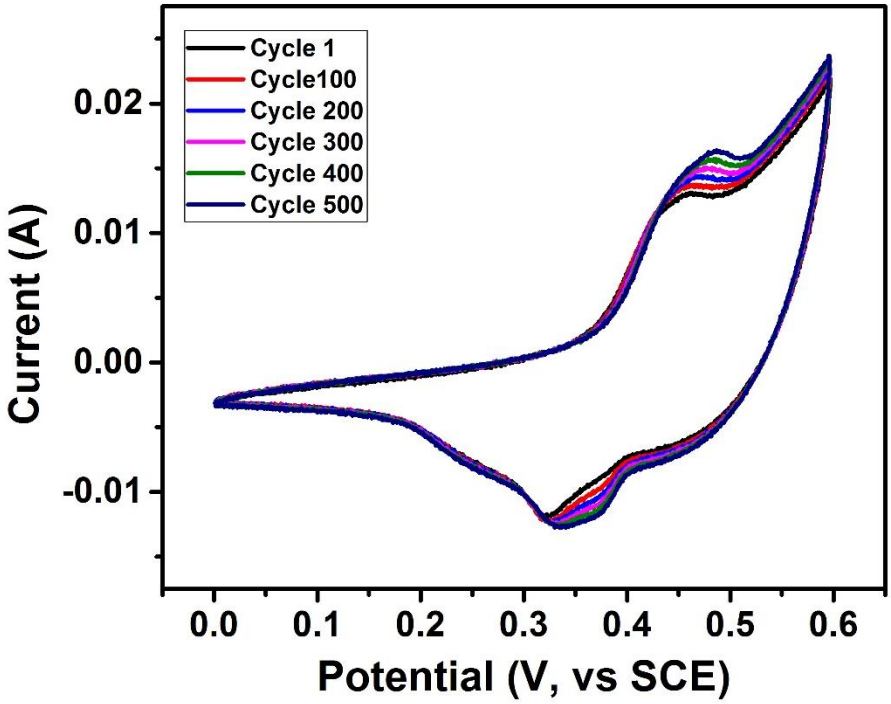

Figure 3.47: Cyclic voltammograms of CS-4 electrode at various cycles in 3M LiOH electrolyte.

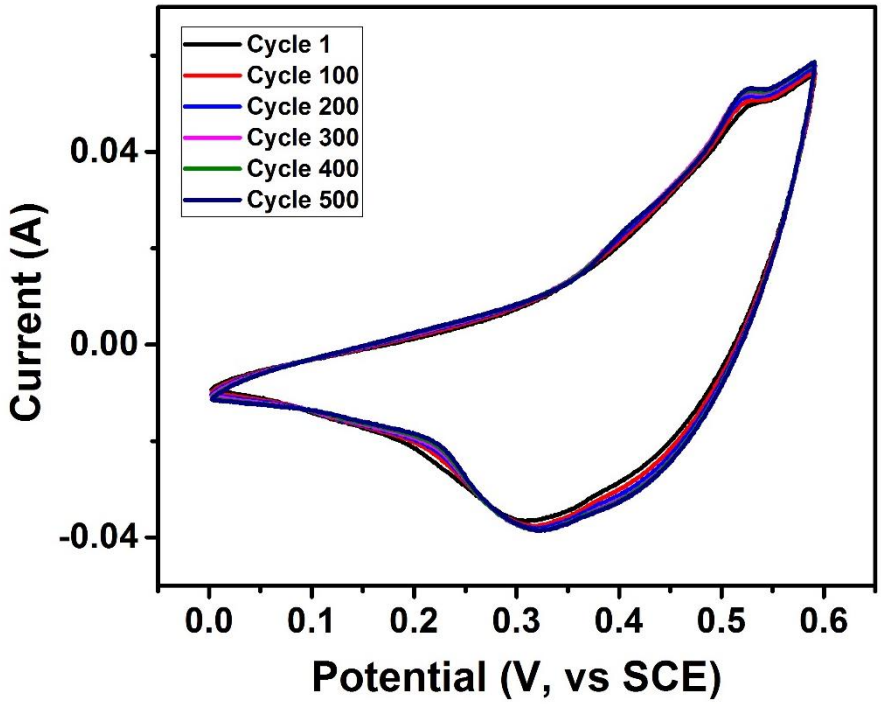

Figure 3.48: Cyclic voltammograms of CS-4 electrode at various cycles in 3M NaOH electrolyte.

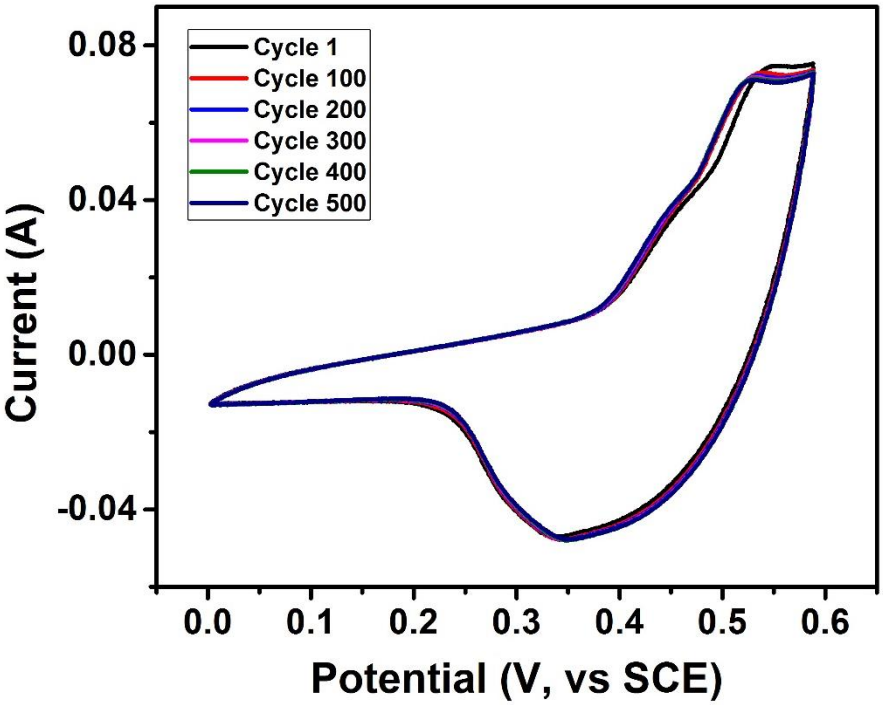

Figure 3.49: Cyclic voltammograms of CS-4 electrode at various cycles in 3M KOH electrolyte.

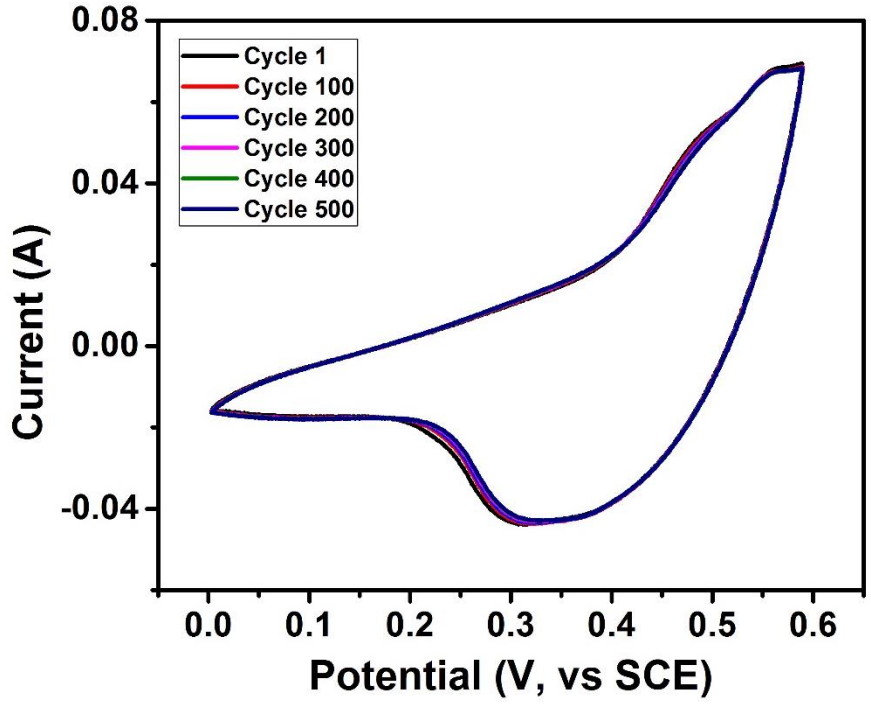

Figure 3.50: Cyclic voltammograms of CS-5 electrode at various cycles in 3M LiOH electrolyte.

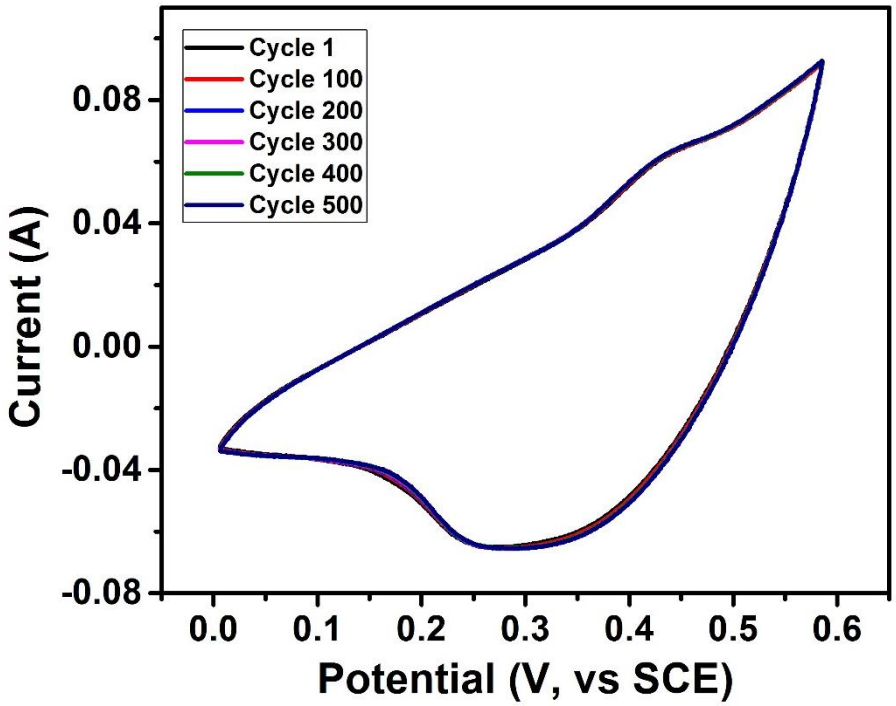

Figure 3.51: Cyclic voltammograms of CS-5 electrode at various cycles in 3M NaOH electrolyte.

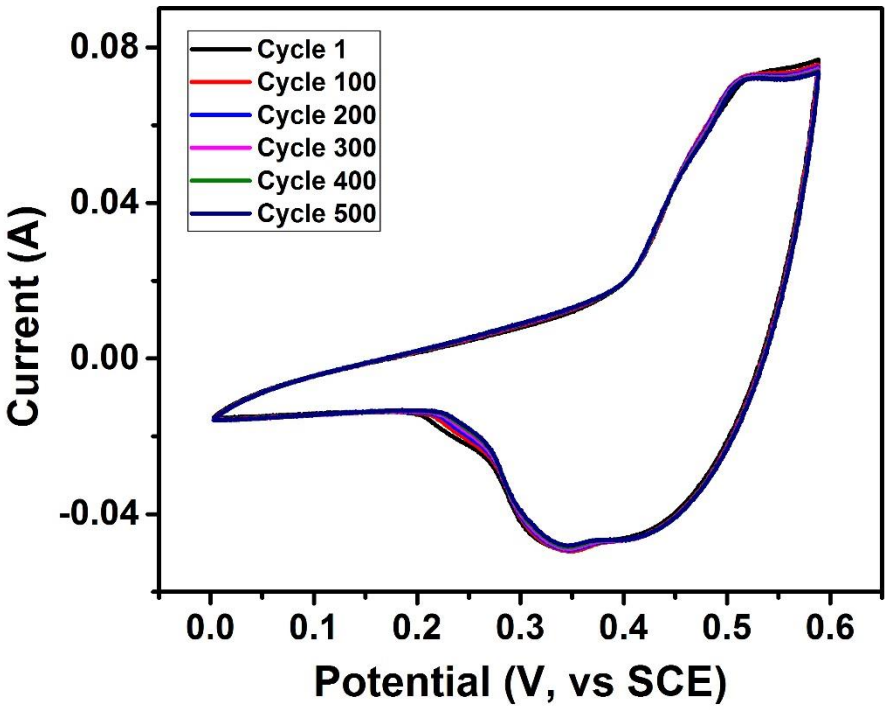

Figure 3.52: Cyclic voltammograms of CS-5 electrode at various cycles in 3M KOH electrolyte.

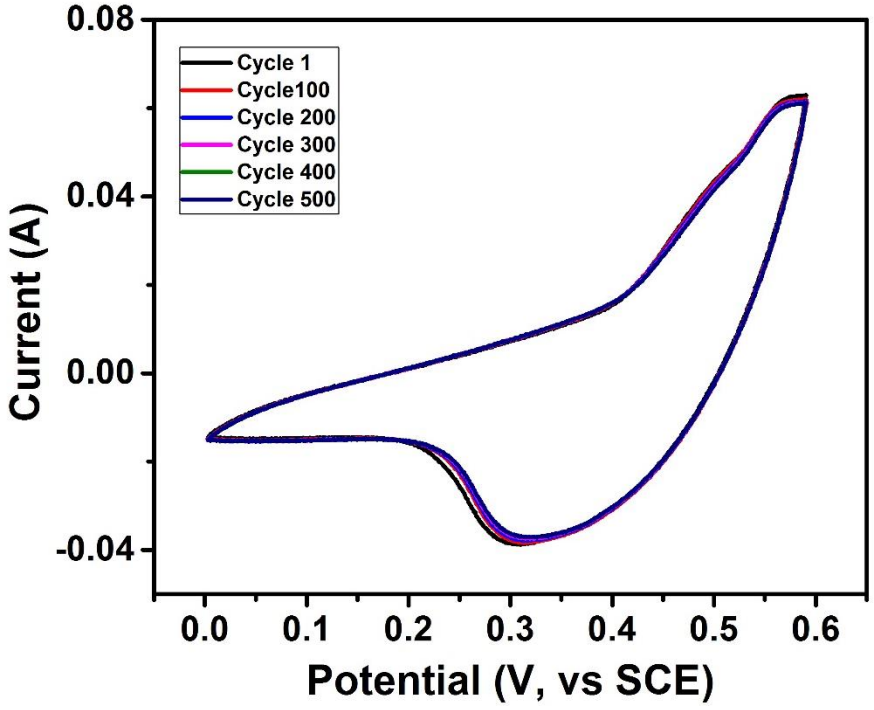

Figure 3.53: Cyclic voltammograms of CS-6 electrode at various cycles in 3M LiOH electrolyte.

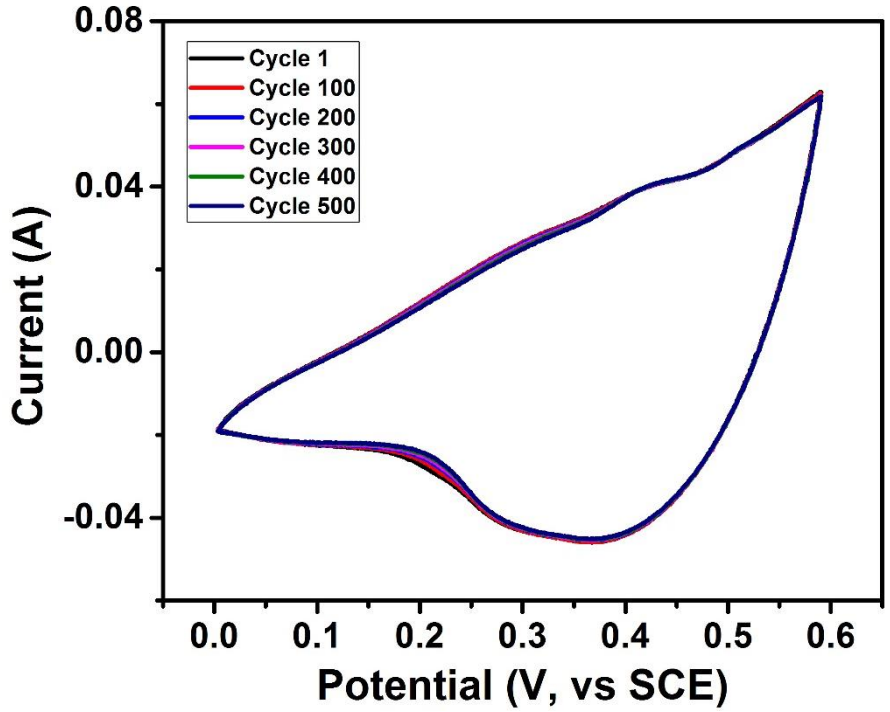

Figure 3.54: Cyclic voltammograms of CS-6 electrode at various cycles in 3M NaOH electrolyte.

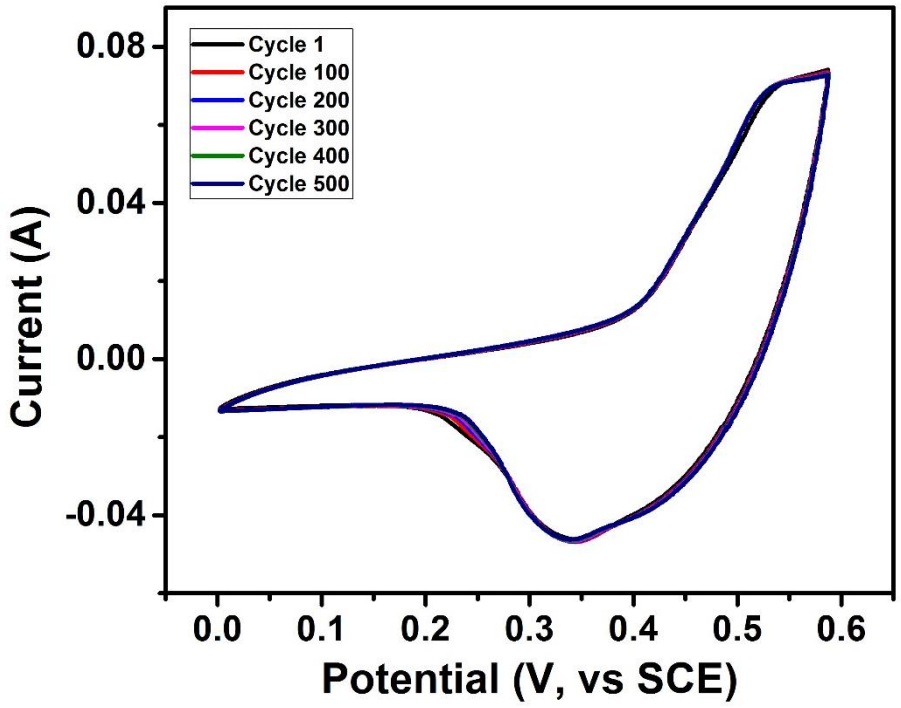

Figure 3.55: Cyclic voltammograms of CS-6 electrode at various cycles in 3M KOH electrolyte.

To further evaluate the potential application of the cobalt sulfides as electrode materials for supercapacitors, galvanostatic charge-discharge measurements were performed. The charge-discharge measurements were performed in three different electrolytes such as 3 M LiOH, NaOH and KOH. The galvanostatic charge-discharge studies were carried out at various applied currents between 0 and 0.6 V (*vs.* SCE). The charge-discharge characteristics of the fabricated cobalt sulfide electrodes (sample CS-1 and CS-6 as representative) are shown in Figures 3.56-3.61. As seen in these figures, the potential-time curves are nearly symmetrical at all currents indicating high charge-discharge coulombic efficiency, low polarization of the electrodes and high electrochemical reversibility of cobalt sulfides [37, 38]. In addition to symmetrical charge-discharge profile, it was also observed that the charge-discharge profile depends on electrolytes.

The specific capacitance of the cobalt sulfide electrodes was calculated using galvanostatic charge-discharge characteristics. The specific capacitance (C_{sp}) of the electrode was calculated using the equation given below [39]:

$$C_{sp} = \frac{I \times \Delta t}{\Delta V \times m}$$

where I is the discharge current (A), Δt is the discharge time (s), ΔV is the potential window (V), and m is the mass of the cobalt sulfide powder. The specific capacitance of the cobalt sulfide electrodes were observed to be decreasing with increasing currents (Figures 3.62-3.67). The decrease in the specific capacitance with the increase of the discharge current could be due to the increase of potential drop and insufficient faradic redox reaction at higher discharge currents [40].

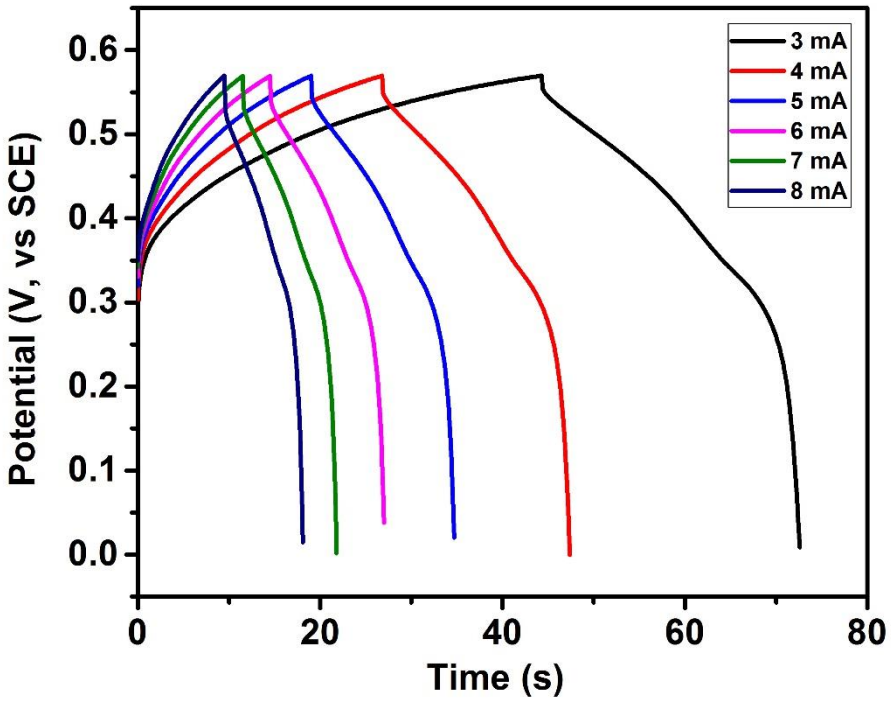

Figure 3.56: Galvanostatic charge-discharge characteristics of CS-2 electrode at various applied currents in 3M LiOH electrolyte.

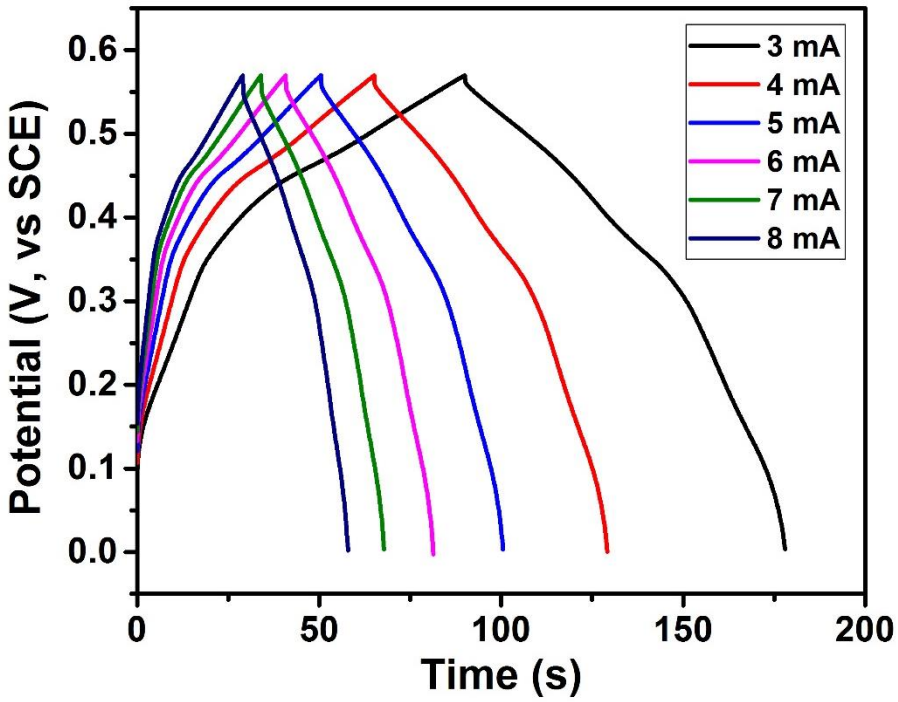

Figure 3.57: Galvanostatic charge-discharge characteristics of CS-2 electrode at various applied currents in 3M NaOH electrolyte.

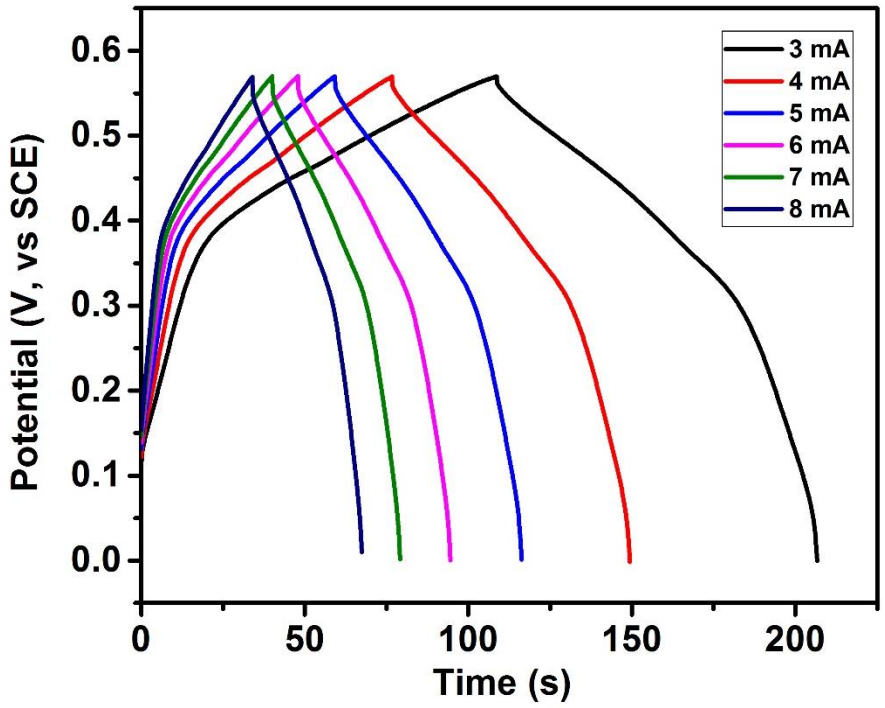

Figure 3.58: Galvanostatic charge-discharge characteristics of CS-2 electrode at various applied currents in 3M KOH electrolyte.

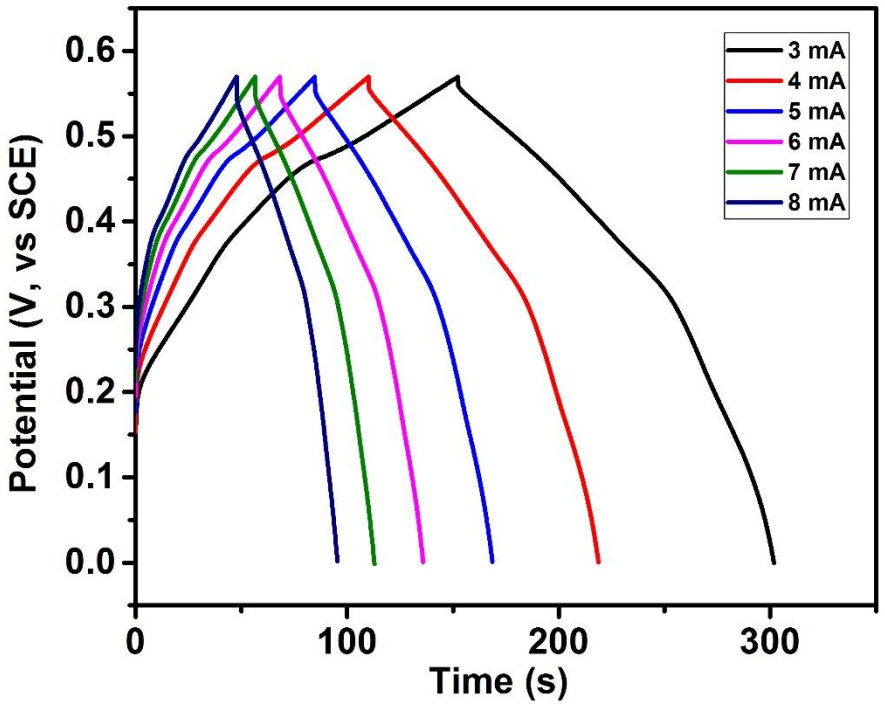

Figure 3.59: Galvanostatic charge-discharge characteristics of CS-6 electrode at various applied currents in 3M LiOH electrolyte.

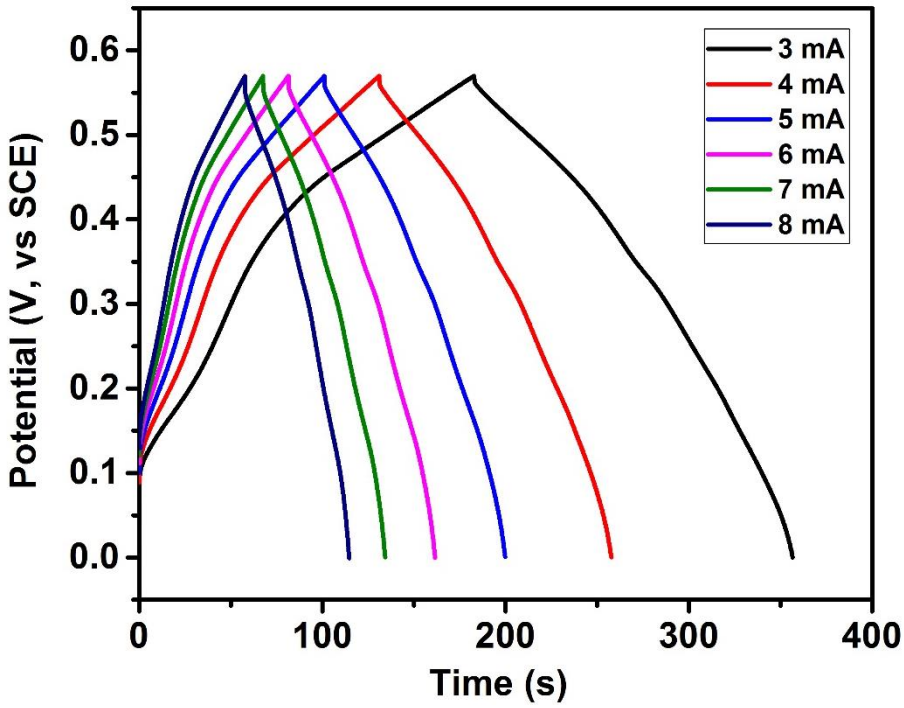

Figure 3.60: Galvanostatic charge-discharge characteristics of CS-6 electrode at various applied currents in 3M NaOH electrolyte.

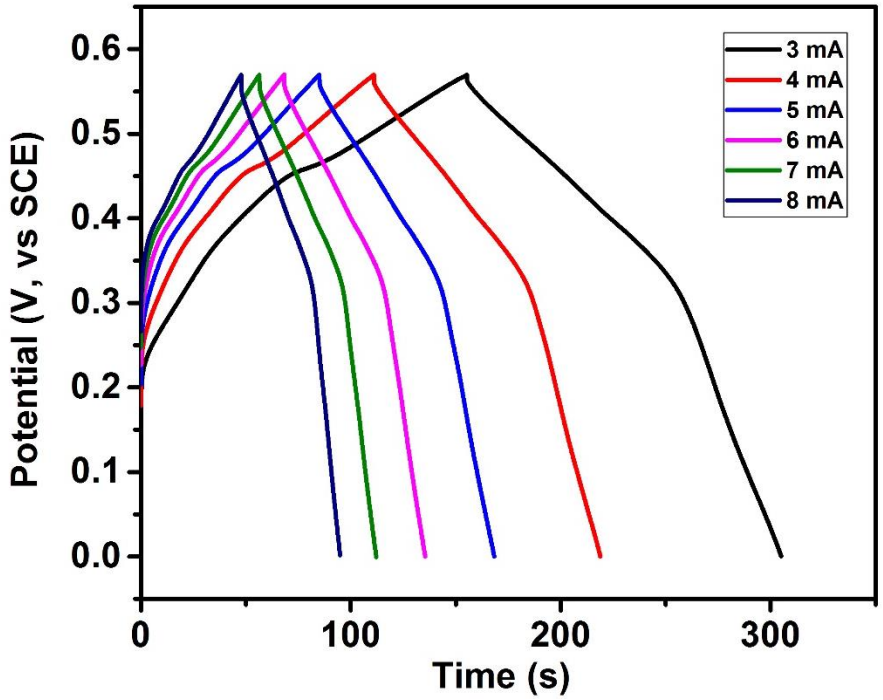

Figure 3.61: Galvanostatic charge-discharge characteristics of CS-6 electrode at various applied currents in 3M KOH electrolyte.

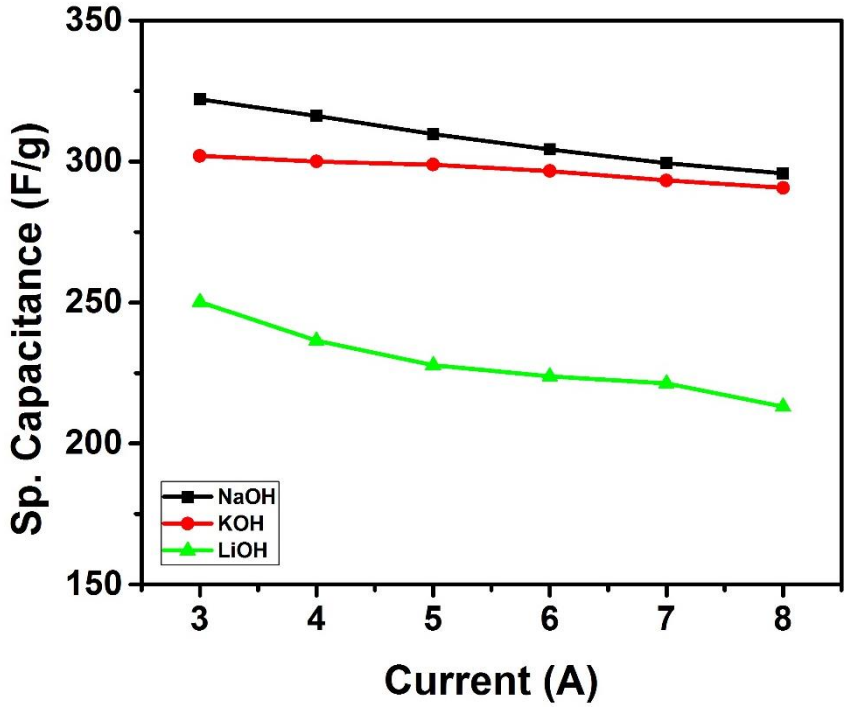

Figure 3.62: Variation of specific capacitance with applied current in different electrolytes for CS-1 sample.

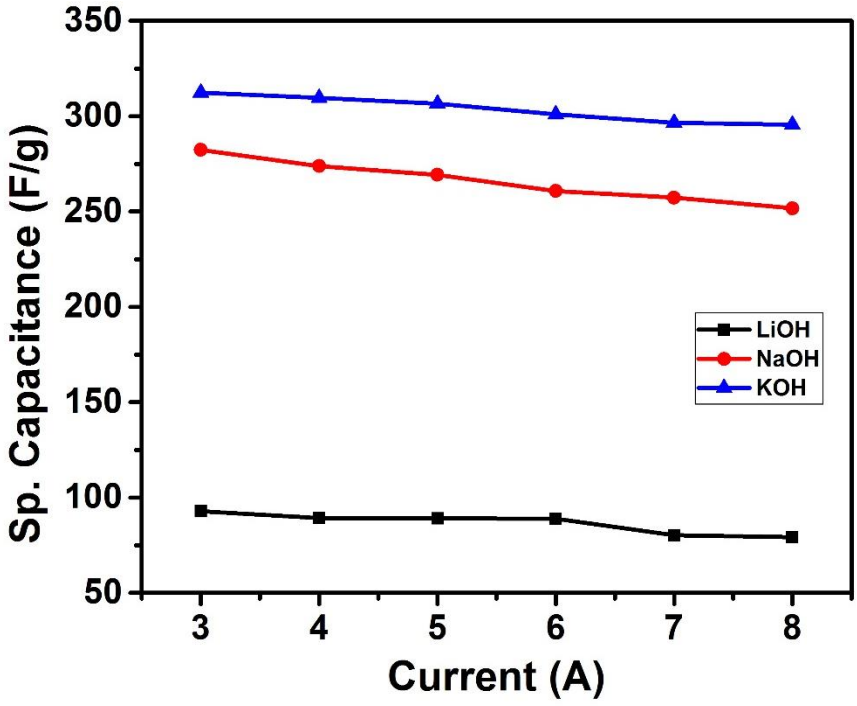

Figure 3.63: Variation of specific capacitance with applied current in different electrolytes for CS-2 sample.

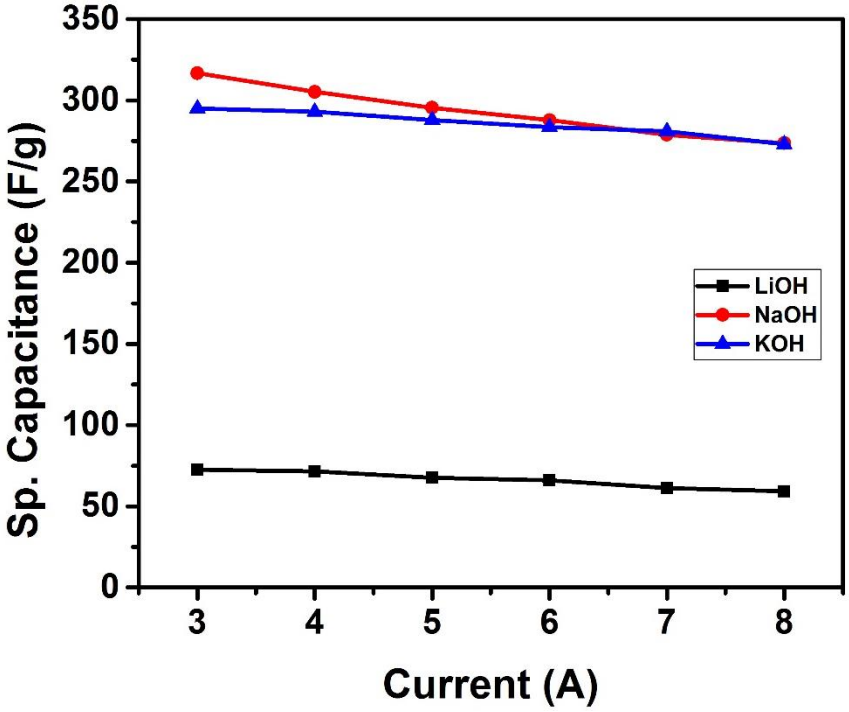

Figure 3.64: Variation of specific capacitance with applied current in different electrolytes for CS-3 sample.

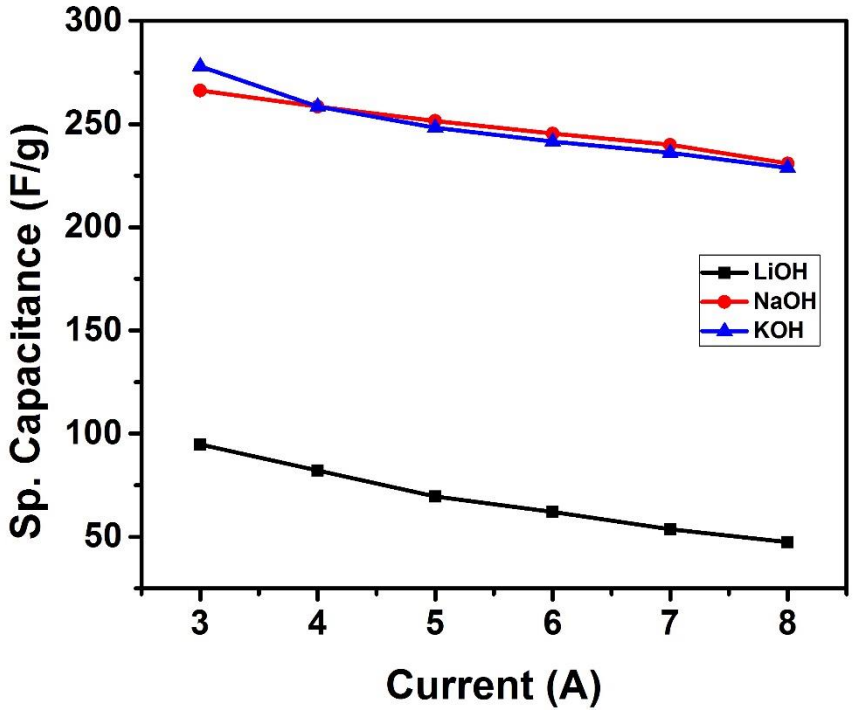

Figure 3.65: Variation of specific capacitance with applied current in different electrolytes for CS-4 sample.

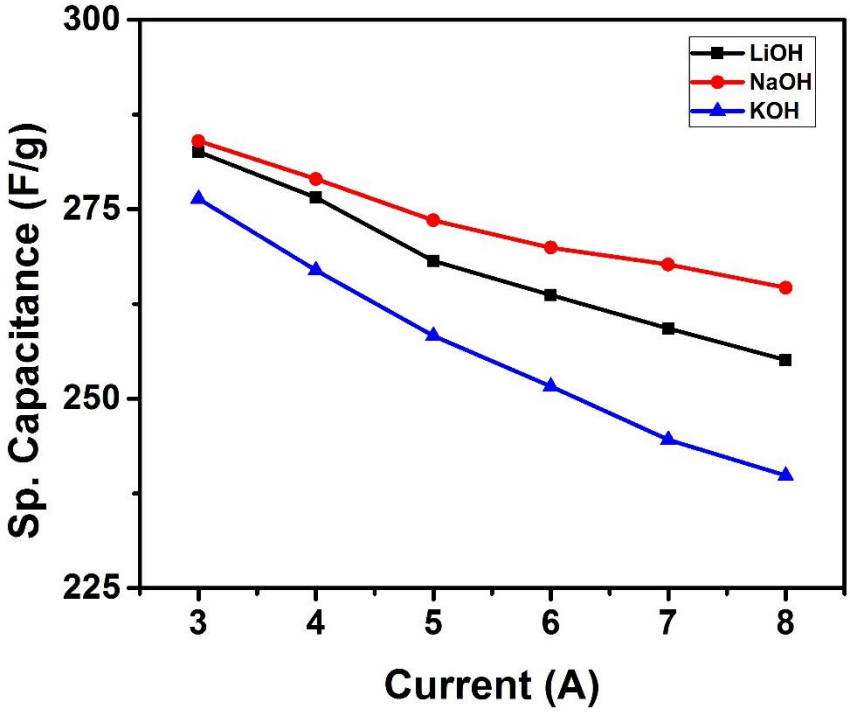

Figure 3.66: Variation of specific capacitance with applied current in different electrolytes for CS-5 sample.

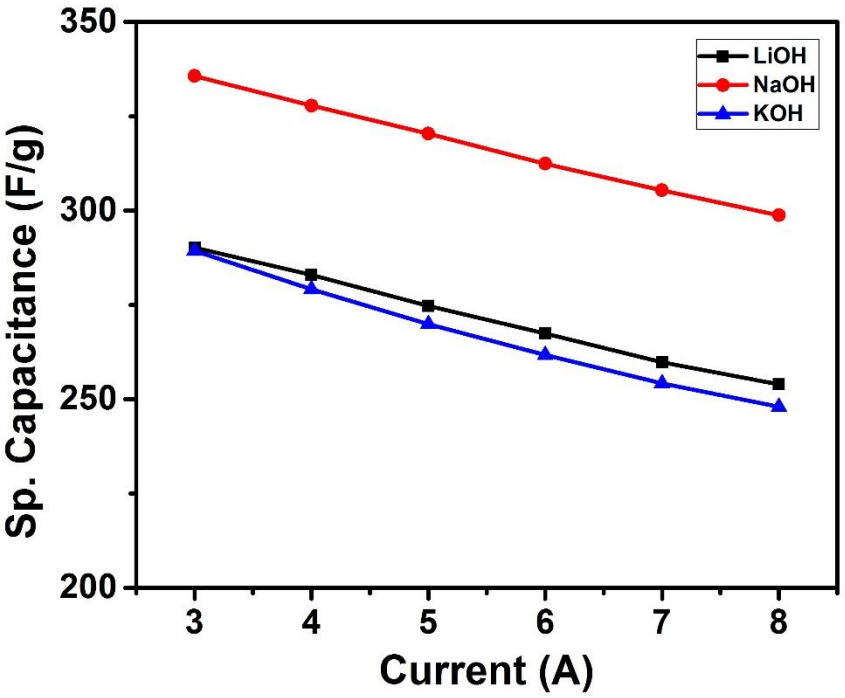

Figure 3.67: Variation of specific capacitance with applied current in different electrolytes for CS-6 sample.

Figures 3.68-3.71 shows the variation of specific capacitance with charge-discharge cycles for the cobalt sulfide samples in 3M LiOH, NaOH and KOH electrolytes. The specific capacitance of the electrodes were observed to be decreasing with cyclic charge discharge study. In some cases, the specific capacitance of the electrode was observed to be slowly increasing with charge-discharge cycles. The increase in the capacitance with cyclic charge-discharge process could be due to activation of the cobalt sulfide surface with time. This makes the surface of cobalt sulfide in full contact with the electrolyte which leads to better electrochemical performance [41, 42].

The performance of the supercapacitors was further evaluated using a Ragone plot which relates energy density to power density of a material. The energy density and the power density for a supercapacitor cell can be calculated using the following equations [8]:

$$E\ \left(\frac{Wh}{kg}\right) = \frac{C_{sp} \times \Delta V^2}{7.2}$$

$$P\ \left(\frac{W}{kg}\right) = \frac{E \times 3600}{t}$$

where C_{sp} (F/g) is the specific capacitance calculated from charge-discharge characteristics, ΔV (V) is the potential window and t (s) is the discharge time. Figures 3.72-3.77 show variation of power density versus energy density for all the cobalt sulfide samples in 3M LiOH, NaOH and KOH electrolytes. As seen in these figures, the higher energy density is observed for the lower discharge currents. On the other hand, power density is higher for the higher discharge currents. The high values of power density and energy density observed in cobalt sulfide electrodes suggest that these materials could be used for high performance energy storage devices.

A quasi-solid state supercapacitor device was fabricated and the performance of the device was studied using cyclic voltammetry and electrochemical impedance spectroscopy. The device was tested at various temperature to validate its applicability in harsh condition. Figure 3.74 shows the cyclic voltammograms of the device fabricated using CS-3 electrodes at different temperature. The shape of the voltammograms are very similar even at higher temperature, indicating near ideal capacitive behavior within this wide temperature window. As seen in Figure 3.75, the specific capacitance of the device increases with increasing temperature. The device showed about 400% improvement in the specific capacitance when the working temperature was increased from 10 to 70 ^{o}C. The results suggest that supercapacitor devices based on cobalt sulfides are more efficient at higher temperature.

The increase in the capacitance of the device with increasing temperature was analyzed using electrochemical impedance spectroscopy (EIS). The main objective of the EIS measurement was to gain insight into the temperature dependence of the resistive and capacitive elements and their effects on the performance of the supercapacitor device. Figures 3.78 and 3.79 (zoomed of Figure 3.78) shows the EIS spectra of the device at various temperatures. As seen in the figure, the equivalent series resistance (ESR) of the device decreases with increasing temperature. The decrease in the ESR value could be due to the enhanced mobility of the ions in the electrolyte which increases the conductivity of the electrolyte [43]. The impedance of the quasi-state supercapacitor device was also observed to decrease with increasing temperature and frequency as seen in Figure 3.80.

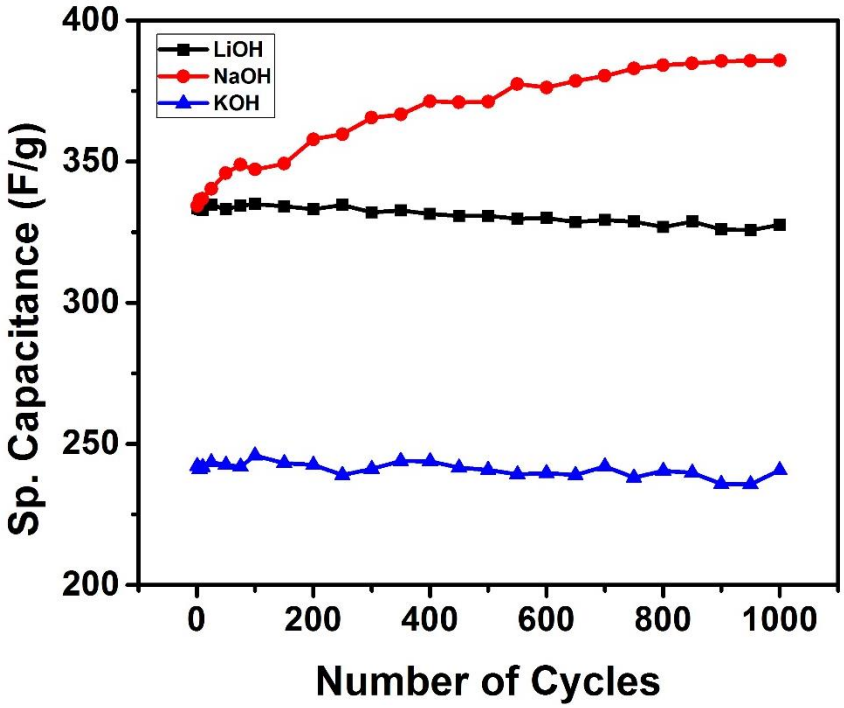

Figure 3.68: Variation of specific capacitance with number of charge-discharge cycles in different electrolytes for CS-1 sample.

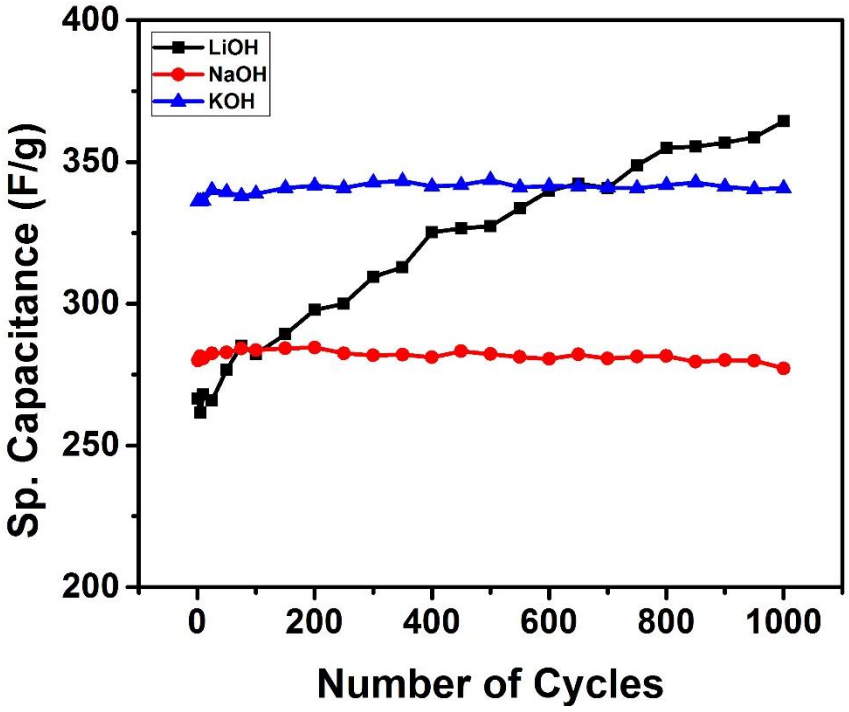

Figure 3.69: Variation of specific capacitance with number of charge-discharge cycles in different electrolytes for CS-2 sample.

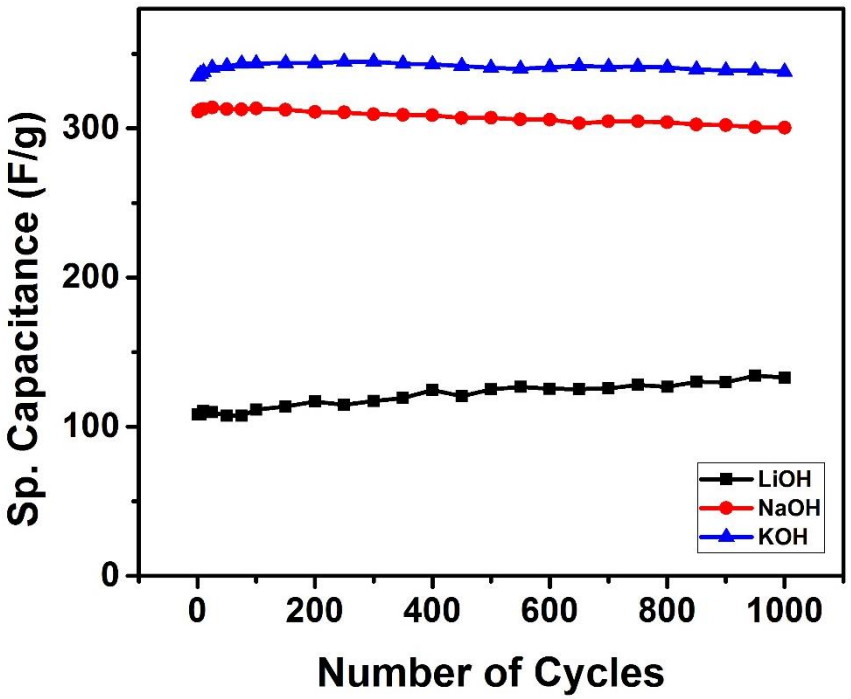

Figure 3.70: Variation of specific capacitance with number of charge-discharge cycles in different electrolytes for CS-3 sample.

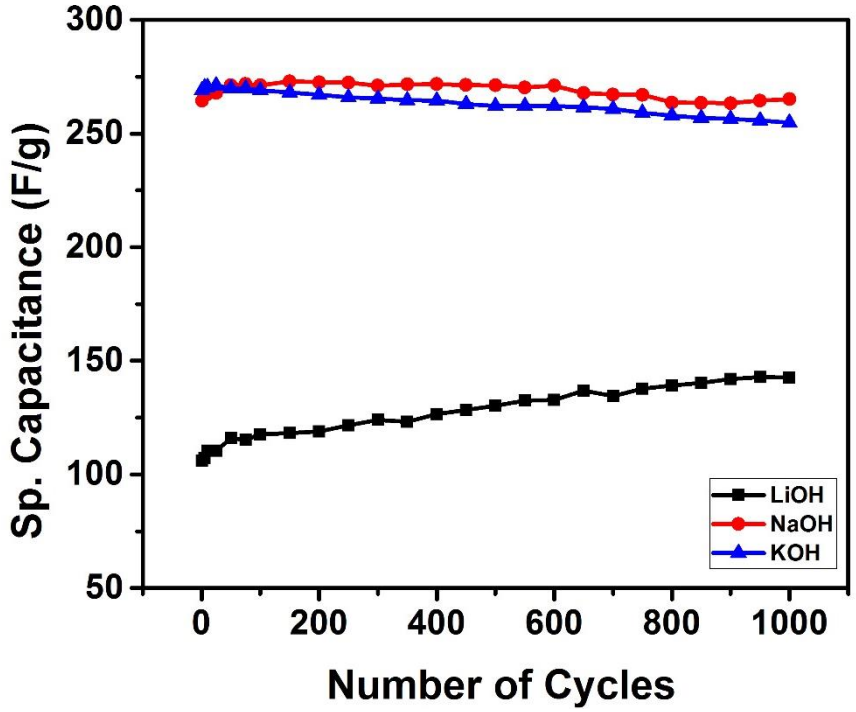

Figure 3.71: Variation of specific capacitance with number of charge-discharge cycles in different electrolytes for CS-4 sample.

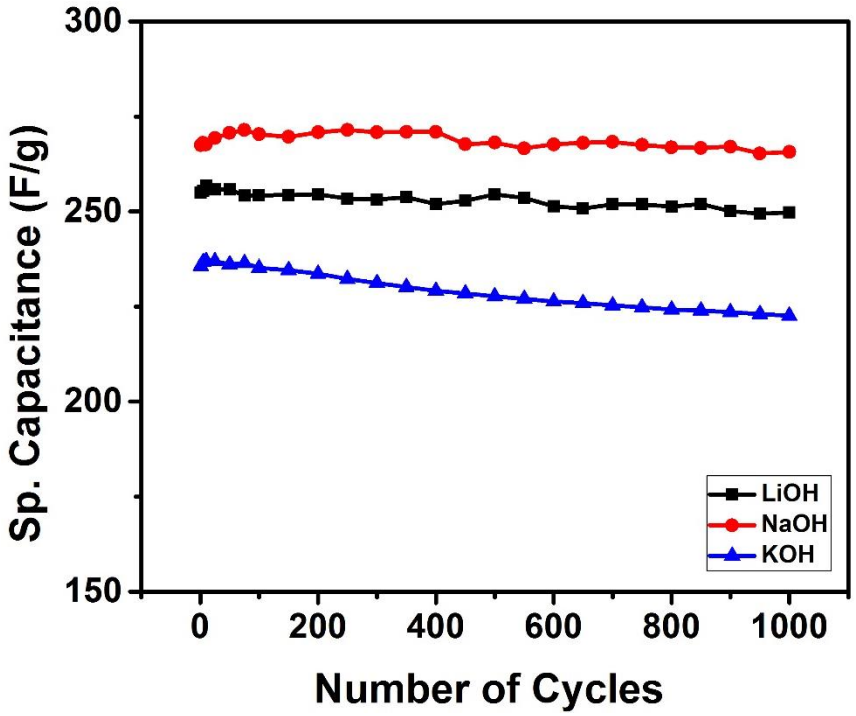

Figure 3.72: Variation of specific capacitance with number of charge-discharge cycles in different electrolytes for CS-5 sample.

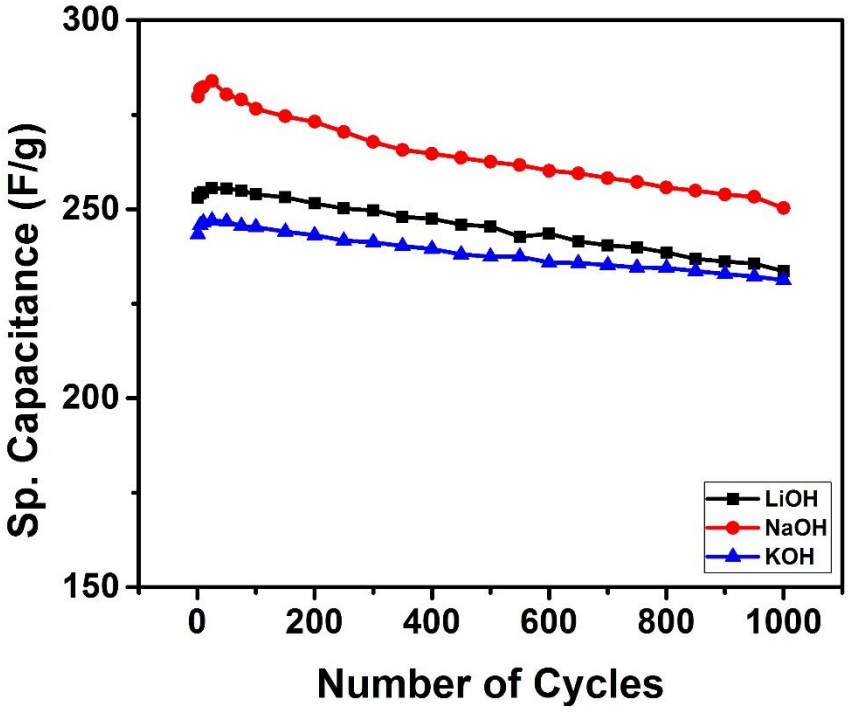

Figure 3.73: Variation of specific capacitance with number of charge-discharge cycles in different electrolytes for CS-6 sample.

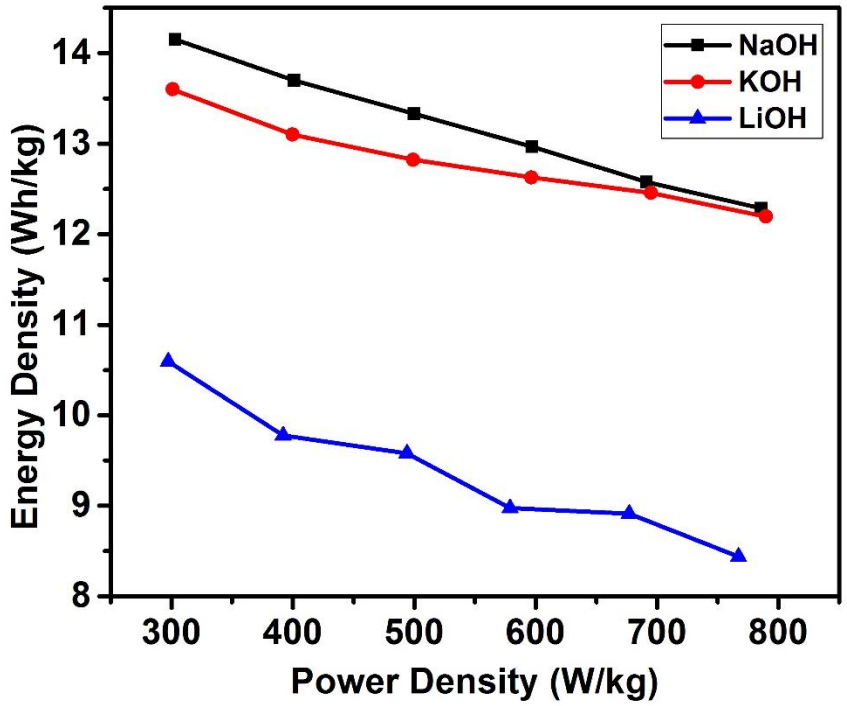

Figure 3.74: Power density versus energy density plots for CS-1 in various electrolytes.

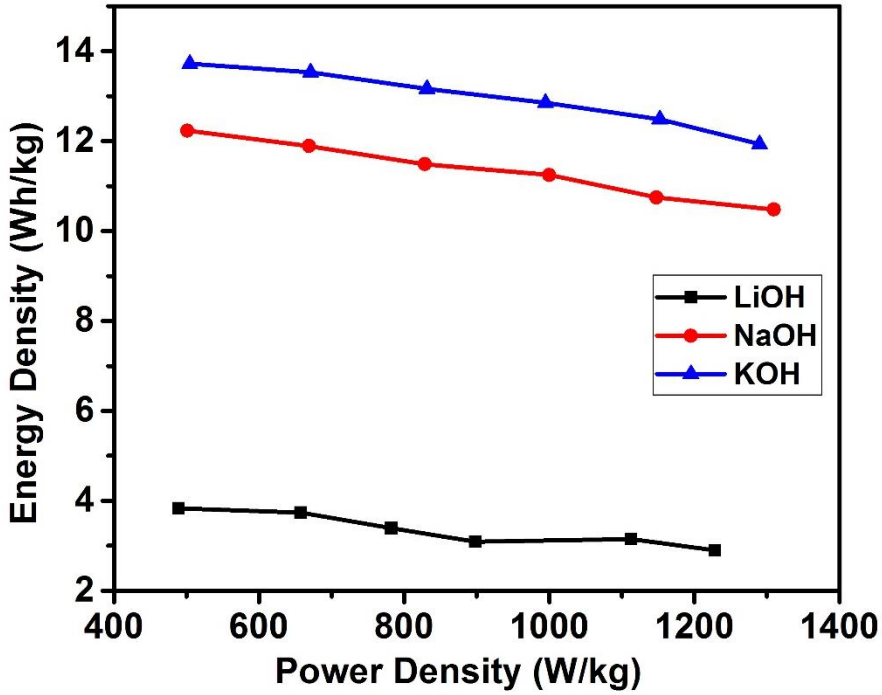

Figure 3.75: Power density versus energy density plots for CS-2 in various electrolytes.

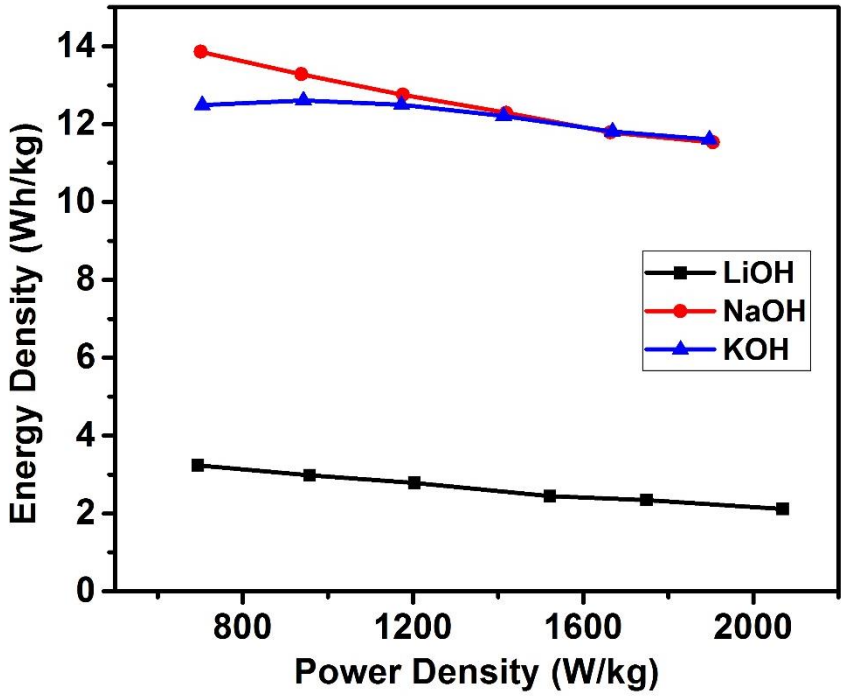

Figure 3.76: Power density versus energy density plots for CS-3 in various electrolytes.

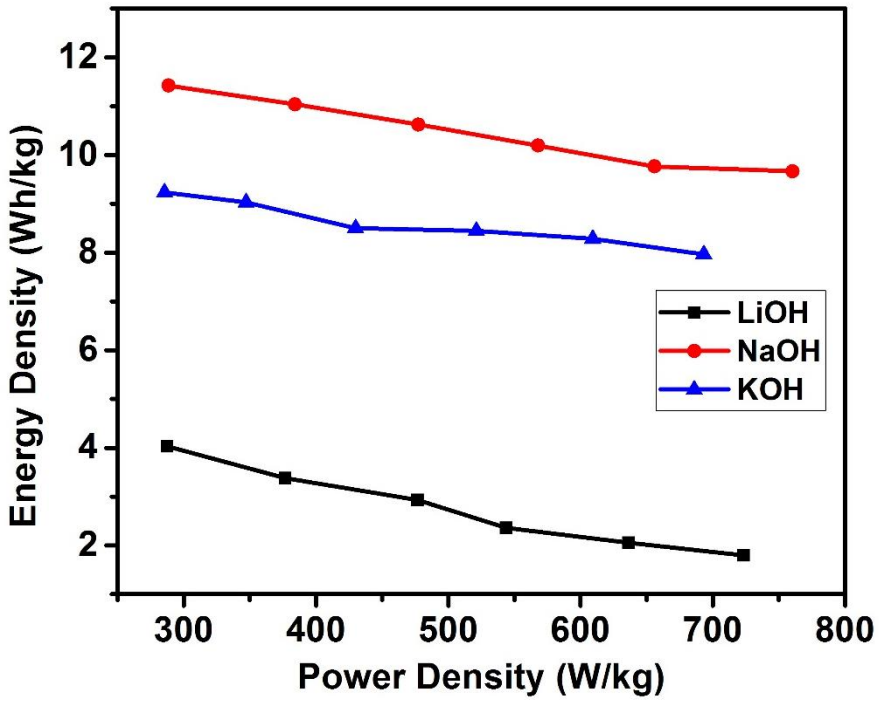

Figure 3.77: Power density versus energy density plots for CS-4 in various electrolytes.

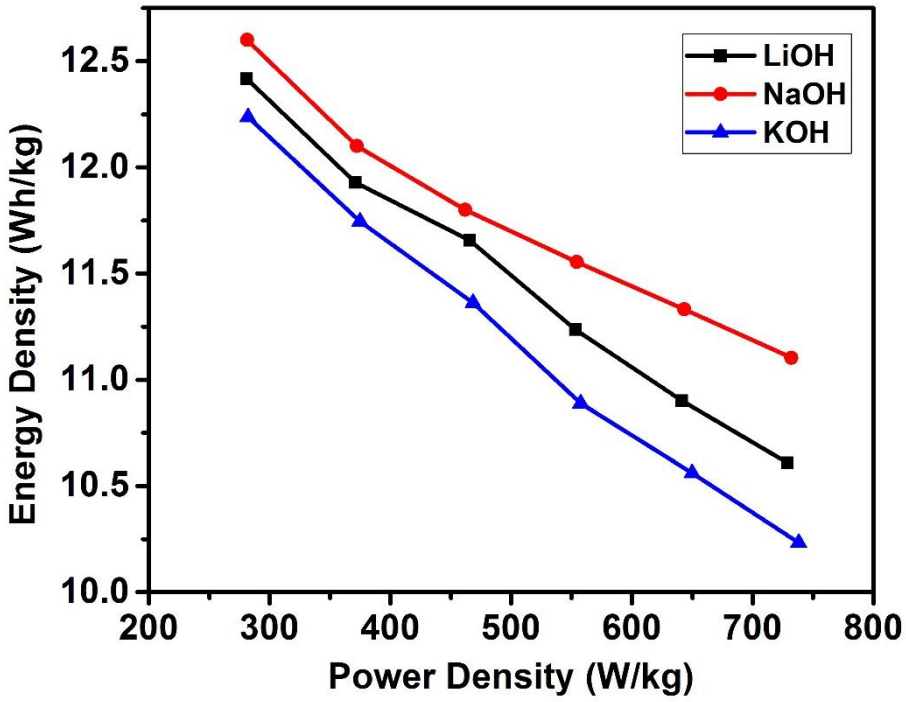

Figure 3.78: Power density versus energy density plots for CS-5 in various electrolytes.

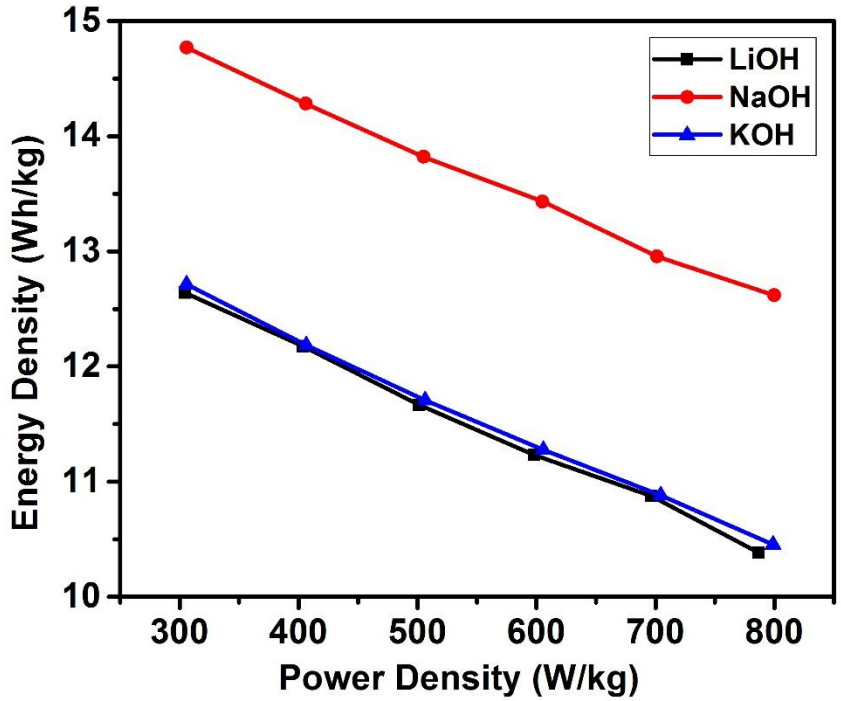

Figure 3.79: Power density versus energy density plots for CS-6 in various electrolytes.

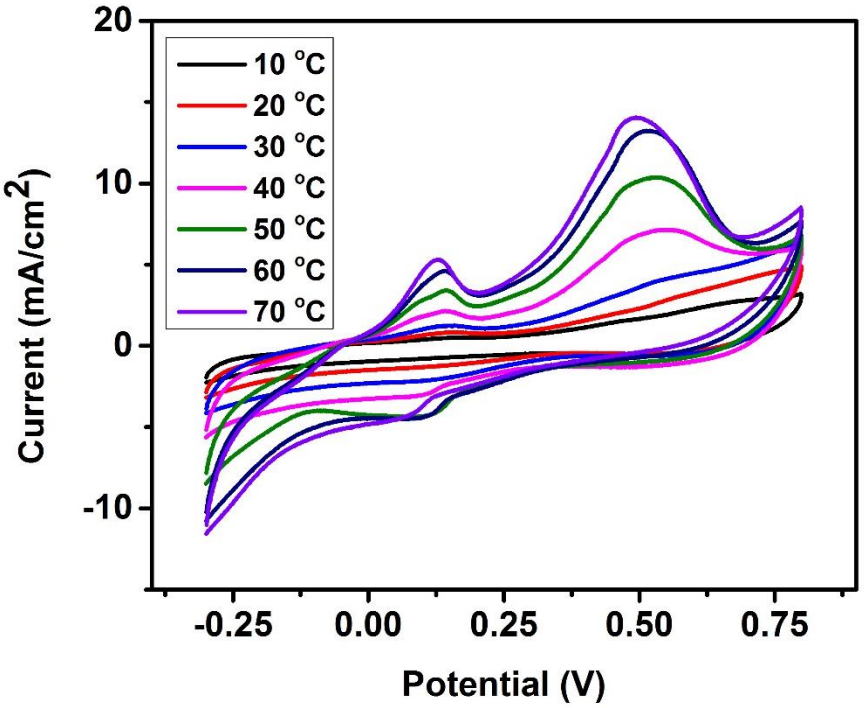

Figure 3.80: Cyclic voltammograms of the device at various temperatures.

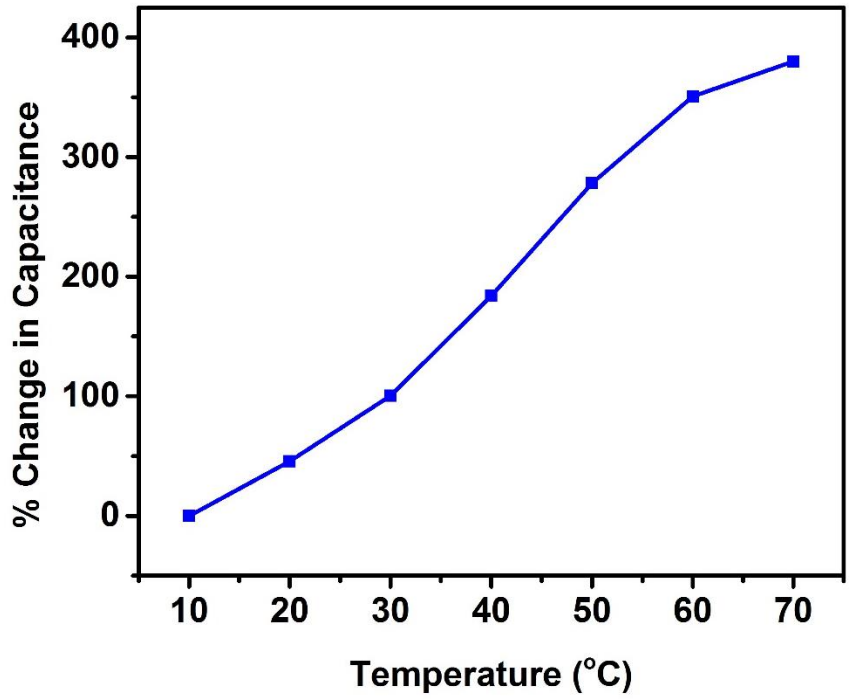

Figure 3.81: % change in specific capacitance of the device versus temperatures.

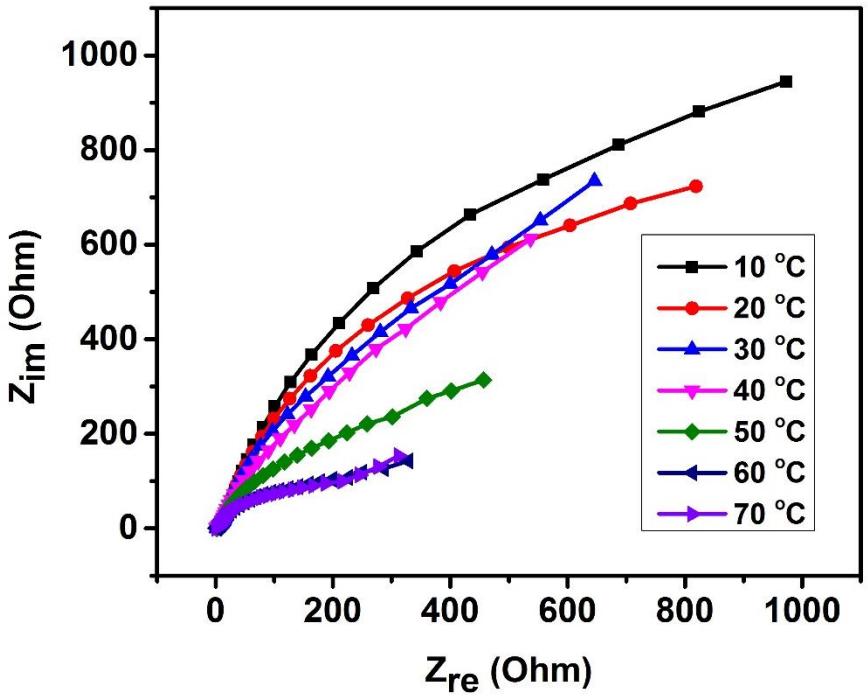

Figure 3.82: Z_{re} versus Z_{im} plots of the device at various temperatures.

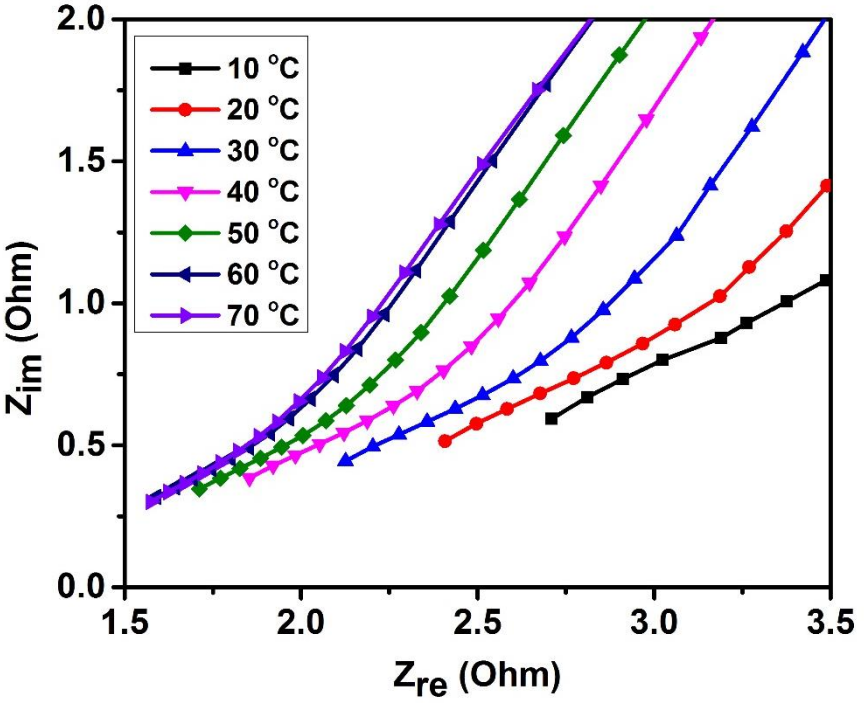

Figure 3.83: Z_{re} versus Z_{im} plots of the device at various temperatures.

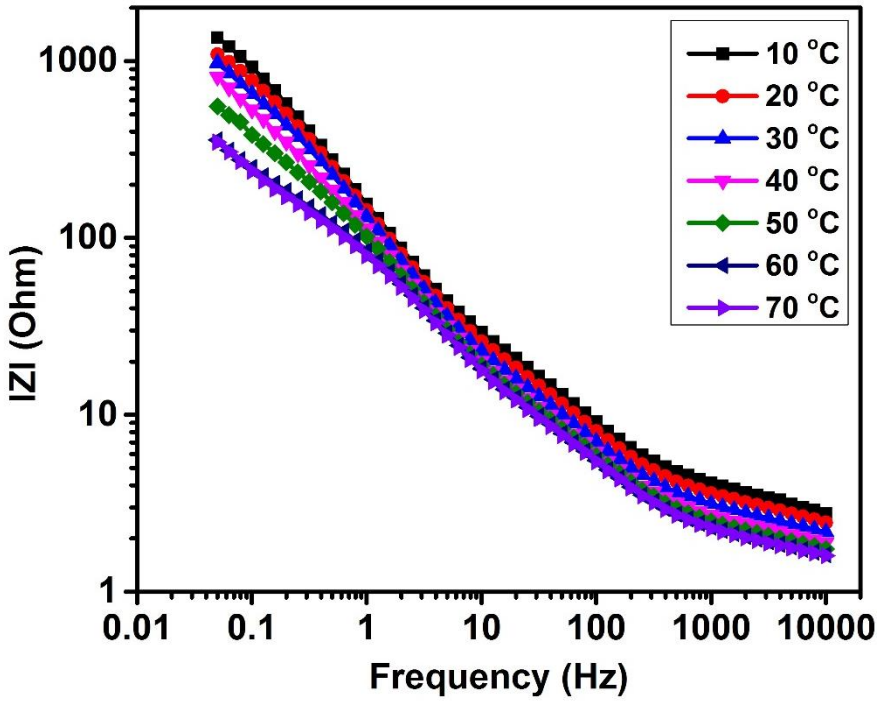

Figure 3.84: Variation of impedance as a function of frequency and temperature.

3.4. Magnetic Properties

Magnetic properties of the cobalt sulfide sample were studied to understand its magnetic nature. The magnetic moment as a function of applied magnetic field at various temperatures for sample CS-3 is shown in Figures 3.85-3.88. As seen in these Figures, CS-3 shows the hysteresis loop at all temperatures. The presence of hysteresis loop even at room temperature indicates that the synthesized cobalt sulfide is ferromagnetic in nature. It is further evident from the magnetization versus magnetic field measurements that the saturated magnetization decreases with increase in the temperature. The coercivity and remanence magnetization of the cobalt sulfide at various temperatures are given in Table 3.2. Liu et al have also observed a similar nature for the nano-octahedron shaped cobalt sulfide [32]. They observed a higher coercive force and remanence

magnetization compare to that of our synthesized cobalt sulfide. The lower values observed in our case could be due to the nanosize of the samples. In general, magnetization decreases with decreasing size.

Figures 3.89-3.90 shows the variation of magnetization as a function of temperature under two different applied magnetic fields. As seen in the magnetization versus temperature measurements, the magnetic moment of the sample decreases with increasing in temperature up to about 120 K and then become almost constant. The high magnetic moments at low temperature can be attributed to the surface spins. The surface spins are aligned in the direction of external magnetic field at high temperature and got frozen during cooling in magnetic field. On increasing the temperature, the magnetic moments decreases due to thermal fluctuations.

Table 3.2: Magnetic properties of cobalt sulfide (CS-3) sample.

Temperature (K)	Coercivity (Oe)	Remanence magnetization (emu/mg)
10	459	59.9
100	177	8.02
200	166	6.96
300	147	6.14

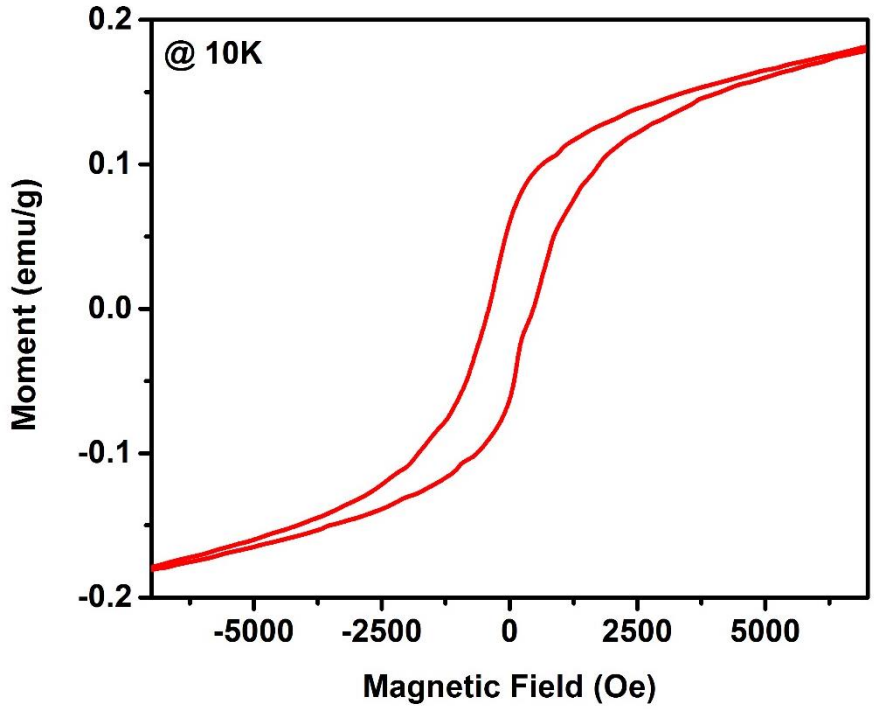

Figure 3.85: M vs. H measurement of cobalt sulfide (CS-3) sample at 10 K.

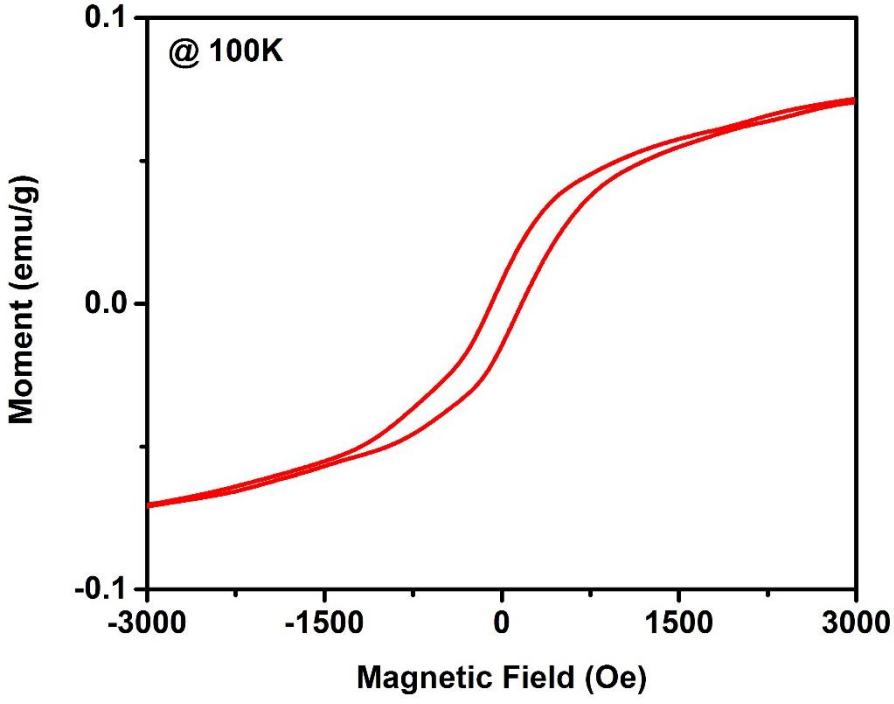

Figure 3.86: M vs. H measurement of cobalt sulfide (CS-3) sample at 100 K.

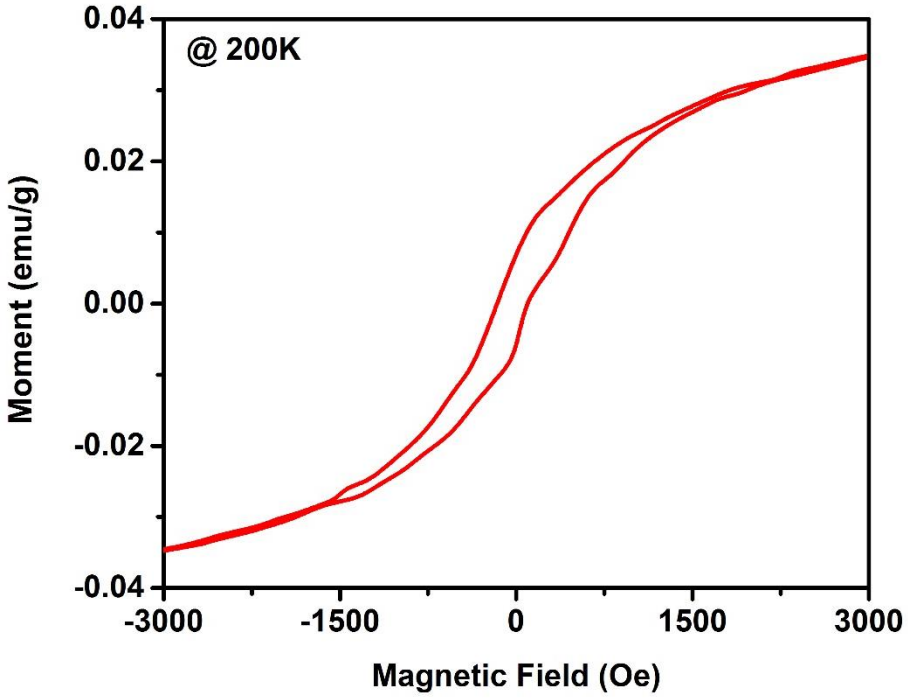

Figure 3.87: M vs. H measurement of cobalt sulfide (CS-3) sample at 200 K.

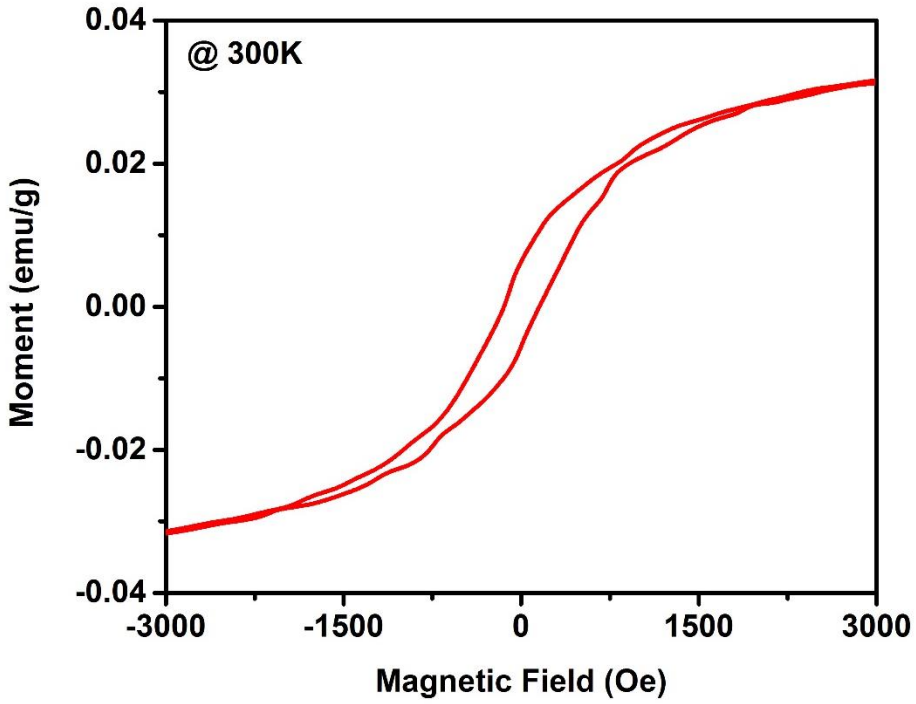

Figure 3.88: M vs. H measurement of cobalt sulfide (CS-3) sample at 300 K.

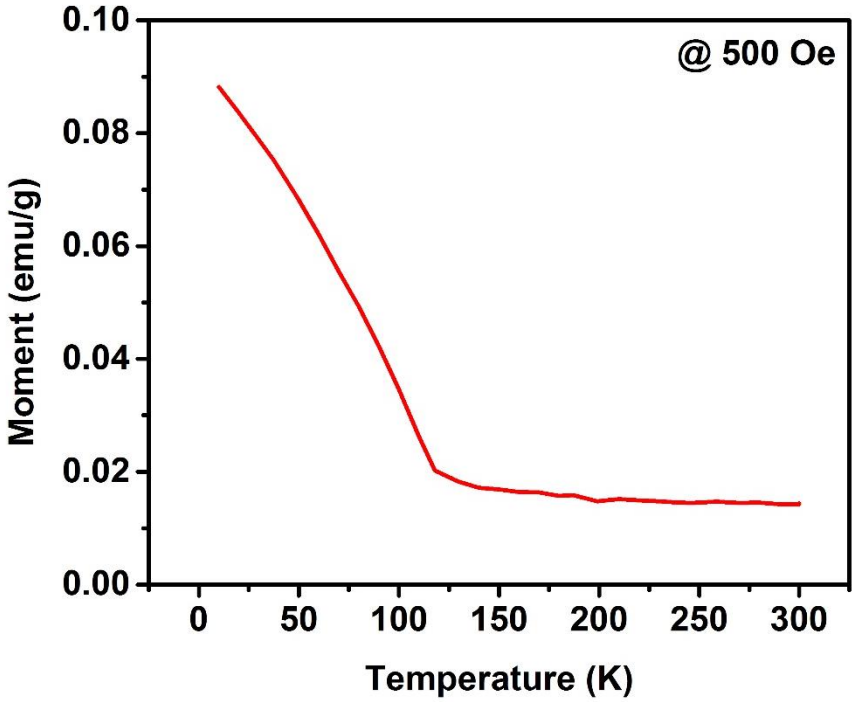

Figure 3.89: M vs. T measurement of cobalt sulfide (CS-3) sample at magnetic field of 500 Oe.

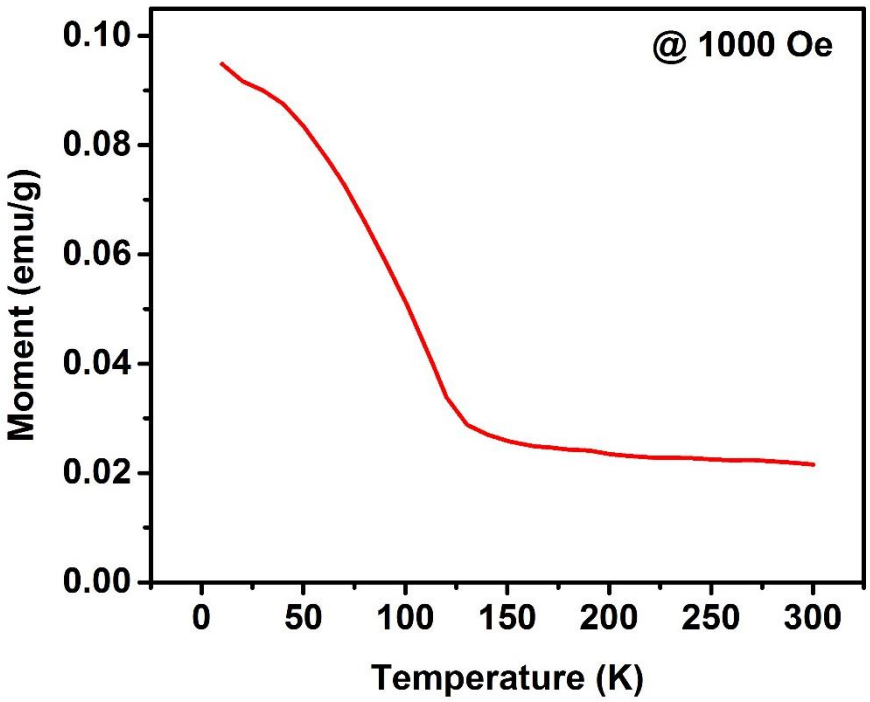

Figure 3.90: M vs. T measurement of cobalt sulfide (CS-3) sample at magnetic field of 1000 Oe.

CHAPTER IV

CONCLUSION

In summary, we have used a facile hydrothermal technique to synthesize cobalt sulfides. It was observed that the growth conditions have a drastic effect on morphology and size of the cobalt sulfides. The synthesized cobalt sulfides were structurally, magnetically and electrochemically characterized. X-ray diffraction, scanning electron microscopy and energy-dispersive X-ray spectrometer were used for structural characterizations. Scanning electron microscopic images revealed that the presence of surfactants during reaction provided morphologies with high surface area. Energy-dispersive X-ray spectrometer was used to further confirm the cobalt sulfide formation. The structural characterizations were further performed using X-ray diffraction technique. The X-ray diffraction patterns of the synthesized powder showed mixed phases of cobalt sulfides such as CoS and CoS_2. The crystallite size of the cobalt sulfide was estimated using XRD data. The average crystallite size of all the samples was in the range of 16.9 to 20.4 nm.

The effect of morphologies and electrolytes on the charge storage capacity of cobalt sulfides were electrochemically evaluated. Electrochemical measurements were performed in a standard three electrode cell. The potential application of the cobalt sulfides for the supercapacitor applications were tested using cyclic voltammeter and galvanostatic charge-discharge measurements. The cyclic voltammograms of cobalt sulfides showed pseudocapacitance behavior with the presence of a pair of redox peaks. It was observed that the specific capacitance of cobalt sulfides depends on scan rate. The specific capacitance was decreasing with increasing scan rate. The specific capacitance was also depending on the morphology of cobalt sulfide and electrolyte. The highest specific capacitance of 702 F/g for sample CS-6 was observed in 3 M NaOH electrolyte at scan rate of 5 mV/s. The cyclic stability test confirmed a high electrochemical stability of the cobalt sulfides. The electrochemical properties were further analyzed using galvanostatic charge-discharge measurements. The specific capacitance of cobalt sulfide electrodes was decreasing with increasing current. A maximum specific capacitance of 335 F/g was observed in 3 M NaOH solution for CS-6 sample. The electrochemical results suggest that cobalt sulfide could be used as an electrode material for fabrication of high capacity supercapacitors. We studied the effect of temperature on the electrochemical behavior of the quasi-solid state device. It was observed that temperature has a drastic effect on the charge storage capacity. The device showed about 400% improvement in charge storage capacity by increasing temperature from 10 to 70 ^{o}C.

Finally, we studied the magnetic properties of the cobalt sulfide. The presence of a hysteresis loop even at room temperature indicated that the synthesized cobalt sulfide

was ferromagnetic in nature. The remanence and coercivity of the cobalt sulfide was decreasing with increasing temperature. The remanence and coercivity at 10K was 59.9 emu/g and 459 Oe, respectively which decreases to 6.14 emu/g and 147 Oe, respectively at 300K. Moreover, the magnetization versus magnetic field measurement indicate that the saturated magnetization decrease with increase in the temperature.

REFERENCES

[1] L. Zhao, N. Baccile, S. Gross, Y. Zhang, W. Wei, Y. Sun, M. Antonietti, M.-M. Titirici, Sustainable nitrogen-doped carbonaceous materials from biomass derivatives, Carbon, 48 (2010) 3778-3787.

[2] Q. Wang, J. Yan, Y. Wang, T. Wei, M. Zhang, X. Jing, Z. Fan, Three-dimensional flower-like and hierarchical porous carbon materials as high-rate performance electrodes for supercapacitors, Carbon, 67 (2014) 119-127.

[3] Y. Han, S. Liu, D. Li, X. Li, Three-dimensionally Hierarchical Porous Carbon Creating High-performance Electrochemical Capacitors, Electrochim. Acta, 138 (2014) 193-199.

[4] V. Subramanian, S.C. Hall, P.H. Smith, B. Rambabu, Mesoporous anhydrous RuO_2 as a supercapacitor electrode material, Solid State Ionics, 175 (2004) 511-515.

[5] U.M. Patil, S.B. Kulkarni, V.S. Jamadade, C.D. Lokhande, Chemically synthesized hydrous RuO_2 thin films for supercapacitor application, J. Alloys Compd., 509 (2011) 1677-1682.

[6] T. Liu, W.G. Pell, B.E. Conway, Self-discharge and potential recovery phenomena at thermally and electrochemically prepared RuO_2 supercapacitor electrodes, Electrochim. Acta, 42 (1997) 3541-3552.

[7] Y.F. Yuan, X.H. Xia, J.B. Wu, X.H. Huang, Y.B. Pei, J.L. Yang, S.Y. Guo, Hierarchically porous Co_3O_4 film with mesoporous walls prepared via liquid crystalline template for supercapacitor application, Electrochem. Commun., 13 (2011) 1123-1126.

[8] C. Xiang, M. Li, M. Zhi, A. Manivannan, N. Wu, A reduced graphene oxide/Co_3O_4 composite for supercapacitor electrode, J. Power Sources, 226 (2013) 65-70.

[9] J.H. Kwak, Y.-W. Lee, J.H. Bang, Supercapacitor electrode with an ultrahigh Co_3O_4 loading for a high areal capacitance, Mater. Lett., 110 (2013) 237-240.

[10] G. He, J. Li, H. Chen, J. Shi, X. Sun, S. Chen, X. Wang, Hydrothermal preparation of Co_3O_4@graphene nanocomposite for supercapacitor with enhanced capacitive performance, Mater. Lett., 82 (2012) 61-63.

[11] J. Zhu, J. Jiang, J. Liu, R. Ding, H. Ding, Y. Feng, G. Wei, X. Huang, Direct synthesis of porous NiO nanowall arrays on conductive substrates for supercapacitor application, J. Solid State Chem., 184 (2011) 578-583.

[12] X. Yan, X. Tong, J. Wang, C. Gong, M. Zhang, L. Liang, Synthesis of mesoporous NiO nanoflake array and its enhanced electrochemical performance for supercapacitor application, J. Alloys Compd., 593 (2014) 184-189.

[13] Z.-H. Gao, H. Zhang, G.-P. Cao, M.-F. Han, Y.-S. Yang, Spherical porous VN and NiOx as electrode materials for asymmetric supercapacitor, Electrochim. Acta, 87 (2013) 375-380.

[14] B.J. Lokhande, R.C. Ambare, S.R. Bharadwaj, Thermal optimization and supercapacitive application of electrodeposited Fe_2O_3 thin films, Measurement, 47 (2014) 427-432.

[15] P.M. Kulal, D.P. Dubal, C.D. Lokhande, V.J. Fulari, Chemical synthesis of Fe_2O_3 thin films for supercapacitor application, J. Alloys Compd., 509 (2011) 2567-2571.

[16] Q. Wang, L. Jiao, H. Du, Y. Wang, H. Yuan, Fe_3O_4 nanoparticles grown on graphene as advanced electrode materials for supercapacitors, J. Power Sources, 245 (2014) 101-106.

[17] Y.-H. Kim, S.-J. Park, Roles of nanosized Fe_3O_4 on supercapacitive properties of carbon nanotubes, Current Applied Physics, 11 (2011) 462-466.

[18] J. Chen, K. Huang, S. Liu, Hydrothermal preparation of octadecahedron Fe_3O_4 thin film for use in an electrochemical supercapacitor, Electrochim. Acta, 55 (2009) 1-5.

[19] X. Zhang, P. Yu, H. Zhang, D. Zhang, X. Sun, Y. Ma, Rapid hydrothermal synthesis of hierarchical nanostructures assembled from ultrathin birnessite-type MnO_2 nanosheets for supercapacitor applications, Electrochim. Acta, 89 (2013) 523-529.

[20] W.-H. Jin, G.-T. Cao, J.-Y. Sun, Hybrid supercapacitor based on MnO_2 and columned FeOOH using Li_2SO_4 electrolyte solution, J. Power Sources, 175 (2008) 686-691.

[21] J. Ge, H.-B. Yao, W. Hu, X.-F. Yu, Y.-X. Yan, L.-B. Mao, H.-H. Li, S.-S. Li, S.-H. Yu, Facile dip coating processed graphene/MnO_2 nanostructured sponges as high performance supercapacitor electrodes, Nano Energy, 2 (2013) 505-513.

[22] E. Mitchell, J. Candler, F. De Souza, R.K. Gupta, B.K. Gupta, L.F. Dong, High performance supercapacitor based on multilayer of polyaniline and graphene oxide, Synth. Met., 199 (2015) 214-218.

[23] L.-J. Sun, X.-X. Liu, K.K.-T. Lau, L. Chen, W.-M. Gu, Electrodeposited hybrid films of polyaniline and manganese oxide in nanofibrous structures for electrochemical supercapacitor, Electrochim. Acta, 53 (2008) 3036-3042.

[24] D. Guan, Z. Gao, W. Yang, J. Wang, Y. Yuan, B. Wang, M. Zhang, L. Liu, Hydrothermal synthesis of carbon nanotube/cubic Fe_3O_4 nanocomposite for enhanced performance supercapacitor electrode material, Materials Science and Engineering: B, 178 (2013) 736-743.

[25] G. Huang, T. Chen, Z. Wang, K. Chang, W. Chen, Synthesis and electrochemical performances of cobalt sulfides/graphene nanocomposite as anode material of Li-ion battery, J. Power Sources, 235 (2013) 122-128.

[26] L. Zhang, H.B. Wu, X.W. Lou, Unusual CoS2 ellipsoids with anisotropic tube-like cavities and their application in supercapacitors, Chem. Commun., 48 (2012) 6912-6914.

[27] H.-W. Chen, C.-W. Kung, C.-M. Tseng, T.-C. Wei, N. Sakai, S. Morita, M. Ikegami, T. Miyasaka, K.-C. Ho, Plastic based dye-sensitized solar cells using Co9S8 acicular nanotube arrays as the counter electrode, Journal of Materials Chemistry A, 1 (2013) 13759-13768.

[28] J.-C. Xing, Y.-L. Zhu, Q.-W. Zhou, X.-D. Zheng, Q.-J. Jiao, Fabrication and shape evolution of CoS2 octahedrons for application in supercapacitors, Electrochim. Acta, 136 (2014) 550-556.

[29] Q.R. Hu, S.L. Wang, Y. Zhang, W.H. Tang, Synthesis of cobalt sulfide nanostructures by a facile solvothermal growth process, J. Alloys Compd., 491 (2010) 707-711.

[30] B. Qiu, X. Zhao, D. Xia, In situ synthesis of CoS2/RGO nanocomposites with enhanced electrode performance for lithium-ion batteries, J. Alloys Compd., 579 (2013) 372-376.

[31] Q. Wang, L. Jiao, Y. Han, H. Du, W. Peng, Q. Huan, D. Song, Y. Si, Y. Wang, H. Yuan, CoS2 Hollow Spheres: Fabrication and Their Application in Lithium-Ion Batteries, The Journal of Physical Chemistry C, 115 (2011) 8300-8304.

[32] B. Liu, F. Wang, D. Zheng, X. Liu, X. Sun, S. Hou, Y. Xing, Hydrothermal synthesis and magnetic properties of CoS2 nano-octahedrons, Mater. Lett., 65 (2011) 2804-2807.

[33] H. Zhang, S.C. Wang, D. Xue, Q. Chen, Z.C. Li, Preparation of nanocrystalline CeO 2 by nanocasting with mesoporous silica, Journal of Physics: Conference Series, 152 (2009) 012070.

[34] J.H. Kim, J.-H. Lee, Y.C. Kang, Electrochemical properties of cobalt sulfide-carbon composite powders prepared by simple sulfidation process of spray-dried precursor powders, Electrochim. Acta, 137 (2014) 336-343.

[35] J. Gomez, E.E. Kalu, High-performance binder-free Co–Mn composite oxide supercapacitor electrode, J. Power Sources, 230 (2013) 218-224.

[36] S.H. Mujawar, S.B. Ambade, T. Battumur, R.B. Ambade, S.-H. Lee, Electropolymerization of polyaniline on titanium oxide nanotubes for supercapacitor application, Electrochim. Acta, 56 (2011) 4462-4466.

[37] F. Zhao, Y. Wang, X. Xu, Y. Liu, R. Song, G. Lu, Y. Li, Cobalt Hexacyanoferrate Nanoparticles as a High-Rate and Ultra-Stable Supercapacitor Electrode Material, ACS Applied Materials & Interfaces, 6 (2014) 11007-11012.

[38] L.-J. Xie, J.-F. Wu, C.-M. Chen, C.-M. Zhang, L. Wan, J.-L. Wang, Q.-Q. Kong, C.-X. Lv, K.-X. Li, G.-H. Sun, A novel asymmetric supercapacitor with an activated carbon cathode and a reduced graphene oxide–cobalt oxide nanocomposite anode, J. Power Sources, 242 (2013) 148-156.

[39] E. Mitchell, F. De Souza, R.K. Gupta, P.K. Kahol, D. Kumar, L. Dong, B.K. Gupta, Probing on the hydrothermally synthesized iron oxide nanoparticles for ultra-capacitor applications, Powder Technol., 272 (2015) 295-299.

[40] E. Mitchell, A. Jimenez, R.K. Gupta, B.K. Gupta, K. Ramasamy, M. Shahabuddin, S.R. Mishra, Ultrathin porous hierarchically textured NiCo2O4-graphene oxide flexible nanosheets for high-performance supercapacitors, New J. Chem., (2015).

[41] W. Tang, S. Tian, L.L. Liu, L. Li, H.P. Zhang, Y.B. Yue, Y. Bai, Y.P. Wu, K. Zhu, Nanochain LiMn2O4 as ultra-fast cathode material for aqueous rechargeable lithium batteries, Electrochem. Commun., 13 (2011) 205-208.

[42] M.-C. Liu, L.-B. Kong, X.-J. Ma, C. Lu, X.-M. Li, Y.-C. Luo, L. Kang, Hydrothermal process for the fabrication of CoMoO4[middle dot]0.9H2O nanorods with excellent electrochemical behavior, New J. Chem., 36 (2012) 1713-1716.

[43] W. Li, K. Xu, L. An, F. Jiang, X. Zhou, J. Yang, Z. Chen, R. Zou, J. Hu, Effect of temperature on the performance of ultrafine MnO2 nanobelt supercapacitors, Journal of Materials Chemistry A, 2 (2014) 1443-1447.